Spatial modelling of mountainous basins

Nederlandse Geografische Studies / Netherlands Geographical Studies

Redactie / Editorial Board
Drs. J.G. Borchert (Editor in Chief)
Prof. Dr. J.M.M. van Amersfoort
Dr. P.C.J. Druijven
Prof. Dr. A.O. Kouwenhoven
Prof. Dr. H. Scholten

Plaatselijke Redacteuren / Local Editors
Drs. R. van Melik,
Faculteit Geowetenschappen Universiteit Utrecht
Dr. D.H. Drenth,
Faculteit der Managementwetenschappen Radboud Universiteit Nijmegen
Dr. P.C.J. Druijven,
Faculteit der Ruimtelijke Wetenschappen Rijksuniversiteit Groningen
Drs. F.J.P.M. Kwaad,
Fysich-Geografisch en Bodemkundig Laboratorium Universiteit van Amsterdam
Dr. L. van der Laan,
Economisch-Geografisch Instituut Erasmus Universiteit Rotterdam
Dr. J.A. van der Schee,
Centrum voor Educatieve Geografie Vrije Universiteit Amsterdam
Dr. F. Thissen,
Afdeling Geografie, Planologie en Internationale Ontwikkelingsstudies Universiteit van Amsterdam

Redactie-Adviseurs / Editorial Advisory Board
Prof. Dr. G.J. Ashworth, Prof. Dr. P.G.E.F. Augustinus, Prof. Dr. G.J. Borger,
Prof. Dr. K. Bouwer, Prof. Dr. J. Buursink, Dr. J. Floor, Prof. Dr. G.A. Hoekveld,
Dr. A.C. Imeson, Prof. Dr. J.M.G. Kleinpenning, Dr. W.J. Meester,
Prof. Dr. F.J. Ormeling, Prof. Dr. H.F.L. Ottens, Dr. J. Sevink, Dr. W.F. Sleegers,
T.Z. Smit, Drs. P.J.M. van Steen, Dr. J.J. Sterkenburg, Drs. H.A.W. van Vianen,
Prof. Dr. J. van Weesep

ISSN 0169-4839

Netherlands Geographical Studies 369

Spatial modelling of mountainous basins

An integrated analysis of the hydrological cycle, climate change and agriculture

Walter Immerzeel

Utrecht 2008

Koninklijk Nederlands Aardrijkskundig Genootschap
Faculteit Geowetenschappen Universiteit Utrecht

This publication is identical to a dissertation submitted for the title of Doctor at Utrecht University; the Netherlands. The public defence of this thesis took place on January 18, 2008.

Promotor:
Prof. Dr. S.M. de Jong

Co-promotoren:
Dr. P. Droogers
Dr. R.A. Quiroz

Examination committee:
Prof. Dr. W.G.M. Bastiaanssen
Prof. Dr. M.F.P. Bierkens
Prof. Dr. J. Bouma
Prof. Dr. N.C. van de Giesen
Dr. J.J. Stoorvogel

ISBN 978 90 6809 411 4

Graphic design, cartography and figures:
GeoMedia (Faculty of Geosciences, Utrecht University)

Copyright © Walter Immerzeel

Niets uit deze uitgave mag worden vermenigvuldigd en/of openbaar gemaakt door middel van druk, fotokopie of op welke andere wijze dan ook zonder voorafgaande schriftelijke toestemming van de uitgevers.

All rights reserved. No part of this publication may be reproduced in any form, by print or photo print, microfilm or any other means, without written permission by the publishers.

Printed in the Netherlands by Labor Grafimedia b.v. – Utrecht

Contents

Figures		9
Tables		11
Abbreviations and acronyms		13
Acknowledgements		15
1	**Introduction**	17
1.1	Background	17
1.2	Mountains and hydrology	17
1.3	Objectives and approach	18
1.4	Innovation and relevance	20
1.5	Thesis outline	21
2	**Understanding precipitation patterns and land use interaction in Tibet using harmonic analysis of SPOT VGT-S10 NDVI time series**	23
	Abstract	23
2.1	Introduction	23
2.2	Methodology	24
2.2.1	Fourier analysis	24
2.2.2	Datasets	26
2.2.3	General	26
2.2.4	Study area	27
2.3	Results	29
2.3.1	NDVI patterns for different land uses	29
2.3.2	NDVI behaviour in relation to precipitation	31
2.3.3	Inter-annual NDVI behaviour	33
2.4	Discussion	35
2.5	Conclusion	36
3	**Historical trends and future predictions of climate variability in the Brahmaputra basin**	39
	Abstract	39
3.1	Introduction	39
3.2	Data and methods	43
3.3	Results	45
3.3.1	Historical trends	45
3.3.2	Future changes	47
3.3.3	Hydrological impacts	49
3.4	Discussion and conclusion	53

4	**Calibration of a distributed hydrological model based on satellite evapotranspiration**	55
	Abstract	55
4.1	Introduction	55
4.2	Study area	57
4.3	Methods	58
4.3.1	SEBAL	58
4.3.2	SWAT	61
4.3.3	PEST	63
4.3.4	Calibration strategy	64
4.4	Results	66
4.5	Discussion and conclusion	71
5	**Integrating remote sensing and a process-based hydrological model to evaluate water use and productivity in a south Indian catchment**	75
	Abstract	75
5.1	Introduction	76
5.2	Study area	77
5.3	Methodology	81
5.3.1	Evapotranspiration mapping	81
5.3.2	Land use classification	82
5.3.3	Data preparation	83
5.3.4	Application of SWAT	83
5.3.5	Model calibration and validation	84
5.3.6	Water productivity analysis	86
5.4	Results and discussion	87
5.4.1	Land use mapping	87
5.4.2	Model calibration and validation	87
5.4.3	Water balance	90
5.4.4	Water productivity analysis	93
5.5	Conclusions	95
6	**Can payments for ecosystem services secure the water tower of Tibet?**	97
	Abstract	97
6.1	Introduction	97
6.2	Materials and methods	99
6.2.1	Study area	99
6.2.2	SWAT	99
6.2.3	MD model for analysis of ecosystem service supply	101
6.3	Results	104
6.3.1	Hydrological modelling	104
6.3.2	Economic model	107
6.3.3	Sensitivity analysis	109
6.4	Discussion and conclusion	111

7 Synthesis **115**
7.1 Introduction 115
7.2 Mapping precipitation using remote sensing 117
7.3 Hydrological implications of climate change in large scale mountainous catchments 121
7.4 Calibrating hydrological models using Remote Sensing 124
7.5 Integrating hydrological and economic modelling to support policy making 128
7.6 Conclusions 129

References **131**
Summary **141**
Samenvatting **143**
Curriculum Vitae **145**

Figures

2.1	USGS global land cover characteristics for Tibet.	28
2.2	Average annual NDVI pattern for Tibet.	29
2.3	Frequency diagram dryland cropland land use.	30
2.4	Modelled and original NDVI curves for dryland cropland.	31
2.5	First two harmonic terms for six different land use types.	31
2.6	Relation between NDVI increment and precipitation.	32
2.7	Inter-annual variation of Fourier-transformed NDVI curves.	34
3.1	Overview Brahmaputra basin.	40
3.2	Box-whisker plot with seasonal climate normals (1961-1990) of temperature and precipitation.	41
3.3	Average number of meterological stations within the correlation decay distance for precipitation and temperature.	43
3.4	Temperature anomalies (°C) and precipitation anomalies (%) per physiographic zone from 1905-2002.	46
3.5	Linear regressions for the TP, HB and FP.	47
3.6	Downscaled temperature and precipitation anomalies from the climate normal 1961-1990.	48
3.7	Box-whisker plot of seasonal temperatures and precipitation for observed data and HadCM3 climate change predictions.	49
3.8	Downscaled spatial temperature anomalies from the climate normal 1961-1990 based on the average of 6 GCMs.	50
3.9	Downscaled spatial precipitation anomalies from the climate normal 1961-1990 based on the average of 6 GCMs.	51
3.10	Average monthly hydrograph at Bahadurabad and basin precipitation and scatter plot between monthly basin precipitation and Bahadurabad discharges.	52
3.11	Projected trends in seasonal discharges at Bahadurabad.	52
3.12	Relation between monthly average and extreme discharges at Bahadurabad.	53
4.1	Upper Bhima catchment boundary, contours of the precipitation sum from June 2004 to May 2005, river network, major reservoirs, and meteorological station.	57
4.2	Monthly precipitation (P), reference evapotranspiration (ET_{ref}) and temperature from June 2004 to May 2005.	58
4.3	Land use based on unsupervised classification of MODIS.	63
4.4	Flowchart of calibration strategy.	65
4.5	Scatter plot of SEBAL vs SWAT of the sum of ET_{ref}.	67
4.6	Box whisker plots of monthly ΔETact (SEBAL – SWAT).	67
4.7	Scatter plots of SEBAL and SWAT ET_{act}.	69
4.8	Eight month sum of ET_{act} for SWAT and SEBAL on sub basin and HRU level.	70
4.9	Historical observed and simulated discharges at the outlet of the catchment.	71

5.1	Upper Bhima catchment boundary and isohyets of total precipitation from June 2004 to May 2005	78
5.2	Monthly precipitation (P), reference evapotranspiration (ET_{ref}), minimum (T_{min}) and maximum temperature (T_{max}) averaged for two meteorological stations.	78
5.3	Average 10-daily NDVI patterns for the agricultural land use classes.	79
5.4	Land use based on unsupervised classification of MODIS time series.	79
5.5	Soil types based on the digital soil map of the world (FAO, 1998)	81
5.6	The root mean square error of modelled actual evapotranspiration versus the number of SWAT model calls required by PEST.	88
5.7	Cumulative ET_{act} from October 2004 to May 2005 derived with SEBAL and simulated with SWAT.	88
5.8	Modelled discharge at the outlet of the catchment (Q_m) versus observed discharge at the outlet of the catchment (Q_o).	90
5.9	Monthly basin average water balance from June 2004 to May 2005.	91
5.10	Cumulative volumetric precipitation (P) and actual evapotranspiration (ET_{act}) from June 2004 to May 2005.	92
5.11	Evaporative depletion per land use from June 2004 to May 2005.	92
5.12	Sugar cane yield (kg/ha) as a function of annual actual evapotranspiration (ETact) and the sum of annual precipitation and irrigation (P+I).	93
6.1	Derivation of the supply of ecosystem services from the spatial distribution of opportunity cost per unit of ecosystem services.	103
6.2	Average annual water balance from 1983 to 2002.	105
6.3	SWAT validation results.	105
6.4	Monthly average precipitation (P), irrigation (I) and actual evapotranspiration (ET_{act}) from 1983-2003 for irrigated and rain fed barley.	106
6.5	Relation between the reduction in irrigation (ΔI) and the reduction in actual evapotranspiration (ΔET_{act}) per HRU based on 20 year averages.	106
6.6	Average annual difference in discharge between the rain fed and irrigated scenario from 1983-2002 in the months April-June at the catchment outlet.	107
6.7	The spatial distribution of opportunity cost per unit of ecosystem service and the derived supply curves.	109
6.8	Catchment results for the base model.	110
7.1	Global water use.	115
7.2	Schematic representation of the systems approach	117
7.3	Two examples of satellite based remotely sensed precipitation (mm) in July 2006.	118
7.4	Projected global surface warming.	122
7.5	Spatial and physical detail of hydrological models	125
7.6	Example of global mass balance changes during august 2005 (cm of water equivalent).	126

Tables

2.1	Regression coefficients (R^2) of NDVI parameters and precipitation.	33
3.1	Overview of the GCMs used, the reference periods and latitudinal and longitudinal spatial resolutions	44
3.2	Seasonal regression models for average discharge at Bahadurabad based on data from 1954-1992.	51
4.1	Date and local acquisition time (+5:30 GMT) of Aqua-MODIS images.	59
4.2	Acreages of different land use and land cover in the catchment	62
4.3	Results of different optimisations runs.	68
5.1	Soil properties of major soils in the catchment based on the digital soil map of the world (FAO, 1998).	80
5.2	Acreages, crops, and growing season of different land use classes in the upper Bhima catchment	82
5.3	SWAT calibration results per land use and per month.	89
5.4	Statistical parameters of yield (Y), actual evapotranspiration (ET_{act}) and water productivity simulated by SWAT per agricultural land use.	94
6.1	Inputs for the economic analysis per Hydrological Response Unit (HRU).	108
6.2	Sensitivity of the total supply of ecosystem service (S), the slope of the supply curve ($\Delta S/\Delta Pe$) and the fraction of farmers participating in a contract (r) at a fixed P_e of 0.15 \$ m^{-3}.	111

Abbreviations and acronyms

4AR	Fourth Assessment Report
AMSU-B	Advanced Microwave Sounding Unit B
AOGCM	Atmosphere Ocean General Circulation Model
AVHRR	Advanced Very High Resolution Radiometer
CAS	Chinese Academy of Sciences
CRU	Climate Research Unit
CV	Coefficient of Variation
CWP	Crop Water Productivity
DDC	Data Distribution Centre
DEM	Digital Elevation Model
DN	Digital Number
ENSO	El Niño Southern Oscillation
ESA	European Space Agency
ET	Evapotranspiration
FAO	Food and Agricultural Organization
FFT	Fast Fourier Transform
FP	Floodplains
GCM	General Circulation Model
GHCN	Global Historical Climatology Network
GLCC	Global Land Cover Characteristics
GML	Gauss-Marquardt-Levenberg
GOCE	Gravity Field and Steady-State Ocean Circulation Explorer
GOES	Geostationary Operational Environmental Satellite
GPCP	Global Precipitation Climatology Project
GRACE	Gravity Recovery and Climate Experiment
GTS	Global Telecommunication System
HB	Himalayan Belt
HKH	Hindu Kush Himalaya
HRU	Hydrological Response Units
IAHS	International Association for Hydrological Sciences
IPCC	Intergovernmental Panel on Climate Change
IR	Infrared
IWMI	International Water Management Institute
JJAS	June, July, August, September
JRC	Joint Research Centre
LAI	Leaf Area Index
MD	Minimum Data
MODIS	Moderate Resolution Imaging Spectroradiometer

NASA	National Aeronautics and Space Administration
NCAR	National Centre for Atmospheric Research
NCEP	National Centre for Environmental Prediction
NDVI	Normalized Difference Vegetation Index
NIVR	Netherlands Agency for Aerospace Programmes
NOAA	National Oceanic and Atmospheric Administration
NUSP	National User Support Programme
PEST	Parameter Estimation
PES	Payments for Ecosystem Services
PR	Precipitation Radar
PUB	Prediction in Ungauged Basin
RFE	Rainfall Estimate
RMSE	Root Mean Square Error
RUE	Radiation Use Efficiency
SEBAL	Surface Energy Balance Algorithm for Land
SRES	Special report on Emission Scenarios
SRON	Space Research Organization of the Netherlands
SRTM	Shuttle Radar Topograghy Mission
SSM/I	Special Sensor Microwave Imager
SWAT	Soil and Water Assessment Tool
TAAAS	Tibetan Academy of Agriculture and Animal Husbandry Sciences
TM	Thematic Mapper
TMI	TRMM Microwave Imager
TOA	Trade-off Analysis
TP	Tibetan Plateau
TRMM	Tropical Rainfall Monitoring Mission
UNL	University of Nebraska Lincoln
USGS	United States Geological Survey
VIRS	Visible Infrared Scanner
WMO	World Meteorological Organization

Acknowledgements

First of all I would like to acknowledge a number of funding agencies that supported part of the work presented in this thesis: the ecoregional fund (chapter 2) and the Netherlands Agency for Aerospace Programmes through their National Users Support Programme (chapter 4 and 5), and FutureWater. Secondly, I would like to express my gratitude to a number of colleagues throughout the world who provided data that supported my work: Dr. Chodok of the Tibetan Bureau of Meteorology, Dr. Lu Changhe of the Institute of Geographic Sciences and Natural Resources Research of the Chinese Academy of Sciences, Dr. Anju Gaur of the International Water Management Institute, Dr. Tarekul Islam of the Institute of Water and Flood Management Bangladesh University of Engineering, Dr. Ji Quimei of the Tibet Academy of Agricultural and Animal Husbandry Sciences, and Sander Zwart of WaterWatch.

From a more personal point of view I would first of all like to thank Roberto Quiroz for initiating this PhD endeavour. I still remember our vivid discussions in Potchefstrom (South-Africa) where you first suggested to consider a PhD based on my work in Nepal, later on this all materialized during a joint field trip to Tibet, your financial support after I returned to the Netherlands and your invitation to come to Lima and work together on unravelling the wavelet mysteries. Your modest but wise suggestions were very much appreciated throughout these years. Many thanks also to Steven de Jong, who immediately enthusiastically agreed to supervise my PhD after I contacted him from Nepal. We worked together more closely after I returned and your endless positivism in combination with a fresh view on many topics were a great source of inspiration. I am also extremely grateful to Peter Droogers. We have worked together since the beginning of 2005 and it has been an interesting learning curve ever since. Thanks for meticulously reading every paper at least three times, for your believe that achieving a PhD degree is instrumental in our field, for your straightforward solutions to (in my view) complex problems, and for pushing me to wrap things up.

I am also grateful to my entire family for motivating me and to keep forcing me to explain what these papers were all about. It certainly helped to get the message straight. A special thanks to my mother-in-law and her irresistible desire to ask me at least twice a week for three years in a row how many paper I finished, what they were about, when the defence was scheduled and more importantly how and where we could celebrate this properly. You surely kept me focused on the final objective.

Finally, Hilde, without you I would not have been able to finish this thesis. Besides your support, unlimited faith and (limited) patience, you commented on many pieces of the jigsaw in a very clear, straightforward and refreshing manner. More importantly, I would probably still be struggling to put it all together weren't it for you and our discussions in the Pyrenees. Final thanks to my little Thijmen for his relentless efforts to keep me focussed on the important things in life, rather then staring at a computer screen.

1 Introduction

1.1 Background

Water is the most essential substance on earth. More than a quarter of the world's population or a third of the population in developing countries live in regions experiencing severe water scarcity (Seckler et al., 1999). The changing climate has an important impact on the spatial and temporal availability of water. It is anticipated that changes in the water cycle will be most significant in mountain areas where the current variability of rainfall, temperature and evapotranspiration is already high. The slow but steady disappearance of the glaciers in mountain areas will also have a significant impact on the discharge patterns of the rivers. The availability of water also has a strong impact on economic activities and potential of an area (Droogers et al., 2001). Our knowledge of how climate change will affect the availability of water is rather limited due to the complexity of the system, the lack of data and observations and model limitations. The use of advanced models driven by inputs from time series of earth observation sensors and from general circulation models and calibrated with field measurements may greatly enhance our insight in the pending impacts of global change. This thesis aims at increasing our knowledge about how water availability will change in the future and at developing practical modelling tools to predict water availability in mountain areas.

1.2 Mountains and hydrology

Mountain areas cover a significant part of the world's surface. Half of the world's population depends directly or indirectly on the water resources provided by mountains. Mountains play an essential role in the survival of global ecosystems, have a profound impact on global and regional weather and climate patterns, and are an important producer of environmental services provided by mountain ecosystems (e.g. fresh water, biodiversity). Because of the altitudinal variation completely different climate regimes are found within short horizontal distances. At the same time mountains are a key element of the hydrological cycle, being the source of many of the world's major rivers and a temporary sink of rainfall water. Mountains can be considered as water towers with increased specific yields for agriculture, seasonal delay of discharge through storage of water in the form of snow and ice, and decreased seasonal discharge variability in comparison to lowlands. Degradation of water resources in mountains therefore does not only affect the mountain population, but also the people in downstream areas. Mountainous regions are considered 'the blackest of black boxes in the hydrological cycle' with respect to data availability and understanding (Klemes, 1998).

It is predicted that climate change in mountain areas will lead to an intensification of the global hydrological cycle and can have major impacts on regional water resources (Arnell, 1999).

Changes in the amount of precipitation and in its frequency and intensity directly affect the magnitude and timing of runoff and the intensity of floods and droughts. However, at present, specific regional effects are uncertain (IPCC, 2001). The impact of climate change on the water resources and agriculture in mountain areas could be significant. Regional changes in precipitation characteristics have the potential to affect mean runoff, frequency, and intensity of floods and droughts. Projected rise in temperature will lead to increased glacial and snow melt (IPCC, 2007), which would lead to increased summer flows in some river systems for a few decades, followed by a reduction in flow as the glaciers disappear and snowfall diminishes. A recent study even showed that climate models predict that temperatures rise faster at higher than at lower altitudes (Bradley et al., 2006). Barnett et al. (2005) argue in a global study that the Hindu Kush Himalaya (HKH) region is the most critical area in which increased melt will affect water supply in the decades ahead. A quantification of these effects as well as an evaluation of adaptation strategies remains however unknown.

1.3 Objectives and approach

A systems approach to the interaction between the hydrological cycle, climate change and agriculture in mountain areas is largely lacking. Research on either of the components has been performed in the past but the integration is severely hampered by the lack of systematic data and/or tools in many cases. Three knowledge gaps can be identified which impede a successful implementation of a systems approach: (i) lack of fundamental data and knowledge about the spatial heterogeneity of climate variables in mountain, (ii) absence of a straightforward technique to calibrate simulation models in data scarce areas and (iii) the missing link between outputs of simulation models and policy changes.

The overall objective of this thesis is:

The development of a systems approach for mountain river basins leading to a better understanding of the hydrological functioning and to the development of tools supportive to decision makers

The thesis is structured across four different topics each addressing a specific research question. The four questions cover the entire range from understanding fundamental hydrological processes using remote sensing to the development of instruments supporting decision making. It should be acknowledged that each research question is a field of science by itself. Therefore a specific topic has been chosen that addresses the main research question. Each topic has resulted in the publication of a peer reviewed paper in an international journal, which will be presented in the subsequent chapters. The following research questions are addressed:

1. How can remote sensing support the quantification of processes of the hydrological balance in highly diverse topographic terrain?
2. Is it possible to make a reliable assessment of climate change and its effects at river basin scale in mountain areas?
3. Is it feasible to develop a methodology to reliably calibrate hydrological models in ungauged basins on the basis of remote sensing derived hydrological parameters?

4. Is it possible to integrate economic and hydrological modelling and if yes, what incentives and economic instruments can best be applied to conserve water in upstream areas of water scarce river basins?

1. How can remote sensing support the quantification of processes of the hydrological balance in highly diverse topographic terrain?

Quantification of different components of the hydrological cycle in time and space is the most important objective of every hydrological simulation model. A precise understanding of the spatial and temporal behaviour of climate parameters in mountain areas is hampered by the lack of observational data (Beniston, 2003). Climate changes rapidly with height and over relative short horizontal distances climatological differences can be extremely large. A common error source of simulation models in mountain catchments therefore is the inaccurate climate representation. More specifically, this thesis focused on understanding precipitation patterns using time series analysis of Remote Sensed vegetation indices on the Tibetan Plateau. The main assumption in the research is that the behaviour of vegetation in semi-arid areas is strongly depending on precipitation. The greenness of the vegetation is measured by the Normalized Difference Vegetation Index and the spatial-temporal patterns are an important determinant of precipitation patterns. Previous studies have revealed that NDVI and rainfall seem to be linearly related in a specific range of rainfall conditions, generally between 200-1200 mm/y and 25-200 mm/month (Davenport and Nicholson, 1993; Malo and Nicholson, 1990).

2. Is it possible to make a reliable assessment of climate change and its effects at river basin scale?

Most applied climate change studies make use of the outputs of general circulation models (GCMs). The use of GCM climate data for modelling impacts on agriculture has been evolving over the past twenty years. Due to the complexity of these models the spatial resolution of the outputs is generally in the range of several hundred kilometres. This is too large for application at local scale, specifically in mountain areas. In order to obtain information at spatial scales, smaller than a grid-box in a GCM, it is necessary to 'downscale' the GCM information. Statistical downscaling uses a time series of local observations which overlap with the reference period of the GCMs (Wilby et al., 1998). This technique assumes conservation of mean and variance during the reference period. In this thesis the temporal and spatial temperature and precipitation patterns in the entire Brahmaputra basin are analyzed. Firstly, a historical analysis of the previous 100 years is performed to detect trends in temperature and precipitation. Trends are explained by multiple regression analysis with a number of variables. Secondly, results of six GCMs are statistically downscaled for two scenarios up to the year 2100. Finally, the downscaled results in time and space are used to assess the hydrological effects of climate change in the basin. Earlier work focused mainly on downscaling GCM output at a specific location, but the combination of spatial and temporal downscaling and the link to basin scale effects on average and extreme river discharges is a new approach.

3. Is it feasible to develop a methodology to reliably calibrate hydrological models in ungauged basins on the basis of remote sensing derived hydrological parameters?

Despite substantial progress in the development of hydrological models, the weakest part is the lack of data to apply and calibrate these models. Traditionally, these models are fine-tuned by a calibration process where observed hydrographs are compared to simulated ones. By adjusting the most sensitive and most unreliable input parameters the model can be calibrated and performs better in describing the current situation. Consequently is it also more reliable to explore water management options for the future. It is clear that in data scarce areas such an approach, which requires observed stream flow data, is impossible. In this thesis it is investigated whether it is possible to autocalibrate the hydrological model SWAT (Neitsch et al., 2001) on the basis of spatial evapotranspiration (ET) measurements derived from Remote Sensing using non-linear parameter optimization tools. Deriving ET from Remote Sensing is an expanding field and several operational tools, based on solving the surface energy balance, are available (Bastiaanssen et al., 1998; Su, 2002). To satisfactory test this approach the highly diverse, both in climate and land uses, mountainous Krishna basin in India is chosen.

4. Is it possible to integrate economic and hydrological modelling and if yes, what incentives and economic instruments can best be applied to conserve water in upstream areas of water scarce river basins?

A critical next step is to decide upon a strategy on how valuable knowledge, generated by these calibrated models, can be integrated with the decision making process. In this thesis an economic approach is integrated with the results of the hydrological simulation model. In agriculture there has been a shift from traditional subsidy and trade policies to conservation and environmental aspects of agriculture by providing farmers with incentives for increasing the supply of environmental services. This project will adopt an economic approach to model the supply of fresh water in mountain areas to illustrate this powerful concept. The minimum data approach developed by Antle and Valdivia (2006) has been used as a starting point. Antle and Stoorvogel (2006) show how the spatial heterogeneity of the physical system can be incorporated in this approach using simulation models. With some adaptation, this approach has proven to be suitable to model the supply of fresh water on the Tibetan plateau.

1.4 Innovation and relevance

Using a systems approach to investigate the relationship between hydrology, climate change and agriculture using simulations models and remote sensing in mountain ecosystems and data poor environments is highly innovative.

The quantification of the spatial heterogeneity of climate variables in mountain areas using Remote Sensing is a new and challenging field of research. Satellites, which enable this type of work, have only recently been developed and systematic methodologies aiming at improving the performance of hydrological simulation models do not yet exist.

Downscaling of GCM data itself is not innovative; however the addition of a spatial component and the basin wide approach is new. Most existing methods downscale to a specific location (usually one meteorological station). The statistical approach to assess basin wide effects of climate change is currently not available, but is in high demand.

Using nonlinear parameter estimation techniques in calibration of models is well investigated in hydrology. These algorithms however always use observed hydrographs. Using spatial information on evapotranspiration in the calibration method is a completely new approach..

The concept of payments for environmental services has received an increasing amount of attention over the years. However, the implementation of the concept is still in its infancy. The possibilities of the integration of physical models and the economic behaviour of farmers are therefore promising.

This thesis has contributed to the development of tools that allow a quantification of the effect of climate change on the water resources as well as the evaluation of an adaptation strategy. These tools are relevant for society and can guide policy makers in taking appropriate, science based action.

1.5 Thesis outline

The research presented in this thesis puts emphasis on mountain catchments in Asia; two chapters focus on (part) of the Tibetan Plateau, one chapter focuses on the Brahmaputra basin covering part of China, India, Bhutan and Bangladesh and two papers analyse a sub-basin of the Krishna basin in the Indian state of Maharasthra. Detailed descriptions of the research catchments are presented in the subsequent chapters.

Each research question has resulted in a peer reviewed paper in a varying range of international scientific journals. The papers are, in modified form, included in this thesis as separate chapters:

- Chapter 2 is titled *Understanding complex spatiotemporal weather patterns and land use interaction in the Tibetan Autonomous Region using harmonic analysis of SPOT VGT-S10 NDVI time series* and is in its original form published in the International Journal of Remote Sensing (Immerzeel et al., 2005).
- Chapter 3 is titled *Historical trends and future predictions of climate variability in the Brahmaputra basin* and is accepted for publication in the International Journal of Climatology. (Immerzeel, 2007)
- Chapter 4 is titled *Calibration of a distributed hydrological model based on satellite evapotranspiration* and is accepted for publication in the Journal of Hydrology (Immerzeel and Droogers, 2007)
- Chapter 5 is titled *Integrating remote sensing and a process-based hydrological model to evaluate water use and productivity in a south Indian catchment* and is accepted for publication in Agricultural Water Management. (Immerzeel et al., 2007a)
- Chapter 6 is titled *Can payments for ecosystem services secure the water tower of Tibet?* and is accepted for publication in Agricultural Systems (Immerzeel et al., 2007b).

Finally chapter 7 forms the synthesis of the five chapters and presents the main conclusions of the thesis. This chapter may be read independently of the preceding chapters and provides a complete overview of and relation between the different research questions addressed.

2 Understanding precipitation patterns and land use interaction in Tibet using harmonic analysis of SPOT VGT-S10 NDVI time series

Based on: Immerzeel, W.W., R.A. Quiroz & S.M. de Jong (2005), Understanding complex spatiotemporal weather patterns and land use interaction in the Tibetan Autonomous Region using harmonic analysis of SPOT VGT-S10 NDVI time series. International Journal of Remote Sensing 11, pp. 2281–2296.

Abstract

Time series analysis of Normalized Difference Vegetation Index (NDVI) imagery is a powerful tool in studying land use and precipitation interaction in data-scarce and inaccessible areas. The Fast Fourier Transform (FFT) was applied to the annual time series of 36 average dekadal NDVI images. The dekadal annual average pattern was calculated from 189 NDVI images from April 1998 to June 2003 acquired with the VEGETATION instruments of the SPOT-4 and SPOT-5 satellites in Tibet. It is shown that the first two harmonic terms of a Fourier series suffice to distinguish between land use classes. The results indicate that the highest biomass production occurs before the monsoon peak. Regression analysis with 15 meteorological stations has shown that the total amount of precipitation during the growing season shows the strongest relation with the sum of the amplitudes of the first two harmonic terms (R^2 = 0.72). Inter-annual NDVI variation based on Fourier-transformed time series was studied and it was shown that, early in the season, the expected NDVI behaviour of the up-coming season could be forecast; if linked to food production this might provide a robust early warning system. The most important conclusion from this work is that harmonic time series analysis yields more reliable results than ordinary time series analysis.

2.1 Introduction

In data-scarce environments time series analysis of the Normalized Difference Vegetation Index (NDVI) can provide valuable information in assessing spatial distributed linkages between climate properties, vegetative phenological cycles and rain-fed land use (Tucker 1979). The NDVI assumes that the difference between the near-infrared and red reflectance divided by the sum of both is a quantitative measure of photosynthetic activity (Prince 1991). Analysis of remotely sensed NDVI imagery has successfully been applied in a variety of fields such as drought assessment (e.g. Liu and Negron Juarez, 2001; Karnieli and Dall'Olmo, 2003), agricultural productivity (e.g. Groten and Ocatre, 2002; Hill and Donald, 2003), climate linkages (e.g. Srivastava et al. 1997; Wang et al. 2001; Ichii et al. 2002; Li et al. 2002; Gurgel and Ferreira, 2003; Roerink et al. 2003), spatial classifications (Azzali and Menenti, 2000) and cloud correction (Roerink and Menenti, 2000).

High temporal and preferably high spatial resolutions are prerequisite for these types of studies and image corrections are required to reduce the effect of atmospheric and geometric distortions on the NDVI values. Traditionally, NDVI images are derived from the Advanced Very High Resolution Radiometer (AVHRR) sensor aboard the National Oceanic and Atmospheric Administration (NOAA) satellite; however since 1998 the VEGETATION instruments aboard the SPOT-4 and SPOT-5 satellites provide another source of data with high spatial and temporal resolution.

The Tibetan plateau is characterized by harsh climatic conditions, and food production is mainly depending on fragile rangelands and irrigated crop production systems. Annual rainfall and temperature are the dominant determinants in ensuring food security in this sensitive landscape (Tashi et al. 2002). Scientific research into the relation between phenological cycles and climatic parameters in Tibet is scarce despite the fact that its understanding could be of great importance for early warning and food security assessments.

The lack of long time series of spatially homogenously distributed meteorological data can be compensated for by establishing a relation between average spatial NDVI patterns and meteorological parameters. The high temporal resolution and the up-to-date character of NDVI imagery enables and facilitates the prediction and spatial interpolation of climate parameters using the relation described above.

The present paper provides an insight into the complexity of relating NDVI derived parameters to precipitation and land use using Fourier analysis. The applicability of using the Fast Fourier Transform (FFT) algorithm is analysed for six different land use complexes. The relation between precipitation and the original and Fourier-transformed NDVI increments is analysed for four different meteorological stations with different land uses, and a relation is established between precipitation amounts during the growing season, total precipitation and different NDVI parameters. The applicability of Fourier-transformed NDVI time series in food security early warning is illustrated for the same four meteorological stations.

2.2 Methodology

2.2.1 Fourier analysis

Satellite measurements of land cover are often disturbed by noise caused by the atmosphere, sensor instability or orbit deviations. In order to derive interpretable characteristics from a noisy pattern, atmospheric transmission models, e.g. Modtran or 6S (Wolfe and Zissis 1993) and geocoding methods can be applied. Alternatively, Fourier analysis can be deployed. Fourier or harmonic analysis is a mathematical technique to decompose a complex static signal into a series of individual cosine waves, each characterized by a specific amplitude and phase angle. Several authors have successfully applied Fourier analysis in analysing time series of AVHRR NDVI imagery (e.g. Azzali and Menenti, 2000; Roerink and Menenti, 2000; Jabubauskas et al. 2001, 2002; Moody and Johnson, 2001).

A process that repeats itself every t seconds can be represented by a series of harmonic functions whose frequencies are multiples of a base frequency. This series of harmonic functions is called a Fourier series. Assume the process can be described by a function F(t). The usual form of the Fourier series is (Pipes and Harvill, 1971):

$$F(t) = \frac{A_0}{2} + \sum_{n=1}^{n=\infty} A_n \cos(n\omega t) + \sum_{n=1}^{n=\infty} B_n \sin(n\omega t) \qquad (1)$$

The constant term in equation 1 is always equal to the mean value of the equation, e.g. the mean NDVI value in a series of satellite imagery and $\omega = 2\pi f_o$, where f_o is de base frequency. Equation 1 can be written in different forms, following basic mathematical laws (Pipes and Harvill, 1971). In this research it was decided to transfer equation 1 to a form that only contains cosine terms which facilitates interpretation. Equation (1) can also be written as

$$F(t) = \frac{A_0}{2} + \sum_{n=1}^{n=\infty} C_n \cos(n\omega t - \phi_n) \tag{2}$$

Equation (2) now has a desirable form with only cosine terms. The signal is decomposed in a series of cosine terms, each with its own amplitude (C_n) and phase angle (ϕ_n), and a constant term ($A_o/2$). When a signal is described using Fourier analysis the values for the coefficients C_n need to be found. An algorithm to recover those coefficients from a discrete signal is the Fast Fourier Transform. In this case we are analyzing a discrete signal of 36 samples (NDVI images) with a fixed interval of 10 days and the Fast Fourier Transform (FFT) is used to find values for the Fourier coefficients C_n. The result of the FFT is a complex vector, and its real part contains the A coefficients and its imaginary part contains the B coefficients of equation (1). The coefficients C_n of equation (2) can be derived from A and B by calculating the length of the vector. There are a few limitations to the FFT related to the underlying mathematics. In the first place in order to correctly recover a signal from the Fourier transform of its samples, the signal must be sampled with a frequency of at least twice its bandwidth (Nyquist frequency) and in the second place only static waves can be analyzed using FFT, which means that both amplitude and phase of the individual terms must be constant over time.

The frequencies, which are recovered by the FFT are given by

$$f_k = \frac{k}{n} f_s \tag{3}$$

where f_k is de frequency of the kth term, n is the number of samples and f_s is de sampling frequency. In this case the smallest frequency, which can be recovered from the time series is 2.778×10^{-3} (1/36 x 1/10), which is equal to a period of 360 days.

The total variance of the Fourier series can be calculated from the amplitude values (Davis, 1986) through:

$$TotalVariance = \sum_{1}^{n} \frac{(amplitude)^2}{2} \tag{4}$$

The percentage variance of each individual term can then be calculated by dividing its contribution by the total. Another recently evolved method to analyse temporal behaviour in a spatial and temporal domain is the wavelet transform (Prasad and Iyengar, 1997). The clear advantage of using the wavelet transform over the Fourier transform is that it allows to decompose time series of images and/or the spatial domain of images in various directions and at various levels of scale; it also allows better detection of frequency and amplitude changes in either domain (Zhu and Yang, 1998; Carvalho, 2001; Epinat et al., 2001). However, the wealth of information and wavelet coefficients are sometimes a bit more difficult to explain on the basis of physiographic landscape information.

2.2.2 Datasets

A dataset containing 189 10-day composite NDVI images derived from the SPOT-4 and SPOT-5 VEGETATION instruments was used, spanning the period April 1998 to June 2003. A land use map was used to average NDVI values and a set of longterm average precipitation values from 15 meteorological stations across Tibet was used to relate precipitation to NDVI increments.

From April 1998 to January 2003 data from the VGT1 sensor aboard the SPOT-4 satellite were used and from February 2003 data from the VGT2 sensor aboard the SPOT-5 satellite were used. Both sensors have the same spectral and spatial resolution. The red spectral band (0.61-0.68 μm) and the near-infrared (NIR) spectral band (0.78-0.89 μm) were used to calculate the NDVI (NIR- RED/NIR + RED) and the imagery had a spatial resolution of 1 km. The synthesized preprocessed S10 NDVI product was used, which is a geometrically and radiometrically corrected 10-day composite image. The periods were defined according to the legal calendar: from the 1st to the 10th; from the 11th to the 20th; and from the 21st to the end of each month.

The land use map was derived from the global land cover characteristics (GLCC) database, which was jointly generated by the US Geological Survey (USGS), the University of Nebraska-Lincoln (UNL) and the European Commission's Joint Research Centre (JRC). It has a spatial resolution of 1 km and 24 different land use classes are distinguished. The map is based on data acquired with the AVHRR from April 1992 to March 1993. A formal accuracy assessment was not conducted for this land cover dataset; however the following validation exercise was conducted. To determine the true cover type, three interpreters independently interpreted either Landsat Thematic Mapper (TM) or SPOT images covering each sample. In order for the AVHRR pixel to be called correct, the majority of the three interpreters (i.e. two of the three) had to agree on the land cover type, as interpreted from Landsat TM or SPOT data, for the sample point. If the land cover type could not be determined the sample was discarded. It was found that 73.5% of the pixels were correctly classified (Scepan, 1999).

Long-term average precipitation values for 15 meteorological stations across Tibet were obtained from the Chinese Academy of Sciences (CAS) and were used to relate NDVI increments with precipitation.

2.2.3 General

A time series of 189 1 km resolution SPOT VGT-S10 dekadal (defined as a 10-day period) NDVI images from April 1998 to June 2003 was processed and analysed for this study.

The region of interest was extracted using CROP-VGT software, and the format was converted in ArcView GIS. The NDVI was calculated from an 8-bit digital number (DN) to NDVI values between 0 and 1 according to the following specified equation:

$$NDVI = -0.1 + 0.004 \cdot DN \tag{5}$$

The datasets were checked and corrected for a DN between 0 and 3 in order to prevent negative NDVI values, which complicates the application of the FFT.

Clouded pixels in the image that needed correction were linearly interpolated using the preceding and subsequent image. The algorithm was only applied when both preceding and subsequent image pixels were cloud-free. Dekadal averages, based on either five or six years, were calculated in ArcView, which resulted in one annual average NDVI pattern captured in 36

images. The GLCC grid was reprojected to the same projection as the NDVI imagery, and the area of interest was extracted.

Firstly, NDVI characteristics per land use complex were studied. For each land use class the average NDVI value was determined for each decadal image in ArcView GIS. A discrete FFT was performed for the main land uses in Tibet using the mathematical software package MathCad. Based on the calculated variance in each frequency a decision was made on the number of cosine terms to be included. The same number of terms was used for all land uses in order to facilitate comparison between the classes. NDVI patterns per land use were interpreted.

Secondly, the relation between precipitation and NDVI increment was analysed. For four different meteorological stations from different agro-ecological zone-land use complexes, temporal patterns of precipitation, based on long-term averages, were related to original and Fourier-transformed NDVI patterns.

A regression analysis using data from 15 meteorological stations was performed between total annual precipitation. Total precipitation during the growing season was related to a number of NDVI pattern characteristics:

- the constant term in equation (2) ($A_0/2$);
- the amplitude of the first harmonic term (A_1);
- the amplitude of the second harmonic term (A_2);
- the sum of the amplitudes of the first two harmonic terms ($A_1 + A_2$);
- the difference between the maximum and minimum of the original NDVI.

The length of the growing season was determined using a modified version of the methodology described by Groten and Ocatre (2002). The following rules were applied in the determination of the start and end of the growing season:

- the start of the growing season was determined by selecting the first dekad (i.e. 10-day period) after March 1 that was followed by two consecutive dekads with positive NDVI increments based on the average Fourier-transformed NDVI time series;
- the end of the growing season was determined by selecting the first dekad after June 1 that was followed by two consecutive dekads with negative NDVI increments based on the average Fourier-transformed NDVI time series.

Eventually the inter-annual Fourier-based NDVI variation was analysed for four different meteorological stations and its applicability for food security early warning was assessed.

2.2.4 Study area

Tibet is situated in the south-western part of China between 27.20° and 36.70° latitude and 78.20° and 99.10° longitude and borders India, Nepal and Bhutan. The total area is over 1.2 million square kilometres. The elevation ranges from 700m above sea level (asl) in the south-east to the summit of Mt. Everest at 8848masl, with an average elevation over 4000masl. Seven different agro-ecological zones, mainly determined by climate and elevation, can be distinguished (Tashi et al. 2002).

These zones vary from a hot humid agro-forestry pastoral zone in the south-east to a cold dry pastoral zone in the north-west. The relation between the physiogeographic units and the

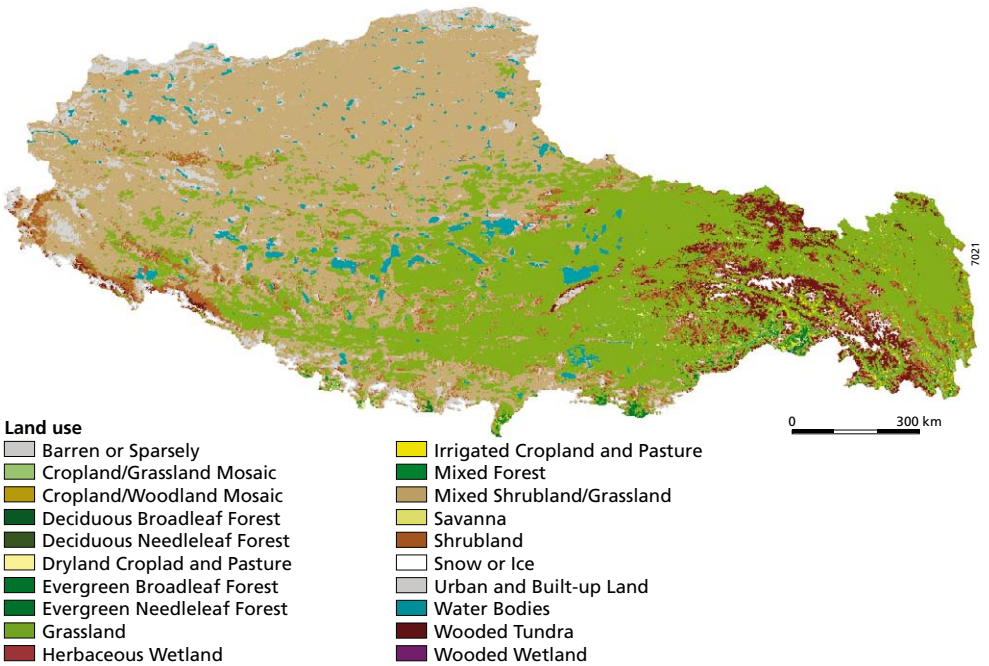

Figure 2.1 USGS global land cover characteristics for Tibet.

agro-ecological zones is evident (Leber et al., 1995). The main agricultural practices are barley production and yak herding. The land use of Tibet (USGS GLCC) is shown in Figure 2.1.

Tibet has only about 230,000 ha of cropland and most of it is concentrated in the Shigatse, Changdu and Lhasa prefectures in the south-eastern part of the country. Barley is the main crop and accounts for 50% of the cropping area. Wheat is the second major crop of (20% of the total cropping area), and both spring wheat and winter wheat are cultivated. Peas, potatoes, forage crops, oils seeds, corn and millet are also grown, but on a much smaller scale. Big gaps between actual and potential production can be noted. In recent years a significant increase in greenhouse vegetable cultivation has occurred. Most of the agriculture is concentrated along the rivers and small-scale canal irrigation systems are used. Tibet has extensive rangelands (77 million ha), part of which is irrigated (4.4 million ha). Yaks, cattle, piannius (a crossbreed between yak and cattle), goats and sheep are the dominant grazing animal species (Qiumei 2003). Overgrazing is a serious problem and many rangelands face serious degradation (Tashi et al., 2002).

There is a clear demarcation between the dry and wet season. At least 80% of the total precipitation (~400-600 mm/yr) falls between June and September, mostly during the night, resulting in a short growing period. Potential evaporation is high (~1600-2000 mm/yr) due to low relative humidity, high wind speeds and radiation. Average temperature ranges from 7 to 15 °C in the warmest month (July) to 21 to 27 °C in the coldest month (January). Temperature is therefore also a major determinant for crop production. A decreasing trend in both temperature and precipitation is observed from south-east to north-west.

2.3 Results

2.3.1 NDVI patterns for different land uses

Figure 2.2 shows the annual NDVI pattern over 12 months based on the decadal images from April 1998 to June 2003. A clear annual NDVI trend is visible in Tibet. The south-east part of Tibet, characterized by a relatively warm climate, shows the highest NDVI values (0.2-0.5) and the largest variation, while the north-western dry and cold area is characterized by very low average NDVI values (0-0.15) with very little variation throughout the year. The growing season in general is short and ranges from approximately four months in the eastern part to hardly any growing season at all in the north-western part of Tibet.

Figure 2.3 shows a frequency diagram for dry croplands. The left-hand vertical axis scales the amplitude in NDVI values for each cosine term; the right-hand vertical axis shows the cumulative percentage explained variance (equation (3)) is shown; the period (1/frequency) of each cosine term is shown on the horizontal axis. The cosine functions with an annual and bi-annual period are by far the most important in the signal. These first two harmonic terms account for 94.2%

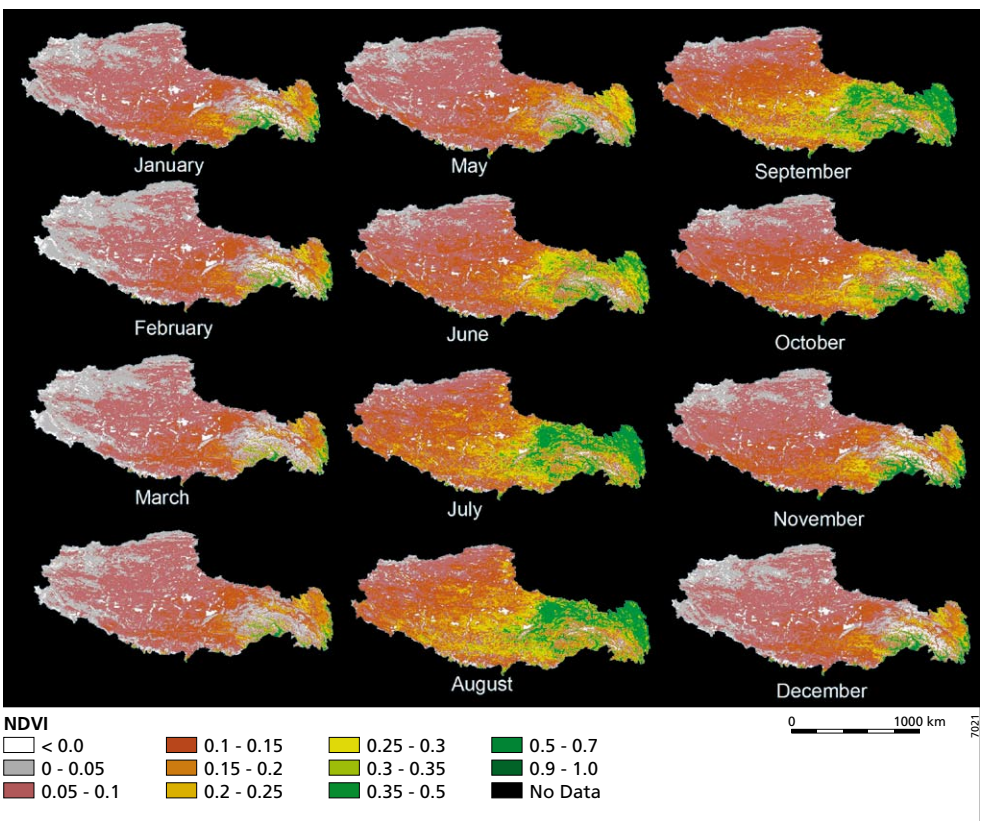

Figure 2.2 Average annual NDVI pattern for Tibet derived from dekadal images from April 1998 to June 2003.

of the total variance. However, it should be noted that there are substantive contributions of the cosine waves with periods of 72 and 60 days, explaining 1.6 and 1.2% of the total variance, respectively, indicating the presence of a temporal phenomenon with a period of approximately two months. The cumulative percentage of the explained variance is used to determine the number of Fourier terms to be included in the modelled signal. In this case we assume that the information contained in the first two harmonic waves is sufficient to be correlated with climatic parameters.

Figure 2.4 shows the original NDVI signal and the modelled Fourier signal including one, two and six different cosine waves for dry cropland areas. The additive term ($A_o/2$) from equation (2) equals 0.23, which is exactly the average NDVI value for the whole year. The original NDVI wave has a clear annual period, and shows two different peaks around 1 August and 1 October. If only one Fourier term is used, most of the annual variation is accounted for (85.2%), however the phase difference during the annual lowest NDVI around March/April is obvious. When two Fourier terms are taken into account (94.2 % of variance explained) this phase difference is no longer apparent. It is only when six Fourier terms are used that the two smaller peaks are modelled well. These smaller peaks relate to cosine waves with a period of 72 and 60 days in the frequency diagram (Figure 2.3). This strange peak behaviour is probably caused by the fact that two different crops (barley and wheat) fall within the same land use category (dry croplands) but they have a different crop calendar resulting in the two different peaks.

Figure 2.5 shows the sum of the first two harmonic terms of six different land uses. The figure clearly illustrates the difference between land uses, and the fact that the NDVI response is a complex mixture of land use and climatic variables. The mixed shrubland/grassland, wooded tundra, grassland and the dryland cropland/pasture land uses show a very similar pattern, although the magnitudes of the classes differ significantly. All exhibit an NDVI peak around the first decade of August. The evergreen needle forest and the irrigated cropland and pasture show a different pattern and gradually peak around the first decade of November. These land uses are obviously less dependent on precipitation, and their annual NDVI pattern might be explained by temperature, radiation and vegetation phenology rather than precipitation. The other land uses

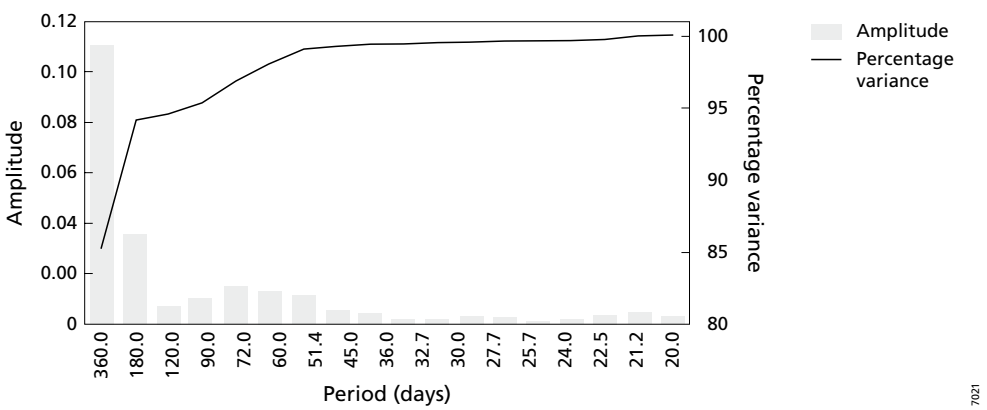

Figure 2.3 Frequency diagram dryland cropland land use.

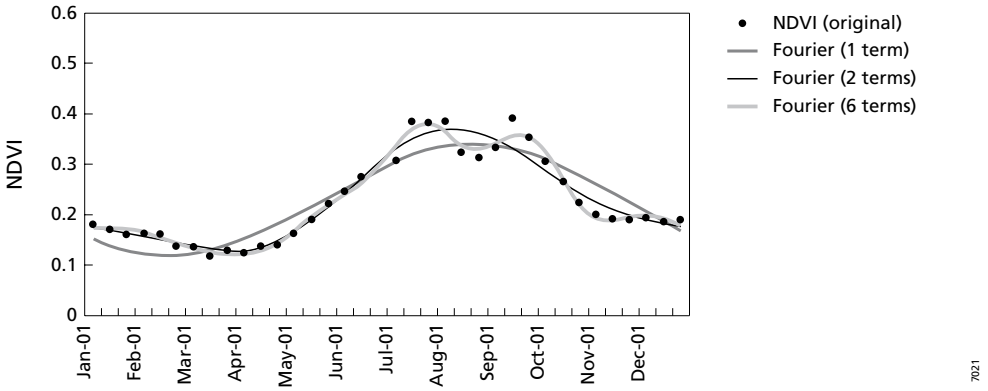

Figure 2.4 Modelled and original NDVI curves for dryland cropland.

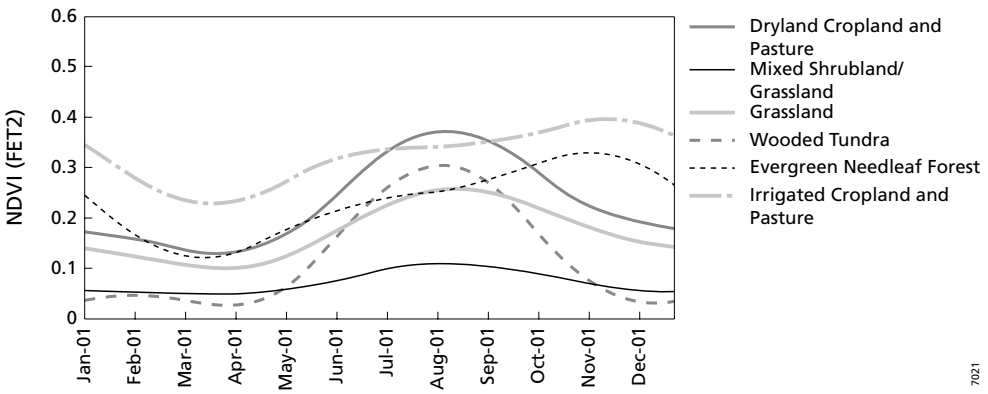

Figure 2.5 First two harmonic terms for six different land use types.

are likely to show a clear relation with annual precipitation patterns. NDVI responds to rainfall with a certain time lag. Land use with higher soil moisture availability will exhibit a longer time lag. In the case of irrigated crops, water availability is ensured through irrigation rather than precipitation. For evergreen needle forest, the relatively higher water availability is the result of a dense and deep root network and a larger buffer capacity because of its higher biomass.

2.3.2 NDVI behaviour in relation to precipitation

Ideally, a quantitative relation between the NDVI and precipitation, valid throughout the year and for every land use, should be found. Figure 2.5 indicates that the Fourier-transformed NDVI curve can only partially be explained by precipitation (80% of the rainfall occurs between June and September), and that the effects of land use are strongly interwoven with climatic parameters. Although the Fourier-transformed NDVI curve for different land use types may not be directly related to annual precipitation patterns, the NDVI increments show the immediate effect of precipitation.

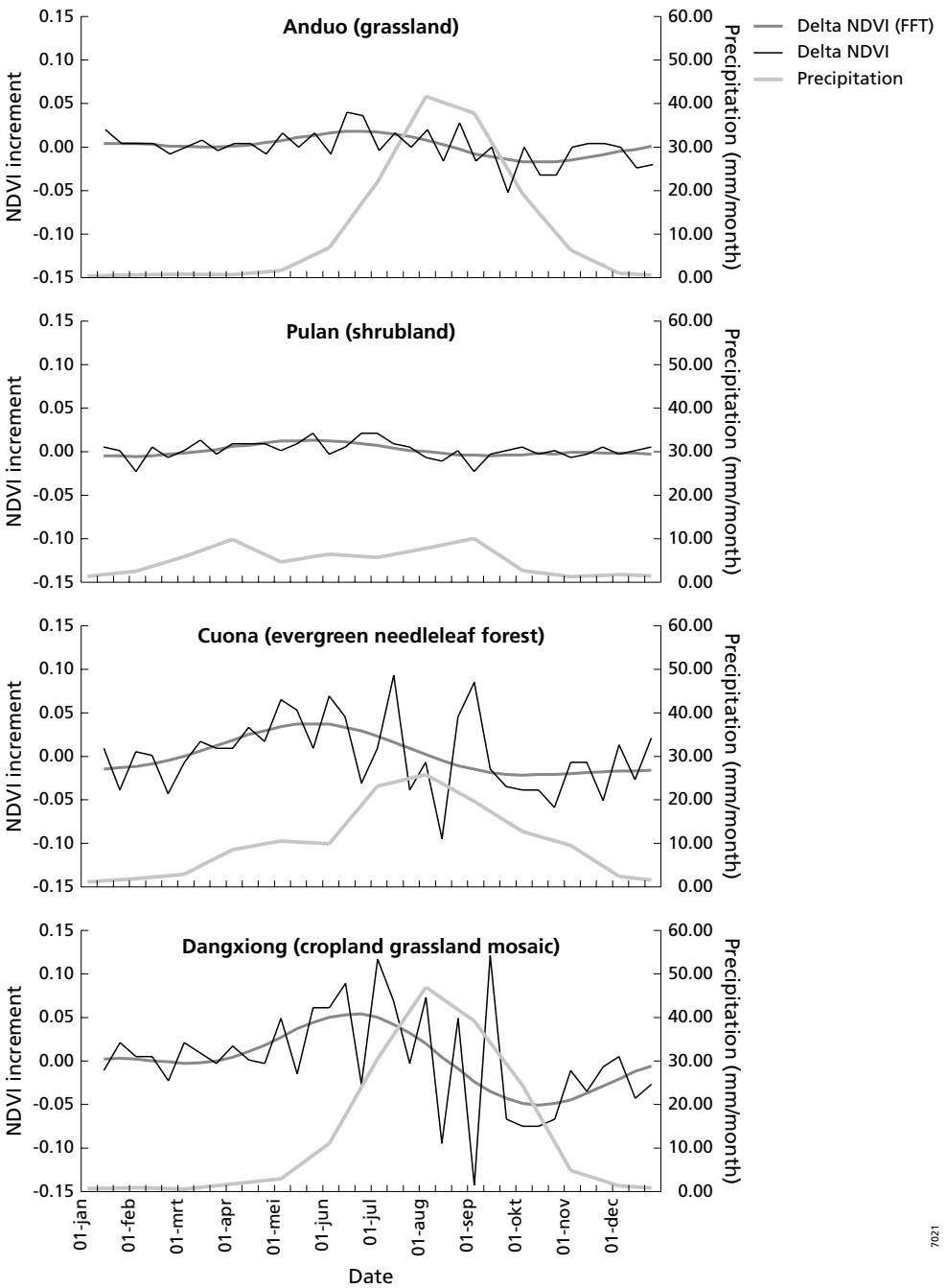

Figure 2.6 Relation between NDVI increment and precipitation for four meteorological stations.

Figure 2.6 shows the average temporal relation between NDVI dekadal increments (original and Fourier-transformed) and monthly precipitation (based on long-term averages) for four different meteorological stations with different land uses. Positive incremental NDVI values indicate growth and an increase in photosynthetic activity. The advantage of the Fourier-transformed NDVI over the original NDVI is evident. All stations respond immediately to the first precipitation in April and exhibit positive incremental values from that date onwards. All stations show an incremental peak before the precipitation peak, indicating that biomass production is maximized before the peak of the monsoon. However, the total amount of green biomass is maximal at that point in time when the increments change sign from positive to negative. The gap between the two peaks is the largest for evergreen needleleaf forest. The cropland grassland mosaic land use exhibits the largest dekadal incremental values (~0.05) and also has the highest precipitation peak (~140 mm/month). Shrubland (Pulan) shows the smallest variation in monthly precipitation amounts and dekadal NDVI increments. Evergreen needleleaf forest has a prolonged growing season compared to the other land uses.

The results of the Fourier analysis, such as the amplitudes and phase angles of the constituent cosine waves, contain information that could be related to variations in precipitation. Fourier analysis provides an insight into the components of a static wave and the outputs of a Fourier analysis can only be related to information valid for the whole signal without a temporal dimension. In other words, the outputs can only be related to, for example, total annual precipitation or total precipitation during the growing season. This is shown in the regression analysis with 15 meteorological stations between total annual precipitation and total precipitation during the growing season and several NDVI parameters pertaining to the whole signal. Table 2.1 shows R^2 values of the regression analysis. In both the total precipitation and the growing season precipitation the R^2 values are the highest for the sum of the amplitudes of the first two harmonic terms, followed by the amplitude of the first harmonic term and then the amplitude of the second harmonic term. In both cases the constant term ($A_o/2$) and the difference between maximum and minimum of the original NDVI correlate poorly to both total and growing season precipitation levels. Slightly higher regression coefficients were obtained when the total amount of precipitation during the growing season was used. The highest value of R^2, 0.72, was found in relating the growing season precipitation to the sum of the amplitudes of the first two harmonic terms.

2.3.3 Inter-annual NDVI behaviour

The average NDVI pattern was analysed for different land uses, and the average Fourier-transformed NDVI increments were related to long-term averages of precipitation. Recent

Table 2.1 Regression coefficients (R^2) of NDVI parameters and precipitation.

Type	R^2	
	Total annual precipitation	Total precipitation growing season
A0/2	0.46	0.47
A1	0.66	0.71
A2	0.62	0.61
A1+A2	0.69	0.72
Max (NDVI) – Min (NDVI)	0.53	0.38

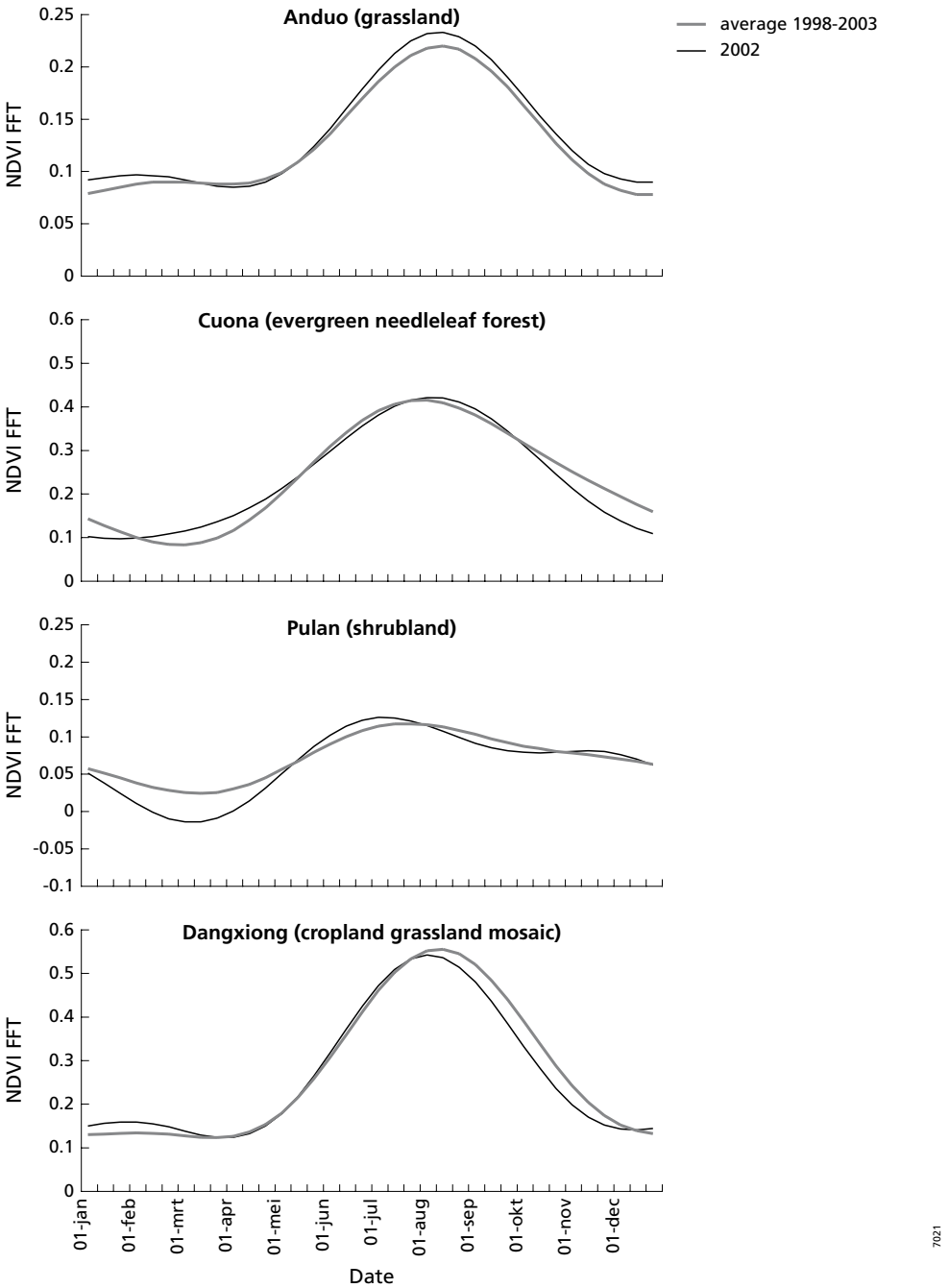

Figure 2.7 Inter-annual variation of Fourier-transformed NDVI curves for four meteorological stations.

homogeneously distributed rainfall data are not available for Tibet; however, the near-real-time availability of NDVI imagery could be an appropriate means for monitoring vegetation and crop development.

Figure 2.7 shows the Fourier-transformed NDVI signal for 2002 and the average Fourier-transformed signal for the period 1998-2003, for the same four meteorological stations. For Anduo and Cuona no difference in the length of the growing season is observed. In Pulan the growing season in 2002 is one dekad shorter and ends earlier, while in Dangxiong the growing season commences one dekad later and ends one dekad earlier. At the onset of the growing season in Pulan the NDVI lags the average 'normal' NDVI curve, but this is compensated throughout the growing season and the peak NDVI is even somewhat higher than normal; the same, but to a lesser extent, is valid for Anduo. The length of the growing season and any deviation from the average situation seriously affects food productivity.

2.4 Discussion

The length of the growing season was determined using a modified version of the methodology developed by Groten and Ocatre (2002). The decision rule for the start is based on the identification of a dekad followed by two dekads with positive increments after a certain first possible date of the growing season. For the end of the growing season a similar decision rule was defined. This work used the same methodology, except that a Fourier-transformed NDVI time series was used – given the noisy pattern of the original NDVI increments (Figure 2.6), it was hoped that this could improve the methodology described by Groten and Ocatre (2002).

Ideally, a quantitative relation between NDVI increment and precipitation valid for every land use and climatic zone should be found. Given the fact that solely longterm average precipitation data (from a different period than the NDVI imagery) are available, total amounts of precipitation have been correlated with NDVI characteristics. However, if a sufficiently long time series with a number of homogeneously distributed meteorological stations covering the same time span as the imagery were available, a more direct relationship could be found. Such a relation could be of great importance in, for example, the spatial interpolation of precipitation patterns. This would require insight into the change of amplitudes and frequencies in spatial and temporal domains, for which application of the wavelet transform might be the appropriate methodology. Such a method can be applied not only to precipitation, but also for estimations of spatial patterns of actual evaporation.

The Fourier-transformed NDVI has also proven to be valuable in analyses of inter-annual NDVI variations. By comparing the Fourier-transformed NDVI patterns of a specific year to a long-term average, anomalies in the growing season can easily be detected. A delayed onset of the growing season may, for example, indicate lower yields or biomass production later in the year. Establishing such Fourier-transformed NDVI patterns and linking them to food production might provide a robust early warning system since very early in the season the expected behaviour of the up-coming season could be forecast.

2.5 Conclusion

Analysis of NDVI time series proves to be a valuable tool to study complex weather patterns in inaccessible and data-scarce regions. Application of the FFT facilitates the extraction of valuable and interpretable characteristics from the time series, which are usually disturbed by atmospheric noise, sensor instability or orbit deviations. Although it is evident that an annual NDVI pattern is the complex resultant of plant phenology and a number of climatic determinants, the results presented in this paper have shown the potential of relating Fourier-transformed NDVI characteristics to both land use and precipitation.

Inclusion of only two harmonic terms in the Fourier series suffices for Tibet, and in the case of dry croplands it was found that 94.2% of the variation in the time series was explained through the first two harmonic terms. However, it also showed that the first two harmonic terms usually relate to natural phenomena with an annual and bi-annual periodicity. If phenomena with a higher frequency are important in the signal, more harmonic terms should be included in the Fourier series. This could be of great importance in areas with higher rainfall regimes than that of the Tibetan plateau or if dual-cropping patterns are prevalent.

Analysis of the average Fourier-transformed NDVI patterns of six different land uses has shown clear separating power, indicating the potential of classification based on high temporal resolution as opposed to high spectral resolution. The use of a different number of Fourier terms to identify differential phenologies and/or cropping seasons might improve our capability of resolving crops or species in mixed systems where the spatial resolution does not suffice. These conclusions match the results found for southern Africa by Azzali and Menenti (2000).

Precipitation-dependent land use/vegetation (dryland cropland/pasture, mixed shrubland/grassland, grassland and wooded tundra) exhibits a clear single peak with different magnitudes roughly following the monsoon cycle. Vegetation/land use that is less dependent on precipitation (evergreen needleleaf forest and irrigated cropland and pasture) does not show this behaviour and its pattern must be explained by other determinants such as temperature constraints during the winter. Fourier-transformed NDVI increments and precipitation show a clear positive relationship for all four meteorological stations studied. FFT NDVI increments are easier to interpret than the original noisy NDVI increments. NDVI increments increase as soon as the first precipitation falls; in some cases they increase even earlier than the first rainfall, indicating the presence of an internal biological calendar. This is most prevalent for evergreen needleleaf vegetation and might be a response to temperature and light triggering growth before the first rains. Initial water availability in that case is provided by the groundwater accessed though a dense and deep rooting network. The maximum biomass production occurs before the precipitation peak, and the total amount of biomass is maximized at the peak of the monsoon at the moment the increments become negative again. Based on this analysis it can be concluded that a relation exists between the total amount of precipitation during the growing season and the amplitudes of the harmonic terms of the Fourier analysis, which are a measure for the total increment.

Regression analysis using 15 meteorological stations across the Tibetan plateau for total annual precipitation and total precipitation during the growing season and several NDVI time series derived parameters has shown that a good relation exists between the different variables. The highest R^2 (0.72) was found between the total precipitation during the growing season and the sum of the amplitudes of the first two harmonic terms. The smallest R^2 (0.38) was found between the total growing season precipitation and the range of the original NDVI. Taking into account

all analysed NDVI characteristics the total growing season precipitation shows a slightly better correlation than the total annual precipitation. This is to be expected as it is the growing season precipitation causing increments in the NDVI, which is reflected in the eventual amplitudes.

3 Historical trends and future predictions of climate variability in the Brahmaputra basin

Based on: Immerzeel, W.W. (2007), Historical trends and future predictions of climate variability in the Brahmaputra basin. International Journal of Climatology (in press)

Abstract

An innovative approach is developed and presented to assess historical climate variations and to quantify future climate change for the entire Brahmaputra basin. Historical trends in temperature and precipitation are analysed from 1900 to 2002 for the Tibetan plateau (TP), the Himalayan belt and the floodplains (FP) using a global 100 year monthly high resolution dataset. Temperature patterns are consistent with global warming and out of the 10% warmest years from 1900 to 2002 six occurred between 1995 and 2002. No clear trends in precipitation were found and annual precipitation in the basin is mainly determined by the strength of the monsoon. Regression analysis is used to further explain monsoon precipitation. A significant inverse relation is found between air temperature differences between the FP and the TP and the strength of the monsoon, whereas the El Niño Southern Oscillation teleconnection does not have a prominent role in explaining variation in monsoon precipitation. Simulation results of six general circulation models are statistically downscaled to the spatial resolution of the observed dataset for two future storylines. The analysis predicts accelerated seasonal increases in both temperature and precipitation from 2000 to 2100. The largest changes occur on the TP and the smallest on the FP. Multiple regression analysis shows a sharp increase in the occurrence of average and extreme downstream discharges for both storylines. The strongest increases are projected for the monsoon season and the largest threat of climate change lies in the associated flooding in the densely populated FP.

3.1 Introduction

It is predicted that climate change will lead to an intensification of the global hydrological cycle and can have major impacts on regional water resources (Arnell, 1999). Changes in the total amount of precipitation and in its frequency and intensity directly affect the magnitude and timing of run-off and the intensity of floods and droughts. However, at present, specific regional effects are uncertain (IPCC, 2001).

The Himalayan range and the Tibetan plateau (TP) are the source of major river systems in Asia. The impact of climate change on the water resources of the region will be significant. Increases in evapotranspiration (ET) combined with regional changes in precipitation characteristics have the potential to affect mean run-off, frequency, and intensity of floods and

droughts. Run-off in the Himalayas for example is affected by snow cover, the monsoon and cyclones. All of which may be affected by climate change (IPCC, 2001).

This study is focusing on the Brahmaputra basin originating mainly in the eastern part of the Himalayas (Figure 3.1). The Brahmaputra is a major transboundary river and drains an area of around 530,000 km^2. The basin is located within four different countries: China (50.5%), India (33.6%), Bangladesh (8.1%) and Bhutan (7.8%). The Brahmaputra springs from a glacier in the Kailash range in Tibet (China) at an elevation of 5300 meters above sea level (m.a.s.l.), has a length of 2900 km and after its confluence with the Ganges, the Brahmaputra flows into the Bay of Bengal. Average discharge of the Brahmaputra is approximately 20,000 m^3/s. The climate of the basin is monsoon driven with a distinct wet season from June to September, which accounts for 60-70% of the annual rainfall.

Three physiographic zones are distinguished in this study, because it is expected that each of these three physiographic units will respond differently to the anticipated climate change. First of all, the TP, covering 44.4% of the basin, with elevations of 3500 m and above in the north of the basin. Secondly the Himalaya belt (HB), covering 28.6% of the basin, with elevations ranging from 100 m.a.s.l. to 3500 m.a.s.l. Finally the agricultural floodplains (FP), covering 27.0% of the basin, of India and Bangladesh with elevation up to 100 m.a.s.l., of which 40% is flood prone.

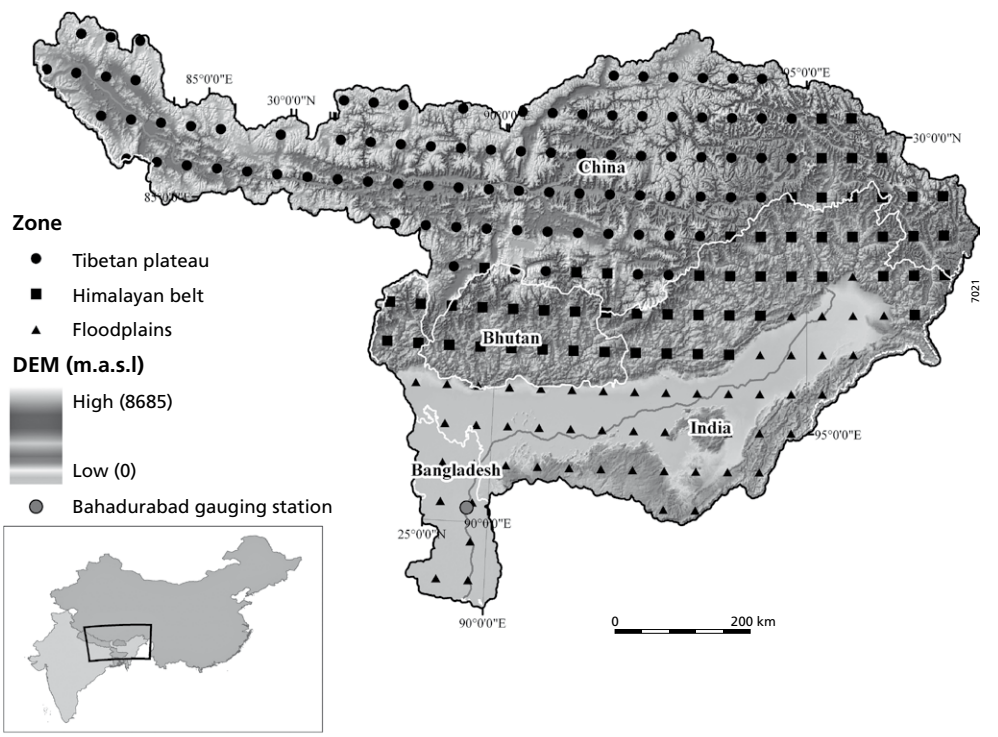

Figure 3.1 Overview Brahmaputra basin; the digital elevation model, location of the CRU TS2.1 grid points of the three physiographic zones, the discharge station at Bahadurabad and country boundaries.

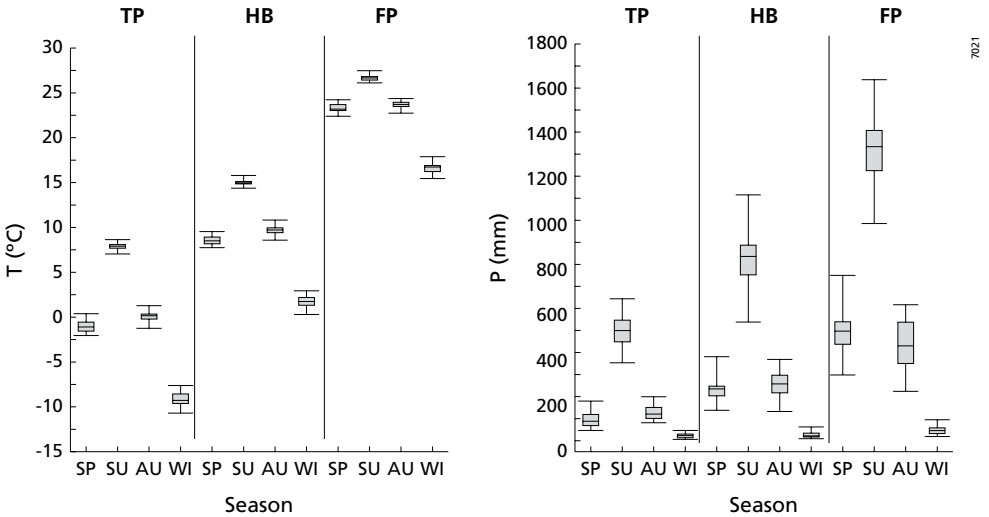

Figure 3.2 Box-whisker plot with seasonal climate normals (1961-1990) of temperature and precipitation for the three different physiographic zones (SP = spring (March, April, May), SU = summer (June, July, August), AU = autumn (September, October, November), WI = winter (December, January, February)).

Figure 3.2 shows the seasonal climate normals from 1961 to 1990 for the TP, the HB and the FP in a boxwhisker plot. The plot shows the median, the upper and lower quartiles and the caps at the end of the box show the minimum and maximum. The TP is the coldest with average temperatures ranging from –10 °C in winter to 7 °C in summer. Winter temperatures in the HB fluctuate around 2 °C, while summer temperatures reach values of approximately 15 °C on average. The FP is the warmest of the three zones with winter temperatures around 17 °C and summer temperatures on average as high as 27 °C. For all zones the seasonal temperature variation is largest in winter and smallest in summer. The annual rainfall is concentrated in the monsoon months June, July, August and September (JJAS) in all zones. The TP located in the rain shadow of the HP is the driest zone in the basin (734 mm/year), while the FP is the wettest with an annual precipitation of 2354 mm. The HB has an average annual precipitation of 1349 mm.

Mountains are a major climate determinant and large scale orography has a pronounced effect on atmospheric flow patterns. A precise understanding of the spatial and temporal behaviour of climate parameters and their projected change in mountain areas is hampered by the lack of observational data in complex topographic terrain and the difficulties to represent large mountain ranges in general circulation model (GCMs) (Beniston et al., 1997). Especially predicting changes in precipitation patterns in mountains pose additional challenges due to the inadequate representation of the local effects of topography on precipitation in most GCMs (Beniston, 2003). In addition to this, there is an intricate set of natural climate determinants that are known to influence the Asian monsoon; the El Niño – Southern Oscillation (ENSO) condition and the Eurasian snow depth levels. The relation between the monsoon and ENSO has been explored by numerous studies (Ropelewski and Halpert, 1989; Walker, 1924; Webster et al., 1999). The general consensus is that during El Niño years anomalous subsidence suppresses

convection over South Asia and this results in a weaker monsoon (Krishna Kumar et al., 1999). Snow pack levels, specifically on the TP, also play a critical role in the variation in inter-annual precipitation. Upper-tropospheric air temperatures above the TP are among the warmest on the planet because of the heating of the elevated land with altitudes of over 3500 m. The troposheric temperature gradient between the TP and the Indian Ocean is shown to be associated with the Indian monsoon rainfall (Fu and Fletcher, 1985). The snow depth on the TP affects the land surface thermodynamics and reduces this thermal gradient. Shaman et al. (2005) report an inverse relationship between the spring snow depth on the TP and monsoon precipitation in Bangladesh. This does however not necessarily mean that these factors have influence on the precipitation in the entire Brahmaputra basin and this is subject of this study.

Climate change will have effects on the hydrology of the Brahmaputra basin. Large parts of the basin depend on the Brahmaputra discharge for irrigation while the lower part of the basin is vulnerable to flooding. Especially Bangladesh suffered severe flooding in 1987, 1988 and 1998 (Mirza, 2003). Climate change will affect the discharge characteristics significantly and will lead to more severe and more frequent flooding (Warrick et al., 1996) both through alterations in climatic conditions and sea level rise. Projected rise in temperature will lead to increased glacial and snow melt, which could lead to increased summer flows in some river systems for a few decades, followed by a reduction in flow as the glaciers disappear and snowfall diminishes. Satellite records have shown a decrease in snow cover extent of about 10% in the Northern hemisphere related to temperature increases in spring and summer since 1966 (Robinson, 1997, 1999). To what extent increased glacial and snow melt influence stream flow is varying strongly in space. Barnett et al. (2005) argue in a global study that the Hindu Kush Himalaya (HKH) region is the most critical area in which increased melt will affect water supply in the decades ahead. Within the Himalayan region there are however large differences in the contribution of melt water in total annual run-off. Rees and Collins (2006) show that the melt water component in the total run-off rapidly decreases from west to east. Summer precipitation declines from east to west. In the western Himalayas in winter at high elevations westerly winds provide precipitation while at lower altitudes arid conditions prevail. Total annual precipitation follows the east to west gradient. Therefore stream flow in basins in the west is for a major part determined by melt water while in the east run-off generated by monsoonal precipitation is the most important constituent of downstream discharge. Rees and Collins (2006) also argue that glaciers experience winter accumulation and summer ablation in the west, but there is predominantly synchronous summer accumulation and summer melt in the east. Singh and Bengtsson (2004) confirm the strong dependence of stream flow on melt water in basins originating in the western part of the basin and stress the difference in melt water contribution to stream flow between rain fed, snow fed and glacial fed river basins. The Brahmaputra basin is located in the eastern Himalayas and river discharges are predominantly rain fed.

Basin wide quantified assessments of climate change and its effects in the entire drainage area of the basin are scarce and not straightforward. Previous work indicates that specifically the TP is extremely sensitive to global climate change (Liu and Chen, 2000). A complete overview of the functioning of the Brahmaputra basin including the impact of climate change on runoff is lacking so far. Therefore this paper will focus on (1) analysis of historical trends in precipitation and temperature, (2) future trends in precipitation and temperature, and (3) the impact of climate change on hydrology.

3.2 Data and methods

Temperature and precipitation patterns were obtained using the most accurate global database currently available: the climate research unit (CRU) dataset. The latest updated version, referred to as the CRU TS 2.1 dataset in this paper, is used to reconstruct the temperature and precipitation patterns in the basin from 1901-2002 (Mitchell and Jones, 2005). The CRU TS 2.1 is a set of monthly climate grids which are constructed for nine climate variables and interpolated onto a 0.5° grid and provide best estimates of month-by month variations. The raw station data are derived from seven different sources and are corrected for in-homogeneities using a modified version of the Global Historical Climatology Network (GHCN) method (Peterson et al., 1998). The centre of the grid cells of the CRU TS 2.1 dataset is shown in Figure 3.1. The interpolated value of a certain grid cell depends on a number of surrounding stations within a correlation decay distance. These distances are 1200 km and 450 km for temperature and precipitation respectively. This does not mean that all stations within this range actually influence the gridded value but it refers to the number of stations with information upon which the grid-box may draw, if necessary (New et al., 2000). The average number of stations in the basin within the correlation decay distance for each grid cell for precipitation and temperature are shown in Figure 3.3. Although this is the most accurate dataset available, the figure shows that some caution is required when interpreting data between 1901 and 1950 and after 1995.

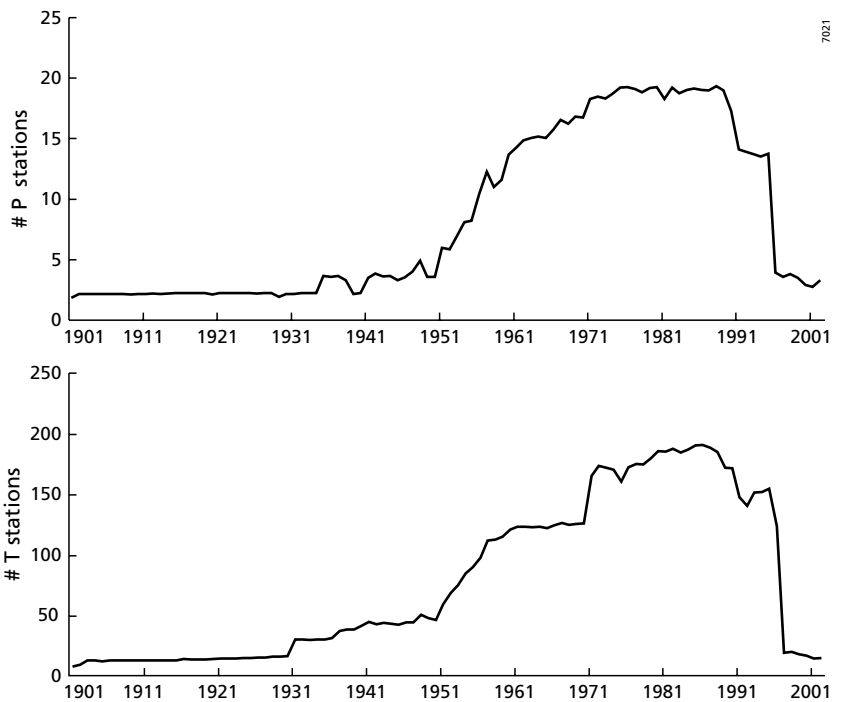

Figure 3.3 Average number of meterological stations within the correlation decay distance for precipitation (top figure) and temperature (bottom figure).

Estimating future precipitation patterns requires understanding of current and past causes of precipitation processes. It is expected that precipitation in the basin is related to ENSO conditions and the thermal gradient between the FP and the TP. To explain precipitation patterns linear regressions were performed to identify relations between the monthly JJAS monsoon precipitation in the TP, the HB and the FP and the Southern Oscillation Index (SOI) (Können et al., 1998), the $NINO_3$ index (Rayner et al., 2003) and the temperature difference between the FP and the TP ($\Delta T_{FP\text{-}TP}$).

GCM monthly precipitation and temperature fields from six different models from 2002 to 2100 are used to analyse the A2 and B2 storylines (Parry, 2002). GCM data were downloaded from the IPCC Data Distribution Centre (IPCC-DDC, http://ipcc-ddc.cru.uea.ac.uk/).

Table 3.1 shows that the different GCMs have a varying spatial resolutions typically in the range of three degrees. In order to capture basin scale variations in temperature and precipitation and the large-scale behaviour of the GCMs a statistical downscaling procedure is applied. The GCM outputs are downscaled to the resolution of the CRU TS 2.1 dataset (0.5° by 0.5°) using a similar procedure as Bouwer et al. (2004). This method ensures conservation of the variability and mean during the reference period.

The average seasonal anomalies (2061-2090 compared to 1961-2000) in precipitation and temperature are determined at the centres of the CRU TS 2.1 grid cells. These anomalies are spatially interpolated to a resolution of 0.05° using a spline tension interpolator with weight one using four CRU TS 2.1 points. This interpolator ensures a smooth (continuous and differentiable) surface, together with continuous first derivative surfaces (Franke, 1982). This approach is appropriate to assess spatial climate patterns at basin scale.

Daily discharge data at the Bahadurabad gauging station (Figure 3.1) from 1956 to 1993 were analysed using a multiple regression based rainfall-run-off model. Average monthly hydrographs in combination with monthly precipitation were assessed on the contribution of snow melt to

Table 3.1 Overview of the GCMs used, the reference periods and latitudinal and longitudinal spatial resolutions

Model	Institute	Acronym	Reference period	Latitudinal resolution	Longitudinal resolution
CCSR	Japanese Centre for Climate System Research, Tokyo, Japan	CCS	1890-2002	~5.54°	~5.63°
CGCM2	Canadian Centre for Climate Modelling and Analysis, Victoria, Canada	CGC	1900-2002	~3.71°	~3.75°
CSIRO-Mk2	Australian Commonwealth Scientific and Industrial Research Organisation, Australia	CSI	1961-2002	~3.19°	~5.63°
ECHAM4/OPYC3	Max-Planck-Institute, Hamburg, Germany	EH4	1990-2002	~2.79°	~2.81°
GFDL-R30	US Geophysical Fluid Dynamics Laboratory, Princeton, USA	GFD	1961-2002	~2.24°	~1.88°
HADCM3	Hadley Centre for Climate Prediction and Research, Bracknell, UK	HAD	1950-2002	~2.50°	~3.75°

annual stream flow. Only if there is sufficient reason to assume that the majority of stream flow is related to rainfall it is legitimate to use a multiple regression run-off model using rainfall data.

Multiple linear regression was used to model average monthly stream flow in month t using three variables; basin precipitation in month t (P_t (mm)), basin precipitation in month t-1 (P_{t-1}(mm)) and ΔT_{FP-TP}(°C) in month t. To capture seasonal variation regression models were derived for summer, winter, autumn and spring separately. These models are of the form:

$$Q_{avg} = a + b1 \cdot P(t) + b2 \cdot P(t-1) + b3 \cdot \Delta T_{FP-TP} \quad (1)$$

where Q_{avg} (m^3/s) is the average monthly discharge, a is the intercept and b1, b2 and b3 are coefficients. Based on these models and the downscaled data of six GCMs seasonal models with monthly time series of average discharges has been generated for the A2 and B2 storylines from 1901-2100.

3.3 Results

3.3.1 Historical trends

Figure 3.4 shows the anomalies in temperature and precipitation from 1900 to 2002 for the three physiographic zones. Six extreme warm years (10% warmest years) have occurred between 1995 and 2002. For the TP, HB and the FP temperature patterns are remarkably consistent with the global warming pattern. The warming trend is obvious throughout the entire basin at an average rate of 0.6 °C/100 yr. Figure 3.4 does not reveal any large difference between the different zones in annual temperature trends. The TP reveals most inter-annual variation. There are however seasonal differences. All zones show the largest warming trend in spring (TP = 1.1 °C/100 yr, HB = 1.0 °C/100 yr, FP = 0.9 °C/100 yr) and the smallest warming trend in summer (TP = 0.2 °C/100 yr, HB = 0.4 °C/100 yr, FP = 0.5 °C/100 yr). There is an obvious difference between the zones in summer temperature trend. Annual trends in precipitation are not observed from 1901-2002. The precipitation pattern in all three zones does not show any resemblance to the global precipitation anomalies, which exhibit a slight positive trend. An approximate 15 year cycle in the annual precipitation pattern is observed. The TP and HB show most inter-annual variation. Other factors evidently play an important role in the inter-annual variation in precipitation. The winter precipitation trends are positive for all zones (TP = 6.7%/100 yr, HB = 6.1%/100 yr, FP = 7.5%/100 yr), while in summer there is a general negative trend for all zones (TP = -6.3%/100 yr, HB = -4%/100 yr, FP = -5.2%/100 yr). Autumn precipitation trends are also positive which could indicate a delay in the onset of the monsoon.

The annual precipitation patterns in the basin are further explained by linear regression analysis. Figure 3.5 shows the results of the linear regressions between the JJAS zonal precipitation and SOI, $NINO_3$ and ΔT_{FP-TP} respectively. The ENSO indices do not have a prominent role in explaining the JJAS precipitation in all three zones, and the correlations found are negligible. A significant relation is however found between ΔT_{FP-TP} and the monsoon precipitation, ranging from R^2 = 0.32 on the TP to R^2 = 0.42 on the FP. Regression analysis between ΔT_{FP-TP} and total JJAS basin precipitation results in an R^2 of 0.45. This leads to the interesting finding that precipitation in the basin is inversely related to the gradient in surface air temperatures between the FP and TP. A small ΔT_{FP-TP} is associated with relatively high air temperatures on the TP and

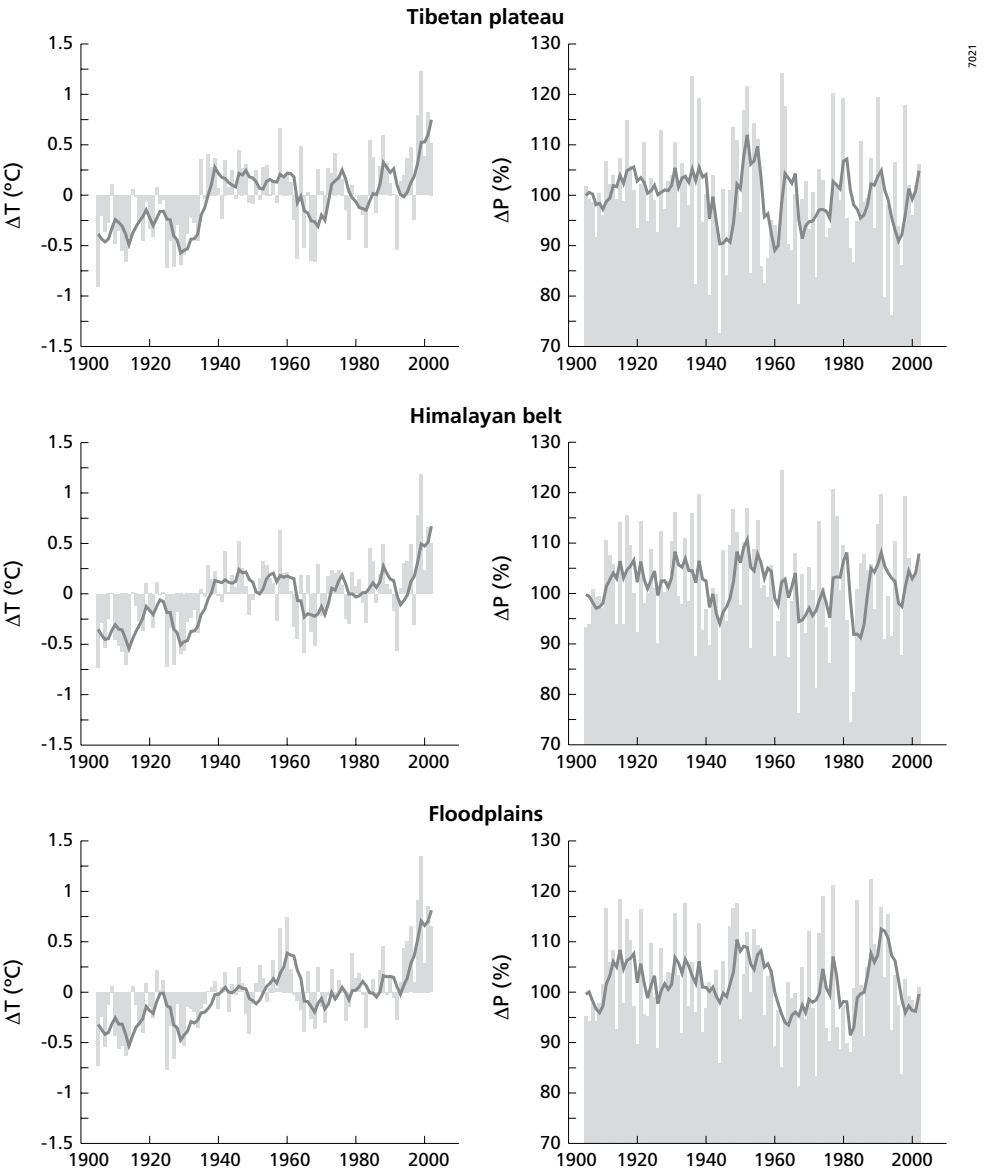

Figure 3.4 Temperature anomalies (°C) (left) and precipitation anomalies (%) (right) per physiographic zone from 1905-2002. The lines indicate the 5 year moving average of temperature and precipitation anomalies from the climate normal 1961-1990. The bars in the graphs indicate the original year temperature and precipitation anomalies respectively.

low air temperatures in the FP. This is indicative of increased warming of the TP land surface and the atmosphere above.

3.3.2 Future changes

Figure 3.6 shows the downscaled temperature and precipitation anomalies from 2000-2100 per physiographic zone. The graphs show the average of all six GCMs. The HADCM3 model is an intermediate model in all projections in all zones. For both temperature and precipitation the HADCM3 model shows the best downscaling results in maintaining the time series characteristics during the reference period, specifically variation in precipitation.

The coefficient of variation between the 6 GCMs in precipitation is on average 9% and the standard deviation in temperature between the GCMs is 0.5 °C for both storylines. There is a slight increasing trend from 2000 to 2100. By the end of the century the A2 storyline shows more extreme changes in precipitation and temperature than the B2 storyline. By 2100 it is projected that on average the temperature in the basin has increased by 3.5 °C and 2.3 °C for the A2 and B2 storylines respectively. The projected changes in precipitation show a more capricious pattern but a consistent increase of 22% and 14% by 2100 for the A2 and B2 storyline respectively is observed. The dips in the precipitation time series at 2080 for the A2 scenario and 2070 for the B2 scenario are caused by anomalous behaviour of the CGC GCM. For both temperature and precipitation

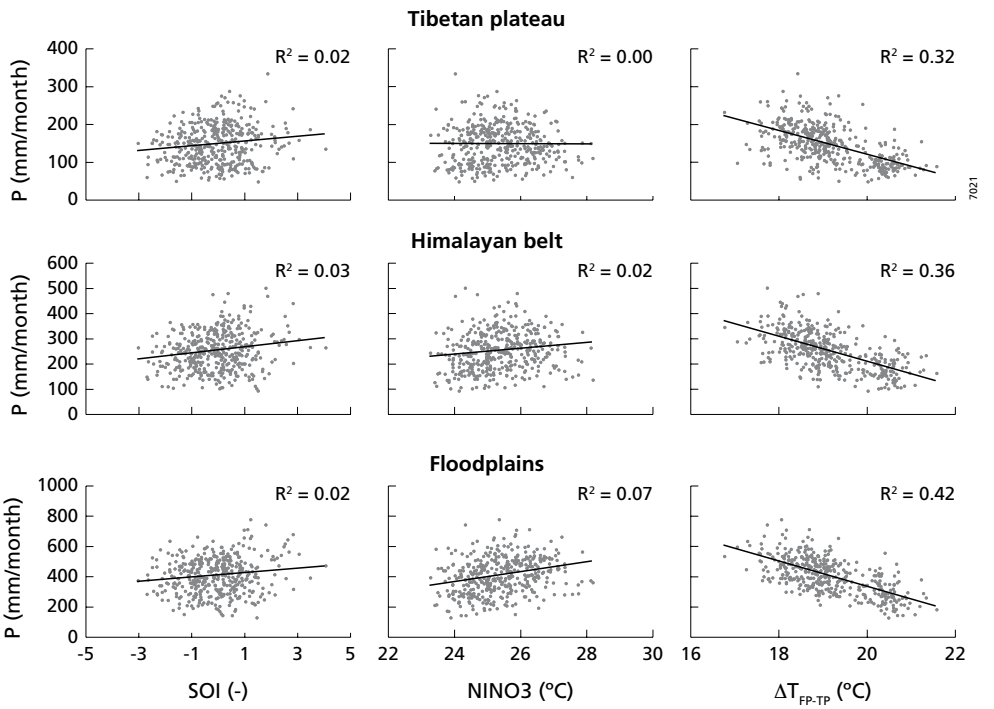

Figure 3.5 Linear regressions for the TP, HB and FP between monthly precipitation in June, July, August and September and SOI, NINO3 and the FP-TP temperature difference for the period 1901-2002.

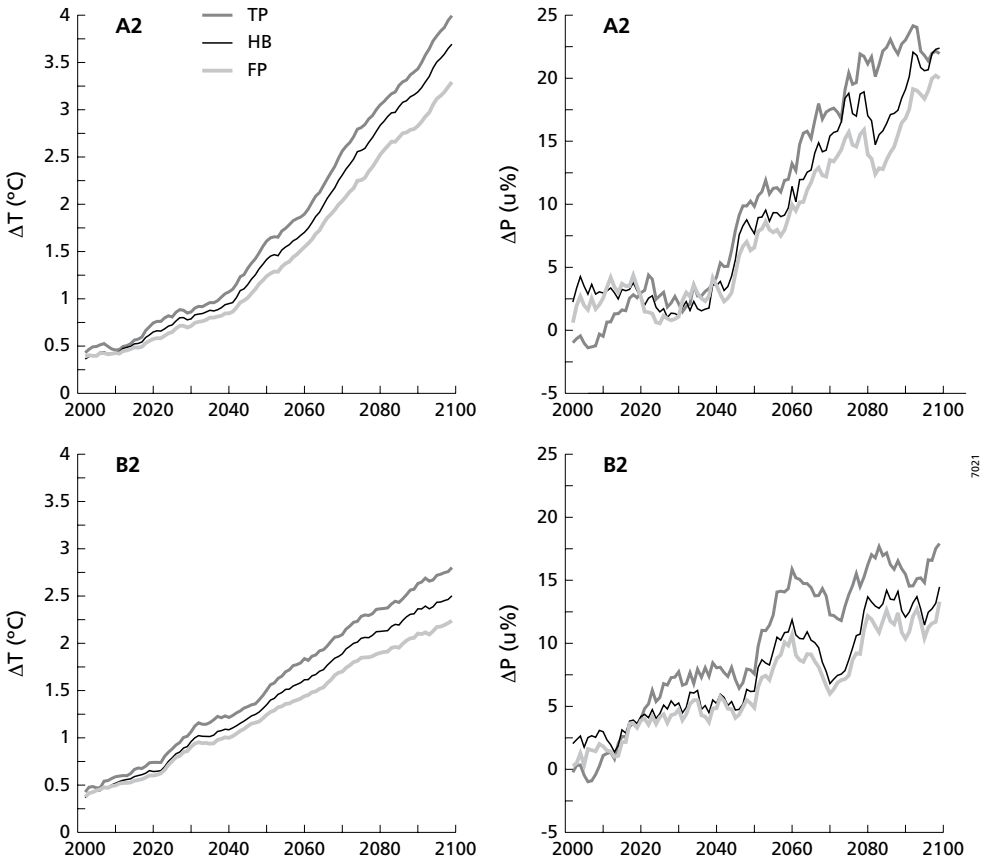

Figure 3.6 Downscaled temperature and precipitation anomalies from the climate normal 1961-1990 based on the average of 6 GCMs from 2002-2100 per physiographic zone.

inter-zonal differences are evident and the TP is the most sensitive to climate change, followed by the HB and the FP for the A2 and B2 storylines. This means that $\Delta T_{FP\text{-}TP}$ will decrease because the TP warms at a faster pace than the FP.

The box-whisker plots in Figure 3.7 shows the basin seasonal shifts in temperature and precipitation. The seasonal climate normals (1961-1990) are compared to 2061-2090 for the A2 and B2 storylines. Data of a single GCM (HADCM3) are used to be able to analyse changes in variation. All seasons show an increase in temperature, which is more pronounced for the A2 scenario than the B2 scenario, except for winter when both scenarios show a similar increase. Autumn shows the largest difference in temperature increase between the two storylines. The difference between the first and third quartiles in summer has increased for both storylines resulting from a wider distribution in temperatures. Seasonal precipitation trends are also positive except for autumn and summer precipitation for the B2 storyline which have the median lower than the 1961-1990 value. The frequency distribution of precipitation is generally widened and the extreme values, especially in summer have increased.

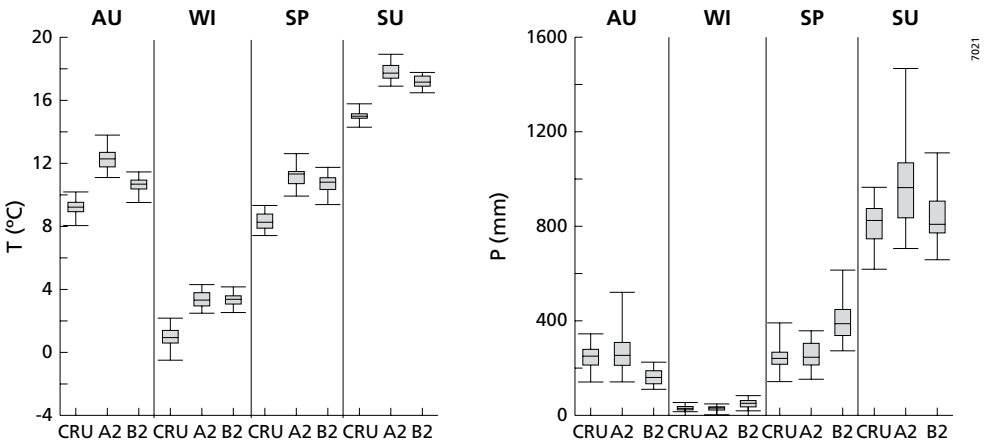

Figure 3.7 Box-whisker plot of seasonal temperatures and precipitation for observed data and HadCM3 climate change predictions for the A2 and B2 scenario (CRU = CRU TS2.1 1961-1990, A2 = downscaled HadCM3 results 2061-2090 for the A2 scenario, B2 = downscaled HadCM3 results 2061-2090 for the B2 scenario).

The spatial patterns in the basin are revealed by the spatially interpolated temperature and precipitation maps in 2020, 2050 and 2080 for the A2 and B2 storylines in Figure 3.8 and Figure 3.9. The Tibetan plateau, specifically the north eastern part shows the largest increase in temperature. Both storylines show similar spatial behaviour and significant spatial differences in temperature between the scenarios become apparent after the 2050s. The Himalayas obviously have a pivotal role in the regional climate system and temperature anomalies generally follow the orography.

The spatial precipitation patterns (Figure 3.9) also shows the strongest increase in precipitation on the TP and the least increase in the FP. The total amount of precipitation in the FP is however more than three times as large than in the TP. The spatial patterns are more capricious than the spatial patterns in temperature. There is a distinct horizontal band around 29°N south of the Brahmaputra River, which shows a remarkably steep increase in precipitation in all years for both storylines. This amounts to a precipitation increase to over 30% in the 2080s for the A2 storyline. The A2 storyline in 2020 shows for large parts of the HB and the FP a remarkable decrease in precipitation. The effects of the Himalayas are also visible in the spatial precipitation patterns.

3.3.3 Hydrological impacts

Figure 3.10 shows the average monthly hydrograph based on daily discharge data from 1956-1993. The hydrograph and scatter plot show that stream flow at Bahadurabad is mainly generated by rainfall. The scatter plot reveals that from the end of the monsoon onwards, when soils are saturated, discharge is relatively high. In the early spring months, when soils have not yet reached saturation, discharge is relatively low. The hydrograph shows that discharge responds directly to rainfall with a typical lag of one month and there is no additional peak in spring related to snow and glacial melt. This does comply with earlier studies that report synchronous accumulation and melt in eastern Himalayan basins (Rees and Collins, 2006). In addition to this summer

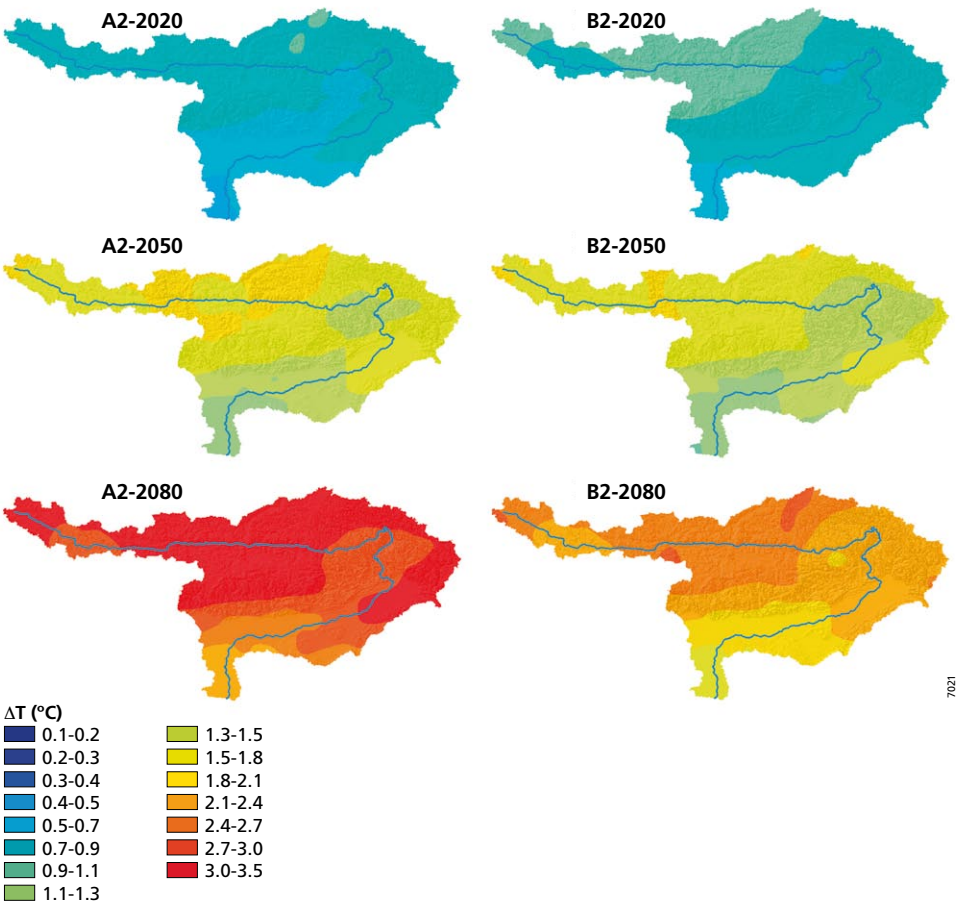

Figure 3.8 Downscaled spatial temperature anomalies from the climate normal 1961-1990 based on the average of 6 GCMs for 2020 (2010-2030), 2050 (2040-2060) and 2080 (2070-2090).

precipitation in all zones is much larger than winter precipitation in the TP and HB (Figure 3.2). Therefore it may be concluded that the overall contribution of snow and glacial melt to downstream discharge in the Brahmaputra will be very small and that it is legitimate to use a simple rainfall-runoff model to gain insight in stream flow patterns. The total average annual precipitation sum between 1956 and 1993 is 1336 mm, while total discharge is on average 1200 mm.

Table 3.2 shows the results of the seasonal regression models. All seasons, except winter, show good results with R^2 ranging from 0.64 in summer to 0.82 in autumn and spring. Winter discharges show limited response to P_t, P_{t-1} and ΔT_{FP-TP}, while average discharge is also relatively low. P_t and P_{t-1} are proportional and ΔT_{FP-TP} is inversely proportional to Q_{avg} in all cases where significant contributions are found.

Using the regression models and the average monthly P_t, P_{t-1} and ΔT_{FP-TP} of the six GCMs the seasonal effects on the discharge from 2000-2100 are determined (Figure 3.11). During the

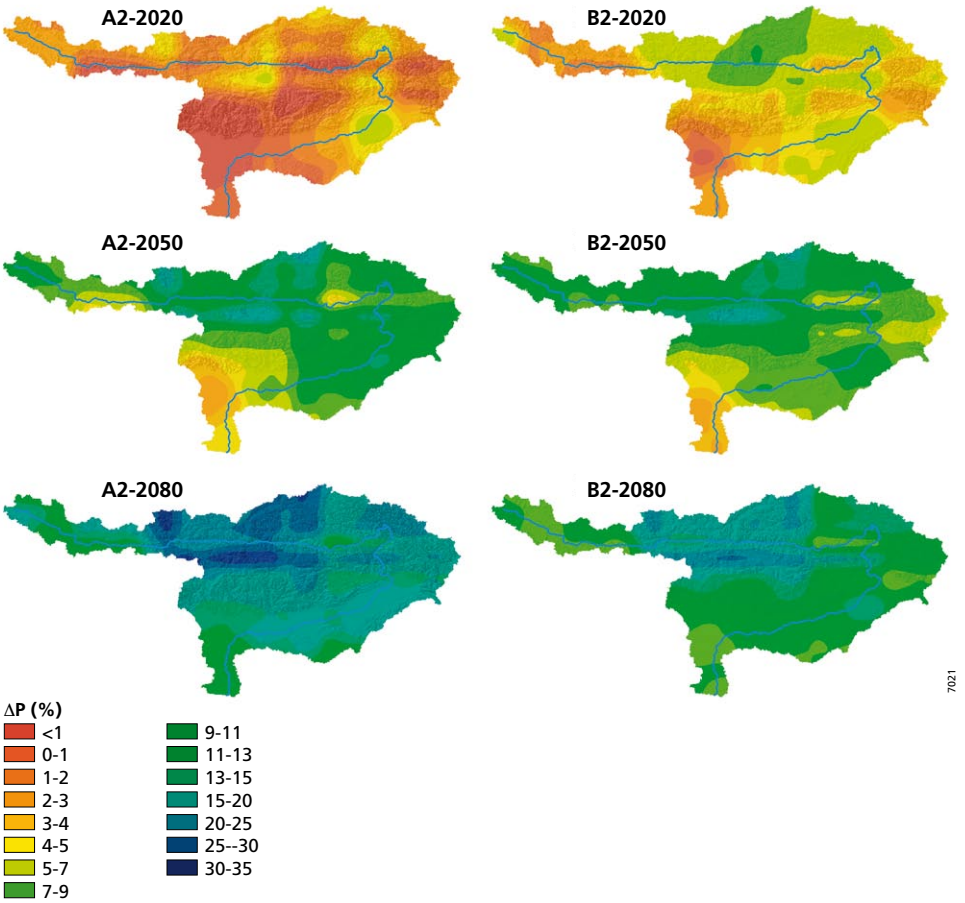

Figure 3.9 Downscaled spatial precipitation anomalies from the climate normal 1961-1990 based on the average of 6 GCMs for the 2020 (2010-2030), 2050 (2040-2060) and 2080 (2070-2090).

Table 3.2 Seasonal regression models for average discharge at Bahadurabad based on data from 1954-1992. Q_{avg} is the average discharge from 1954-1992. R2 is the multiple R squared, a is the intercept and b1, b2 and b3 are the coefficients in the multiple regression equation. A "*" indicates significant contribution at the 95% confidence level.

	Autumn		Winter		Spring		Summer	
Q_{avg} (m^3/s)	25267		5518		9247		40204	
R^2	0.82		0.06		0.82		0.64	
a	-254		14275	*	28253	*	73630	*
b1	97	*	-10		35	*	72	*
b2	73	*	33		38	*	68	*
b3	242		-347	*	-964	*	-3635	*

monsoon in summer the strongest increase in discharge is expected and projections range between 20% and 30% increase of average monthly discharge for the B2 and A2 scenarios respectively. Winter discharges show little change and discharge is mainly fed by groundwater base flow. Autumn and spring show intermediate increases in discharge. The increase in summer is critical and this will most likely also entail an increase in the number of extreme discharges, since there is a strong relation between average monthly discharge and maximum monthly discharge (R^2 = 0.61; Figure 3.12).

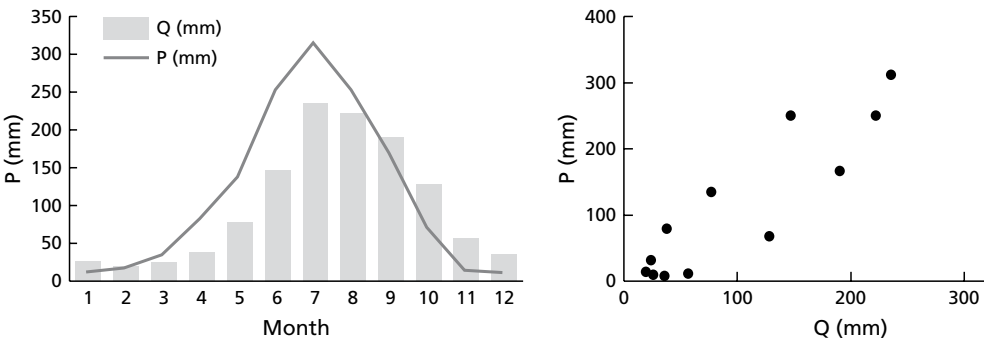

Figure 3.10 Average monthly hydrograph at Bahadurabad and basin precipitation (left figure) and scatter plot between monthly basin precipitation and Bahadurabad discharges (right figure) (1956-1993 data).

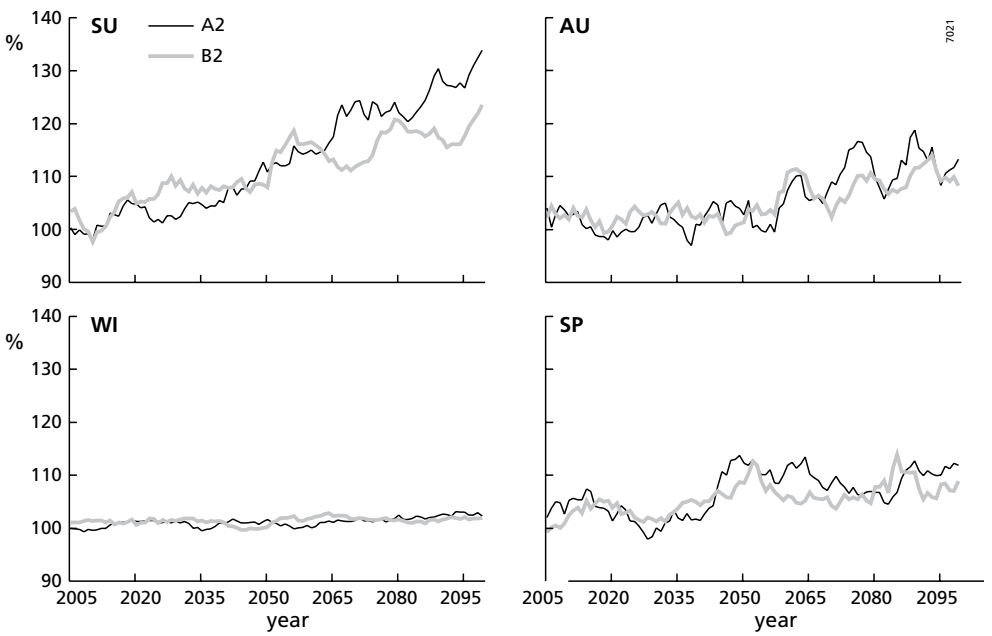

Figure 3.11 Projected trends in seasonal discharges at Bahadurabad based on multiple linear regression models and average data of six GCMs.

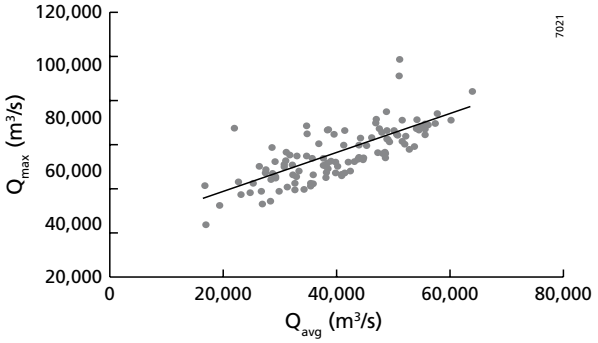

Figure 3.12 Relation between monthly average and extreme discharges at Bahadurabad.

3.4 Discussion and conclusion

The historical analysis of precipitation and temperature revealed that there is a clear increasing trend in temperature at an average rate of 0.6 °C/100 year, with the largest increases in spring. No distinct drying or wetting trends are observed over the last 100 year and annual precipitation is primarily controlled by monsoon dynamics.

The GCM simulations show an accelerated increase in both temperature and precipitation. Projected changes on the TP are more profound than in the other two physiographic zones. The widening distribution of summer precipitation indicates a potential increase in extreme events.

In this paper an analysis is provided of the historical climatic variations at the scale of a large river basin. The CRU TS 2.1 dataset is not always suitable to provide time series analysis at the scale of an individual grid box. The grids are optimised in space rather than in time, resulting in instantaneous best estimates of spatial patterns. The analysis also revealed a large variation in time in the number of stations within the correlation decay distance. For these reasons the time series analysis conducted in this research on the dataset was mainly conducted per physiographic zones and problems caused by local inhomogeneities at a specific location were avoided.

The historical analysis showed clear temperature trends, however no clear trends in precipitation were observed although seasonal variations were apparent. This study reveals no significant relation between ENSO and monsoon precipitation, which is not in agreement with earlier findings (Krishna Kumar et al., 1999) and should be subject to further research. A large part of the variation in monsoon precipitation is however explained by the surface air temperature gradients between the FP and the TP. Relatively high temperatures on the TP and low temperatures on the FP generally yield stronger monsoons. Previous studies (Barnett et al., 1989; Shaman and Tziperman, 2005) argue how thermodynamics on the TP reduce the strength of the monsoon through a decrease of the upper-tropospheric temperature gradient between TP and the Indian Ocean. They argue that the reduction of the thermal gradient is caused by an increased TP snow pack resulting in a number of thermodynamic effects which all result in lower air temperatures of the atmosphere above the TP; (i) an increased snow pack yields a higher albedo leaving less solar radiation for the sensible heat flux, (ii) of the energy which is left a substantial part is required for sublimation and (iii) the melting of the snow leaves a wetted surface and a large part of the energy is consumed by the latent heatflux. In other words low air temperatures on

the TP (= high $\Delta T_{FP\text{-}TP}$) generally yield weak monsoons, which is in agreement with findings of this study. Kripalani et al. (2004) found that the well-documented negative relationship between winter snow and summer rainfall has recently changed into a positive relation ship in the western Himalayas, and argue that a possible cause might be found in global warming and the interaction between snow depth and cover.

The future precipitation increase simulated by the GCMs is assumed to be driven by global warming rather than changes in atmospheric dynamics. The study revealed an inverse relation between $\Delta T_{FP\text{-}TP}$ and precipitation. The GCM analysis showed that this gradient will decrease in the years ahead, which would result in higher precipitation according to the relation found.

To which extent remains however largely unknown and this should be topic of future research and some caution is warranted. A number of recent studies have, for example, investigated the influence of black carbon aerosols on the South Asian monsoon, suggesting a competing effect with increasing concentrations of greenhouse gases (Lau et al., 2006; Ramanathan et al., 2005; Chung and Ramanathan, 2006). These specific aerosols are not included in the climate models.

The hydrological analysis showed that it is likely to assume that the majority of downstream stream flow in the Brahmaputra is generated by rainfall and to a much lesser extent by snow and glacial melt. It was also found that the average difference between annual precipitation and discharge only leaves 136 mm for evapotranspiration. Assuming that the soil water storage balance is close to zero this is not realistic given the high potential evapotranspiration rates. The logical explanation is that the CRU precipitation, based on a limited number of stations, underestimates the precipitation in the floodplain due to orographic effects in the Meghalaya hills and the Himalayan foothills. Nijssen et al. (2000) found similar results. Through relative simple multiple regression analysis interesting relations are found between JJAS discharges and precipitation. It showed that trends in average and extreme discharges can be reasonably well predicted, but that the most extreme discharge events are missed by the regression model. There are several potential reasons. Extreme discharges are often the result of precipitation events with a daily timescale. Extreme discharges at Bahadurabad are combination of processes and the upstream hydro-meteorological processes are not the only cause for floods in Bangladesh. The combination of simultaneous discharge peaks of the tributaries, high runoff from the Meghalaya Hills, heavy rainfall in Bangladesh, high groundwater tables and spring tides will results in a very high peak discharges at Bahadurabad (Messerli and Hofer, 2006).

In this research direct relationships with zonal precipitation were investigated. This study provides a baseline against which process based hydrological models may be built and used to simulate the complete anticipated effects on the hydrological cycle. Changes in snowfall, evapotranspiration and groundwater recharge can thus be modelled and related to food production in a changing environment.

4 Calibration of a distributed hydrological model based on satellite evapotranspiration

Based on: Immerzeel, W.W. & P. Droogers (2007), Calibration of a distributed hydrological model based on satellite evapotranspiration. Journal of Hydrology (in press)

Abstract

Calibrating spatially distributed hydrological models is complex due to the lack of reliable data, uncertainty in representing the physical features of a river catchment, and the implementation of hydrological processes in a simulation model. In this paper, an innovative approach is presented which incorporates remote sensing derived evapotranspiration in the calibration of the Soil and Water Assessment Tool (SWAT) in a catchment of the Krishna basin in southern India. The Gauss-Marquardt-Levenberg algorithm is implemented to optimise different combination of land use, soil, groundwater, and meteorological model parameters. In the best performing optimisation, the r^2 between monthly sub-basin simulated and measured actual evapotranspiration (ET_{act}) was increased from 0.40 to 0.81. ET_{act} was more sensitive to the groundwater and meteorological parameters than the soil and land use parameters. Traditional calibration on a limited number of discharge stations lumps all hydrological processes together and chances on the equifinality problem are larger. In this study we have shown this problem can be constrained by using spatially distributed observations with a monthly temporal resolution. At a spatial resolution below the sub-basin level further study is required to fine-tune the calibration procedure.

4.1 Introduction

Calibration of physically based, distributed hydrological models is complex given limitations of the input data, complexity of the mathematical representation of hydrological processes, and incomplete knowledge of basin characteristics. A priori, it is not clear whether a unique set of model parameters exists for a given catchment. While comparing model outputs to observations the main question is what the causes of these differences are (Duan et al., 2003)? Model calibration is usually based on the comparison between modelled and observed hydrographs for a limited number of locations and a small number of input parameters are varied in a trial and error mode to achieve a desired response (Gupta et al., 1998; Anderston et al., 2002). In a complex distributed hydrological model with numerous parameters with a high spatial and temporal heterogeneity this approach can be cumbersome. To overcome these difficulties a number of different auto-calibration or parameter optimisation methods have been developed that deploy a systematic approach to parameter estimation.

The type of optimisation algorithm applied is the dominant distinguishing factor in parameter estimation (Singh and Woolhiser, 2002). The objective function describes the difference between the observed and model simulated values. RMSE statistics and the Nash-Sutcliffe criterion (Nash and Sutcliffe, 1970) are amongst the most commonly used. Minimizing the objective function is complex; because most discharge based objective functions in distributed hydrological models have multiple extremes. Optimisation algorithms adopt either a gradient (Levenberg (1944); Marquard (1963)) or a global search method such as the shuffled complex evolution algorithm (Kuczera, 1997) and genetic algorithms (Wang, 1991). Global optimisation algorithms are designed for locating the global optimum. Local search algorithms have been criticized for getting trapped in local minima. The most important advantage of a local search is nonetheless its efficiency; e.g., the number of model calls required to find the optimum set of parameters. Skahill and Doherty (2006) show how the algorithms underlying the Gauss-Marquardt-Levenberg (GML) method of computer-based parameter estimation can be improved to enhance the possibility to find the global minimum while retaining the model run efficiency.

Using a limited number of discharge stations in the optimisation may well lead to the equifinality problem; e.g., there are more than one parameter combination leading to similar results (Beven, 1993; Beven, 2000; Beven, 2001; Beven and Freer, 2001; Beven 2006; Franks et al., 1997). High spatial heterogeneity in combination with a large number of model parameters inhibits the identification of one set of parameters describing the natural system. If river discharges in a catchment are mainly governed by human decisions (e.g., dams and reservoirs) they may not be usable in determining the natural characteristics of the system. Hydrological parameters measured using remote sensing, which has a high spatial and temporal observational resolution, could provide a suitable solution in this respect. Deriving hydrological parameters such as evapotranspiration and soil moisture using remote sensing is a growing field of research (Bastiaanssen et al., 1998; Hall et al., 1992; Kite and Droogers, 2000; Su, 2000). The use of remote Sensing in the parameterisation of hydrological models is an even newer field; Wood (1995) empirically evaluates scale issues using remote sensing data and a hydrological model. Other studies use remote sensing to parameterise hydrological models (Boegha et al., 2004; Houser et al., 1998; Kite and Pietroniro, 1996; Shuttleworth, 1998). Less work has been done in the use of remote sensing in the actual calibration using optimisation algorithms of hydrological models. Campo et al. (2006) show the use of remote sensing derived soil moisture in the calibration of a distributed hydrological model using a local search algorithm developed by Nelder and Mead (1965).

In summary five partially overlapping fields of expertise can be identified that deal with the topic of this study: (i) deriving hydrological fluxes by remote sensing, (ii) optimisation algorithms used in calibration of simulation models, (iii) equifinality in parameter optimisation, (iv) use of remote sensing in parameterisation of hydrological models and (v) the use of remote sensing in the calibration of hydrological models in data scarce areas. The focus of this paper is on the last topic (v). The objective was to evaluate the method of using remote sensing derived actual evapotranspiration (ET_{act}), based on the Surface Energy BALance algorithm (SEBAL; Bastiaanssen et al., 1998), to calibrate the process-based hydrological model Soil and Water Assessment Tool (SWAT; Arnold et al., 1998), in the water scarce Upper Bhima catchment in southern India. The Parameter ESTimation (PEST) software (Doherty, 2005), incorporating the gradient search GML optimisation method, was used for this purpose.

4.2 Study area

The Upper Bhima catchment (45,678 km²) is located in the upstream part of the Krishna basin in southern India and originates in the Western Ghat mountains and covers part of the Maharasthra state (Figure 4.1). The catchment is located between 16.5°-19.5° latitude and 73.0°-76.5° longitude. The elevation ranges from 414 meter in the east to 1458 meter in the Western Ghat mountains and 95% of the catchment is below 800 meter and relatively flat. The average slope of the catchment is 2%.

The catchment has two main tributaries, the Sina River which drains the north eastern part and the Bhima River which drains the remainder. The catchment is an important source of water for the entire Krishna basin as a major part of the precipitation falls in the Western Ghat range in the east of the catchment and is retained and released to downstream areas through an intricate set of reservoirs, especially along the Bhima tributary. Flows in the rivers are, therefore, mainly human controlled and respond less directly to variations in the climate excitations and biophysical conditions and are hence less suitable to use for calibration. The reservoirs accumulate water during the monsoon season (June to September), and this is gradually released throughout the irrigation season (October to May).

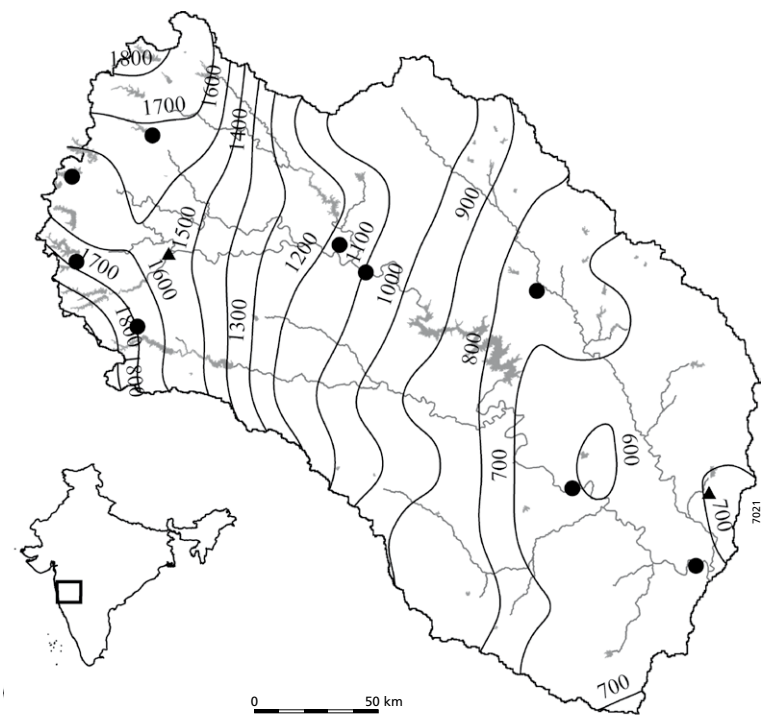

Figure 4.1 Upper Bhima catchment boundary, contours of the precipitation sum from June 2004 to May 2005, river network, major reservoirs, and meteorological station (circles represent precipitation stations; triangles represent precipitation, temperature, wind speed, relative humidity and radiation stations)

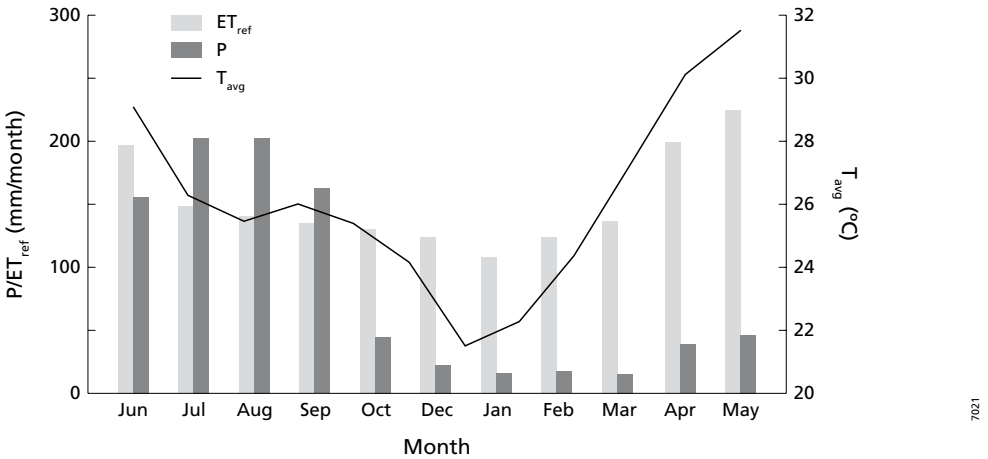

Figure 4.2 Monthly precipitation (P), reference evapotranspiration (ET_{ref}) and temperature from June 2004 to May 2005.

The catchment has a highly diverse climate mainly caused by the interaction between the monsoon and the Western Ghat mountain range (Gunnel, 1997). The precipitation ranges from less than 600 mm in the eastern part of the basin to over 1800 mm in the mountains in the west with an average of 941 mm during the averagely wet irrigation year 2004-2005 (Figure 4.1). Figure 4.2 shows the monthly precipitation (P) and reference evapotranspiration (ET_{ref}) in the basin. ET_{ref} is calculated using Penman-Monteith (Monteith, 1965) and alfalfa as reference crop. The catchment has a high annual ET_{ref} (1814 mm) ranging from 224 mm/month in May to 108 mm/month in December. More than 75% of the annual precipitation occurs during the monsoon. Between October and May, large precipitation deficits occur with the peak in May (179 mm) just before the onset of the monsoon.

The state of Maharasthra has a diverse cropping pattern characterized by cultivation of sugarcane, sorghum, wheat, corn, millet, groundnut, grass fodder, and a variety of horticultural crops (Neena, 1998). Three main types of agricultural systems were identified in the catchment: (i) rain fed agriculture with a single crop (e.g. sorghum) cultivated during the monsoon, (ii) supplemental irrigated agriculture with one rain fed crop during the monsoon (e.g. sorghum) and a (groundwater) irrigated crop planted in October and harvested in February (e.g. winter wheat) and (iii) irrigated perennial sugarcane which has a growing period of 11 months and which is grown throughout the year and irrigated from water released by the reservoir system. Other natural land covers include rangelands, mixed forests, evergreen forests and water surfaces.

4.3 Methods

4.3.1 SEBAL

The Surface Energy Balance Algorithm for Land (SEBAL) formulated by Bastiaanssen et al. (1998) was used to derive bi-weekly ET_{act} from October 2004 to May 2005. Spectral radiances in the visible, near-infrared, and thermal infrared part of the spectrum derived from 16

MODIS satellite images were used. Two cloud free images were selected each month and the MOD02HKM product was used in the analysis. This Level 1B product contains calibrated and geolocated radiances. The thermal band is downscaled and the final resolution of the ET_{act} images is 250 meter. This downscaling algorithm is based on the assumption that a unique relationship between radiometric surface temperature relationship and vegetation index exists at multiple resolutions and is similar as described by Agam et al., 2007. It should be noted that this sharpening procedure does not account for sub-pixel variability in soil moisture conditions, and therefore does not work as well for areas where the irrigated areas are smaller than the nominal MODIS thermal pixel size of 1 km (Agam et al., 2007b).

The acquisition dates and overpass time are shown in Table 4.1.

SEBAL converts satellite radiances into land surface characteristics such as surface albedo, leaf area index, vegetation index, and surface temperature, which were used in solving the instantaneous energy budget equation given by

$$L_v E = Q^* - G_0 - H \quad (1)$$

Where L_vE is the latent heat flux (W/m^2), Q* is the net radiation flux at the surface (W/m^2), G_o is the soil heat flux (W/m^2), and H is the sensible heat flux to the air (W/m^2).

The net radiation (Q*) was computed by subtracting all outgoing radiant fluxes from all incoming radiant fluxes according to

$$Q^* = Q_{s\downarrow} - \alpha Q_{s\downarrow} + Q_{L\downarrow} - Q_{L\uparrow} - (1-\varepsilon_0) Q_{L\downarrow} \quad (2)$$

Where $Q_{s\downarrow}$ is the incoming short-wave radiation (W/m^2), α is the surface albedo (dimensionless), $Q_{L\downarrow}$ is the incoming long wave radiation (W/m^2), $Q_{L\uparrow}$ is the outgoing long wave radiation

Table 4.1 Date and local acquisition time (+5:30 GMT) of Aqua-MODIS images.

Date	Time
16/10/2004	1:40 PM
21/10/2004	2:00 PM
04/11/2004	2:10 PM
22/11/2004	2:00 PM
03/12/2004	1:40 PM
17/12/2004	1:50 PM
07/01/2005	2:10 PM
18/01/2005	1:50 PM
12/02/2005	1:45 PM
19/02/2005	1:50 PM
14/03/2005	2:00 PM
23/03/2005	1:50 PM
10/04/2005	1:40 PM
19/04/2005	1:35 PM
14/05/2005	1:25 PM
17/05/2005	1:55 PM

(W/m^2), and ε_o is the surface thermal emissivity (dimensionless). In Eq. 2, the amount of net short-wave radiation ($Q_{S\downarrow} - \alpha Q_{S\downarrow}$) that remains available at the surface is a function of the surface albedo (α). The broad band surface albedo α was derived from the narrow band spectral reflectances $\alpha(\lambda)$ measured by each MODIS satellite band (Zhong and Li, 1988). The incoming short-wave radiation ($Q_S\downarrow$) was computed using the solar constant, the solar incidence angle, a relative earth-sun distance, and a computed broad band atmospheric transmissivity. This transmissivity was estimated from sunshine duration or inferred from pyranometer measurements. The incoming long wave radiation ($Q_L\downarrow$) was computed using a modified Stefan-Boltzmann equation with an apparent emissivity that is coupled to the shortwave atmospheric transmissivity and a measured air temperature. Outgoing long wave radiation ($Q_L\uparrow$) was computed using the Stefan-Boltzmann equation with a calculated surface emissivity and surface temperature. Surface temperatures were computed from the satellite measurements of thermal radiances.

Soil heat flux was empirically calculated as a G_o/Rn fraction using vegetation indices, surface temperature, and surface albedo. Sensible heat flux was computed using wind speed observations, estimated surface roughness, and surface to air temperature differences (ΔT), that were obtained through a sophisticated self-calibration between dry ($L_vE \approx 0$) and wet ($H \approx 0$) pixels. The wet and dry pixels were manually selected in the image. For the wet pixel it is assumed that $\Delta T = 0$. For the dry pixel ΔT is given by:

$$\Delta T = \frac{Hr_{ah}}{\rho_{air} c_p} \tag{3}$$

Where r_{ah} (s m^{-1}) is the near surface aerodynamic resistance to heat transfer, ρ_{air} (kg m^{-3}) is the moist air density and C_p (J kg^{-1}) is the specific heat at constant pressure. SEBAL solves this implicit equation iteratively. Empirically it has been shown that under many conditions there is a linear relation between surface temperature (T_o) and ΔT. This relation was used to estimate ΔT for all pixels in the image.

Knowing the instantaneous soil, latent, and sensible heat fluxes made it possible to calculate the evaporative fraction given by:

$$\Lambda = \frac{L_v E}{Q^* - G} \tag{4}$$

SEBAL assumes that the evaporative fraction is constant during the day and this assumption allows the conversion of an instantaneous L_vE value to a daily value. Experimental work has demonstrated that this is a reasonable assumption for cases when soil moisture and atmospheric conditions do not significantly change (e.g., Shuttleworth et al., 1989; Brutsaert and Sugita, 1992; Nicols and Cuenca, 1993; Kustas et al., 1994; Crago, 1996; Franks and Beven, 1997).

For periods longer than one day it may be assumed that the (time-integrated) soil heat flux equals 0. The 24hr latent heat flux could therefore be determined by

$$L_v E_{24hr} = \Lambda Q^*_{24hr} \tag{5}$$

The final step was to derive biweekly evapotranspiration data. This was achieved by inserting L_vE_{24hr} into the Penman-Monteith equation (Monteith, 1965). Using this approach it was possible to inversely determine the surface resistance (r_s). There are some known associated problems with

this approach. There is a strong relationship between the aerodynamic (r_a) and surface resistances (r_s) and uncertainty in r_a leads to incorrect estimates of r_s (Beven, 1979; Franks et al., 1997). By using a consistent r_a from meteorological data the error in the eventual ET estimate is however minimal. Knowing the spatial distribution of the surface resistance made it possible to calculate ET_{act} based on the Penman-Monteith equation and meteorological data for all days without satellite imagery (Bastiaanssen and Bandara, 2001). Meteorological data on radiation, temperature, wind speed, relative humidity for two stations were used for this purpose (Figure 4.1). SEBAL has been extensively validated (Bastiaanssen et al., 1998[b]).

The 16 biweekly ET_{act} images of the Upper Bhima catchment were accumulated to eight monthly images from October 2004 to May 2005, and these were used in the calibration of the SWAT model. SEBAL could not be applied during the monsoon months (June to September) due to the lack of cloud free imagery.

4.3.2 SWAT

A SWAT model was built and simulations were run on a daily basis from June 2004 to May 2005. SWAT is a distributed hydrological model providing spatial coverage of the integral hydrological cycle including atmosphere, plants, unsaturated zone, groundwater, and surface water. The model is comprehensively described in literature (Arnold et al., 1998; Srinivasan et al., 1998).

Conceptually SWAT subdivides the catchment into sub-basins and a river network based on a digital elevation model (DEM). Based on unique combinations of soil and land use, the sub-basins were further detailed into hydrological response units (HRUs), which were the fundamental units of calculation. A total of 115 sub basins and 768 HRUs were delineated in the Upper Bhima catchment.

The Penman-Monteith method (Monteith, 1965) was used in SWAT to calculate daily reference evapotranspiration for alfalfa (ET_{ref}) and potential plant transpiration (ET_p). Daily data on radiation, wind speed, relative humidity, and air temperature for two different meteorological stations were used (Figure 4.1). Potential daily plant transpiration is calculated using actual daily crop height and leaf area index (LAI), required to determine the aerodynamic resistances and canopy resistances respectively. Potential soil evaporation is an exponential function of ET_{ref} and the soil cover and is further reduced during periods with high plant water use. Actual soil evaporation is limited by the soil water content (θ) and is reduced exponentially when θ drops below field capacity.

To calculate actual plant transpiration the potential plant water uptake is defined by

$$w_{p,z} = \frac{ET_p}{[1-e^{\beta_w}]} \cdot \left[1-e^{\left(-\beta_w \cdot \frac{z}{z_{root}}\right)}\right] \qquad (6)$$

Where $w_{p,z}$ (mm H_2O) is the potential plant water uptake from the soil surface to a specified depth from the soil surface on a given day, ET_p (mm H_2O) is the maximum plant transpiration on a given day, β_w (-) is the water use distribution parameter, z is the depth from the soil surface (mm), and z_{root} is the depth of root development in the soil (mm). Actual plant water uptake equals actual plant transpiration and is, similarly to soil evaporation, reduced exponentially when θ drops below field capacity. Actual evapotranspiration (ET_{act}) is the sum of interception, actual soil evaporation, and actual plant transpiration.

Meteorological data in SWAT are parameterized on sub-basin level. No precipitation data was available for the simulation period and to be able to capture the spatial heterogeneity in precipitation, monthly gridded precipitation estimates with a spatial resolution of 25 km derived with the Tropical Rainfall Monitoring Mission (TRMM; Kumerrow et al., 1998) was used. To correct the TRMM data the monthly grids were scaled using linear regression with 11 meteorological stations between 1998 and 2004 (Figure 4.1). For each month and each station a linear relationship between observed and TRMM precipitation was established. Using these relationships between observed precipitation and the TRMM data during the simulation period, monthly grids of precipitation were generated from June 2004 tot may 2005. The grid based monthly data were aggregated per sub-basin and converted to daily precipitation using a simple weather generator, since no long term statistics on daily rainfall distributions are available. The weather generator maintains the monthly sums, days with rain are randomly selected, and a maximum daily precipitation threshold is used. This threshold is higher during the monsoon months (100 mm) than in other months (20 mm). A total of 115 hypothetical meteorological stations were thus inferred on the model.

The major reservoirs (20) are mainly located along the Bhima branch. For modelling purpose, the reservoirs are clustered into two reservoirs. Because the simulation year was an average year, the assumption was made that over the entire year there was no net increase or decrease in reservoir storage. The reservoirs inflow was largest during the monsoon season and throughout the irrigation year the water was used for irrigation. The unused excess water was released using a monthly distribution derived from historical measurements.

Land used in this study was based on a 15 class unsupervised land use classification using a time series of 16 MODIS derived Normalized Difference Vegetation Index (NDVI) images with a spatial resolution of 250 meter. The same imagery was used for the land use classification and the SEBAL analysis (Table 4.1). Based on existing land use map and field surveys 15 classes were clustered into six land use classes defined in Table 4.2.

The results were visually verified with high resolution satellite imagery. The final land use map is shown Figure 4.3.

The FAO digital soil map of the world (FAO, 1995) was used to derive soil properties. Ten different soil units are identified in the catchment. The alluvial plains are predominantly characterized by vertisols and the Western Ghats and steeper slopes by luvisols.

To initialize the model, in particular soil moisture, a model spin up period of one year was used by simulating the period June 2004 to May 2005 twice consecutively and the calibration on ET was performed on the latter year from October 2004 to May 2005. Initial soil moisture

Table 4.2 Acreages of different land use and land cover in the catchment

Class name	Code	Area (km^2)	Area (%)
Water surfaces	WATR	411	1
Rangelands	RNGB	12242	27
Rain fed agriculture	AGR1	15348	34
Supplemental irrigated agriculture	AGR2	6121	13
Irrigated sugarcane	AGR3	9090	20
Evergreen forest	FRSE	1416	3
Mixed forest	FRST	1051	2

was set at field capacity and nearly all soils were again at field capacity after the monsoon of the second year of simulation at the start of the calibration period.

4.3.3 PEST

In this study PEST (2005 version) was used to calibrate the SWAT model using ETact derived with SEBAL. PEST is a non-linear parameter estimation package that can be used to estimate parameters for just about any existing computer model (Doherty, 2005). PEST is able to run a model as many times as it needs to while adjusting its parameters until the discrepancies between selected model outputs and a complementary set of field or laboratory measurements is reduced to a minimum.

PEST uses the GML algorithm to optimize the model. The theory underlying the GML method is derived from the linear parameter estimation theory. The relation between a hydrological model (X), a set of parameters (p), a set of observations (H) and residuals in the observations (ε) can be described as:

$$X \cdot p = H + \varepsilon \tag{7}$$

The goal of PEST is to find that p that minimises the objective function, which is defined as the sum of squared deviations between model generated values and experimental observations and can be written as:

$$\Phi = (H - Xp)^{t} Q (H - Xp) \tag{8}$$

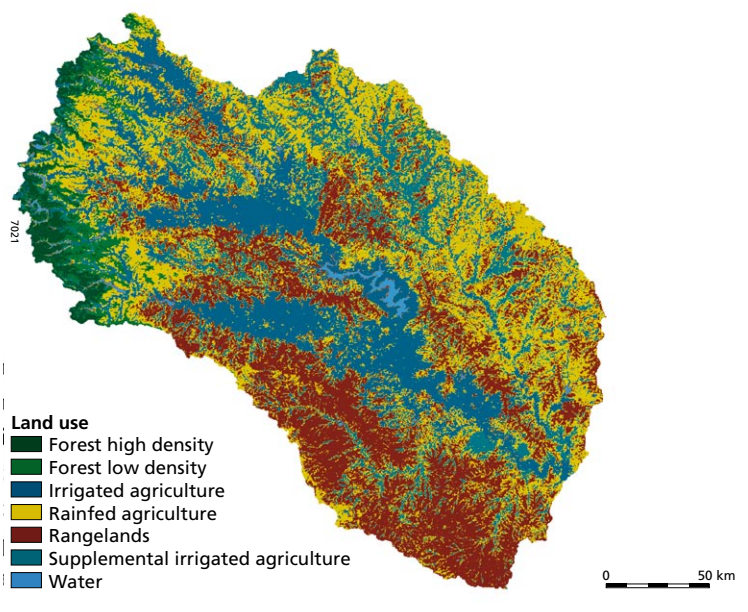

Figure 4.3 Land use based on unsupervised classification of MODIS time series of NDVI imagery.

Where Q is proportional to the inverse of C(ε), the covariance matrix of measurement noise. The objective function used in PEST is closely related to the commonly used root mean square error (RMSE) through:

$$RMSE = \left(\frac{\Phi}{N}\right)^{\frac{1}{2}} \tag{9}$$

Φ is minimized when

$$p = (X^t Q X)^{-1} X^t Q b \tag{10}$$

For linear models optimisation can be achieved in one step, whereas for non-linear problems it is an iterative process. At the beginning of each iteration the relationship between model parameters and model-generated outputs is linearised by formulating a Taylor expansion about the currently best parameter set; hence, the derivatives of all observations with respect to all parameters must be calculated. This linearised problem is then solved for a better parameter set, and the new parameters tested by running the model again.

However, one of the most relevant restrictions in the GML algorithm, a gradient based method, is sensitivity to local minima. Recent advances in the GML algorithm have improved the capability to identify the global minimum in surface water models (Skahill and Doherty, 2006). The most pronounced advantage of the GML method is that it can generally complete a parameter estimation process with an extremely high level of model run efficiency.

4.3.4 Calibration strategy

The core of the calibration as tested in this study consists of a comparison of seven different parameter set estimations. The entire flowchart of the calibration strategy, including pre and post-calibration steps, is summarized in Figure 4.4.

Because ET_{ref} is the basis for the ET_{act} calculations, first, a simple adjustment was performed on the SWAT input solar radiation to ensure that calculated SWAT ET_{ref} and SEBAL ET_{ref} were equal. In general SWAT ET_{ref} is lower than SEBAL ET_{ref} and there are two possible reasons. Firstly, to account for impacts of slope and aspect on incident solar radiation SEBAL incorporates a digital elevation model (DEM) based correction. Another source for slight deviations between SEBAL and SWAT ET_{ref} is the fact that SEBAL ET_{ref} assumes grass as a reference crop and SWAT assumes alfalfa. For grass the reference crop height equals 0.12 m and r_s equals 70 m s^{-1}, while for alfalfa a reference height 0.40 m and a r_s of 100 m s^{-1} are taken. To correct these difference the SWAT input radiation was incremented iteratively for each sub basin until SWAT ET_{ref} matched SEBAL ET_{ref}.

After adjusting of ET_{ref}, it was verified through a set of box whisker plots whether ΔET_{act} (ET_{act} SEBAL – ET_{act} SWAT) was explained by variation in land use, different soil type, month, or precipitation zone. Precipitation zones were delineated based on annual precipitation.

This analysis leads to the identification of a number of PEST optimisation runs for a primary variable. Each PEST run optimizes a set of sub-variables related to either of these primary variables. The results of each PEST run (Φ reduction and r^2) were used to identify a number

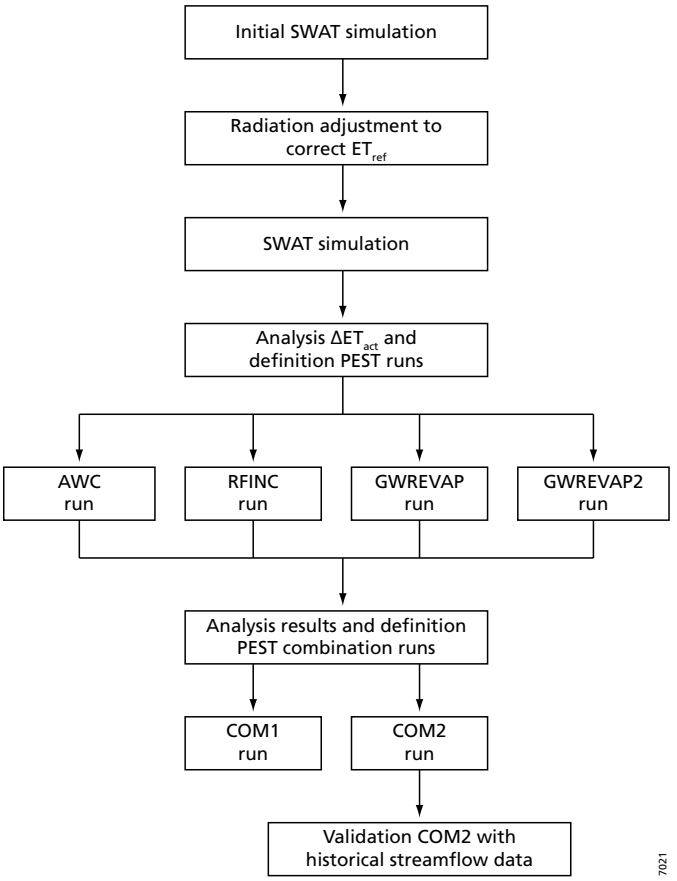

Figure 4.4 Flowchart of calibration strategy.

of combination PEST runs. Final results were analyzed at basin, sub-basin, and HRU level. All ET_{act} optimisation runs calculated the **Φ** based on monthly data at sub basin level. A total of 920 observations (8 months times 115 sub basins) were used in the objective function. The following optimisation runs were formulated (Figure 4.4):

- Available water capacity (AWC). The AWC is defined as the difference between the field capacity of the soil and the permanent wilting point. It is defined per soil layer per soil type and determines, to a large extent, the water holding capacity of the soil. Ten different soil types with two layers each resulted in 20 different sub-variables to be optimized. AWC is bound by the range 0.05 mm/mm and 0.60 mm/mm.
- Maximum potential leaf area index (BLAI). The LAI is the leaf area divided by the land area. The BLAI is one of six parameters that determine leaf area development of a crop in SWAT and determines the maximum threshold. BLAI is specified per land use type (Table 4.2) and, excluding water surfaces, resulted in 6 sub-variables to be optimized (one per land use). The bounding range is between 2.0 and 8.0 for AGR1, AGR2, FRSE and FRST, between 5.0 and 12.0 for AGR3 and between 1.0 and 8.0 for RNGE.

- Monthly rainfall increment (RFINC). The RFINC is specified per month and per sub-basin and is defined as the relative monthly adaptation in rainfall. The assumption was made that the spatial distribution of the TRMM derived precipitation was correct, however that for specific months the scaled absolute amounts of precipitation could be incorrect. This led to one sub-variable to be optimized per month. RFINC is allowed to vary between -200% and 200% of the original monthly precipitation.
- Groundwater revap coefficient (REVAP1 and REVAP2). Water may conceptually move from the shallow aquifer into the overlying unsaturated zone. The process of water being evaporated from the capillary fringe in dry periods is referred to as groundwater revap and in SWAT quantified by the revap coefficient (β_r) multiplied by ET_{ref}. Two optimisation runs were designed. For the first optimisation run one β_r for each land use, except water, was defined (REVAP1, 6 sub-variables). For the second optimisation run it was assumed that β_r varies per land use and per elevation zone. Four different elevation zones were defined (0-500 m, 500-600 m, 600-700m and >700m). In combination with land use this resulted in 21 unique β_r resulting from unique combinations of elevation zone and land use class (REVAP2, 21 sub-variables). For both optimisation runs the revap coefficient may range between 0.0 and 0.5.

Two combined optimisation runs were performed based on the results of the individual runs (COM1 and COM2). COM1 combined AWC, RFINC and GWREVAP1 and COM2 combined AWC, RFINC and GWREVAP2. Two combinations runs were evaluated to check if the ability of PEST to converge to an optimum was not jeopardized by the relatively large number of parameters of COM2.

The results of the best performing combination run were validated using historical stream flow data.

4.4 Results

Monthly analysis of the ET_{ref} differences between SEBAL and SWAT revealed that the differences between SEBAL and SWAT typically range from 6.1 mm $month^{-1}$ in May 2005 to 29.9 mm $month^{-1}$ in March 2005 with an average monthly difference of 16 mm $month^{-1}$. Figure 4.5 shows the results of the ET_{ref} adjustments. The unadjusted SWAT ET_{ref} (base) is consistently lower than SEBAL ET_{ref}. With a modest relative adaptation of solar radiation per month and per sub-basin, the monthly differences were reduced to minimal (adjusted). On average radiation values were increased by 3.5% with a maximum of 7% for one sub basin in March.

SWAT simulated ET_{act} with the base model (base) in the 2004-2005 irrigation year was 775 mm with the highest ET_{act} in August (112 mm) and the lowest in February (34 mm). Figure 4.6 shows box-whisker plots of monthly ΔET_{act} per land use, soil type, month, and precipitation class respectively. The order of magnitude of SWAT ET_{act} is similar to SEBAL, ΔET_{act} is on average slightly positive indicating that ET_{act} derived using SEBAL is slightly higher than SWAT simulated values. The distribution of ΔET_{act} resembles a normal distribution for most cases, but ranges between the first and third quartile are considerable and vary between land uses, soil types, months and precipitation classes.

Table 4.3 presents the results for the different optimisation runs. In the base run the root mean square error (RMSE), defined as the average difference between monthly ET_{act} SWAT and ET_{act} SEBAL, was equal to 24 mm/month and ET_{act} SWAT was generally higher than the ET_{act}

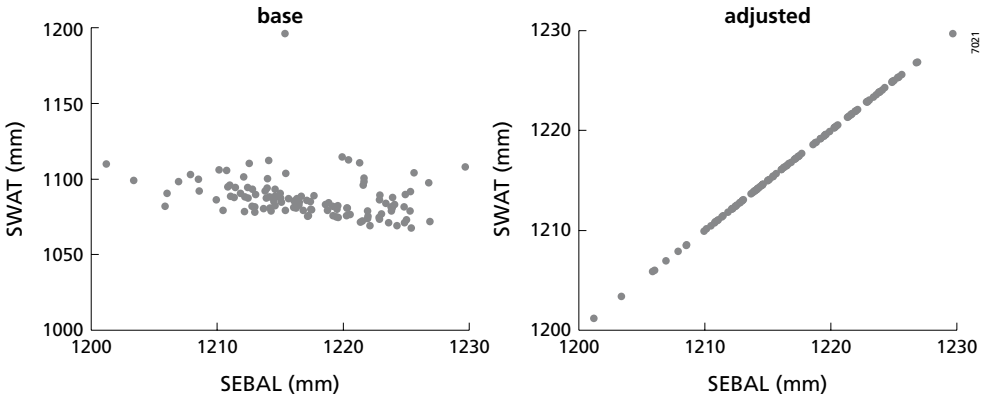

Figure 4.5 Scatter plot of SEBAL vs SWAT of the sum of ET_{ref} from October 2004 to May 2005 per sub basin.

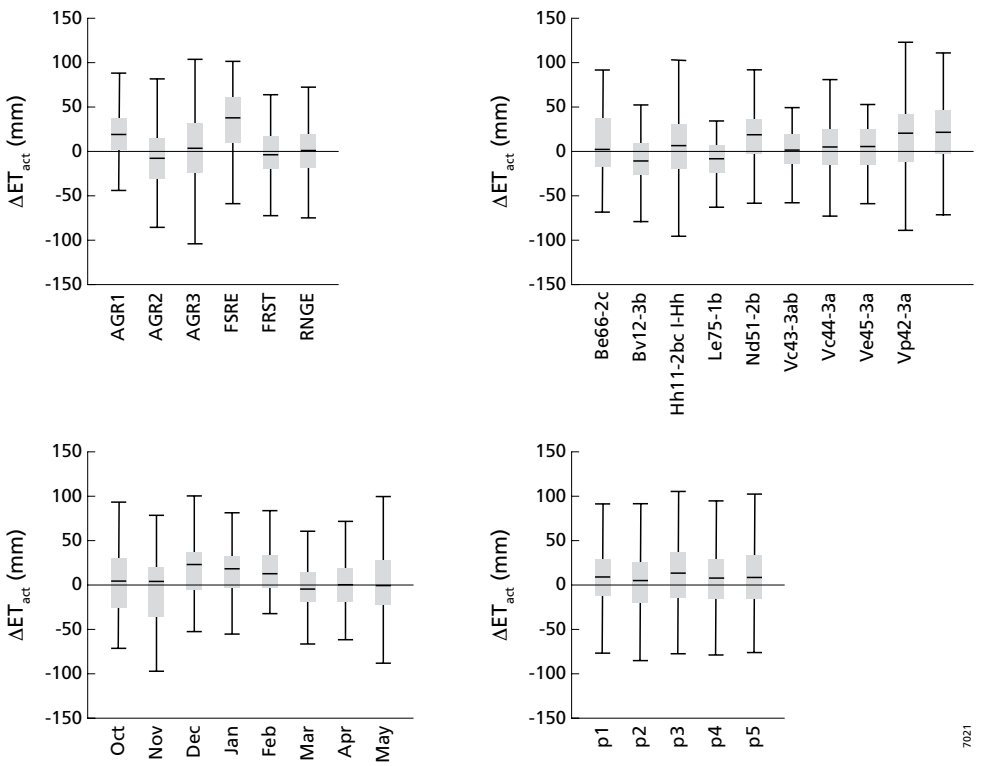

Figure 4.6 Box whisker plots of monthly ΔETact (SEBAL – SWAT) per land use class (top left), soil class (top right), month (bottom left) and precipitation class (bottom right; p1 = 0-800 mm yr-1, p2 = 800-1100 mm yr-1, p3= 1100-1400 mm yr-1, p4=1400-1700 mm yr-1, p5=1700-2000 mm yr-1) The box-whisker plots show the median, first and third quartiles. The caps at the end of the boxes show the extreme values.

SEBAL (ε = 5.2 mm/month). The AWC run reduced the RMSE to 22 mm and the average value for the AWC after optimisation was 0.22 mm/mm, while the average initial value was 0.15 mm/mm. The model was relatively insensitive to maximum plant leaf area index (BLAI). The RMSE was not reduced and the average of the residuals only decreased by 0.4 mm/month. The RFINC optimisation run had a significant effect and the r^2 increased from 0.40 to 0.70. The average adjustment in monthly precipitation during the calibration months was limited (-13 mm/month) with a maximum in December (21 mm) and a minimum in April (-29 mm). ET_{act} SWAT was also sensitive to the groundwater revap coefficient. The GWREVAP run (6 variables) resulted in a RMSE of 17 mm and ε was reduced to 1.6 mm/month. GWREVAP2 (21 variables) yielded a slightly higher r^2 but no significant improvements in RMSE and ε were observed. The best results were achieved by the combination runs (COM1 and COM2). COM2 yielded the best results in the optimisations: 2987 model calls were required to increase r^2 from 0.40 to 0.81. The RMSE in that case equalled 13 mm/month and ET_{act} SWAT was on average only 0.5 mm/month higher. The COM1 results were also good, but significantly less model calls were required (1610). In the COM1 run the average available water content increased from 0.15 mm/mm to 0.21 mm/mm, the rainfall adjustment on average was -2% during the calibration months and the groundwater revap coefficient equalled 0.1.

There are several ways to evaluate the reliability of any optimisation of a distributed hydrological model across time and space. Figure 4.7 shows the scatter plots for run COM1 between SEBAL ET_{act} and the optimized SWAT ET_{act} on catchment, sub-basin and HRU level respectively. It also shows the individual monthly data and the eight month sum of $ET_{act.}$ The figure shows that the goodness of fit decreases with spatial and temporal detail. The r^2 of monthly catchment ET_{act} for example is as high as 0.90, while at HRU level the r^2 is only 0.35. In time

Table 4.3 Results of different optimisations runs. #sub and #obs are the number of sub-variables and observations used in the optimisations. The **Φ** (Eq. 8) is the sum of the squared deviations between monthly SEBAL and SWAT ET_{act} summed over all sub basins (objective function), RMSE is the Root Mean Square Error, defined as the average difference between monthly ETact SWAT and ETact SEBAL (Eq. 9), ε is the average of the residuals and # model calls is the number of model calls required to reach the optimisation results.

PEST run	Primary variable	#sub	#obs	Φ	RMSE (mm/month)	r^2	ε (mm/month)	# model calls
BASE	-	0	920	5.29E+05	24.0	0.40	5.20	-
AWC	Available water content	20	920	4.49E+05	22.1	0.49	5.90	664
BLAI	Maximum plant leaf area index	6	920	5.19E+05	23.8	0.41	5.50	68
RFINC	Monthly rainfall increment	12	920	2.54E+05	16.6	0.70	0.80	324
GWREVAP	Groundwater revap coefficient	6	920	2.78E+05	17.4	0.68	1.60	55
GWREVAP2	Groundwater revap coefficient	21	920	2.66E+05	17.0	0.70	1.70	792
COM1	Available water content, monthly rainfall increment, groundwater revap coefficient	38	920	1.77E+05	13.9	0.79	-0.45	1610
COM2	Available water content, monthly rainfall increment, groundwater revap coefficient	53	920	1.63E+05	13.3	0.81	0.50	2987

we see similar patterns. The r^2 at monthly sub basin level is 0.81 while if the eight month sum is analyzed the r^2 increase to 0.92.

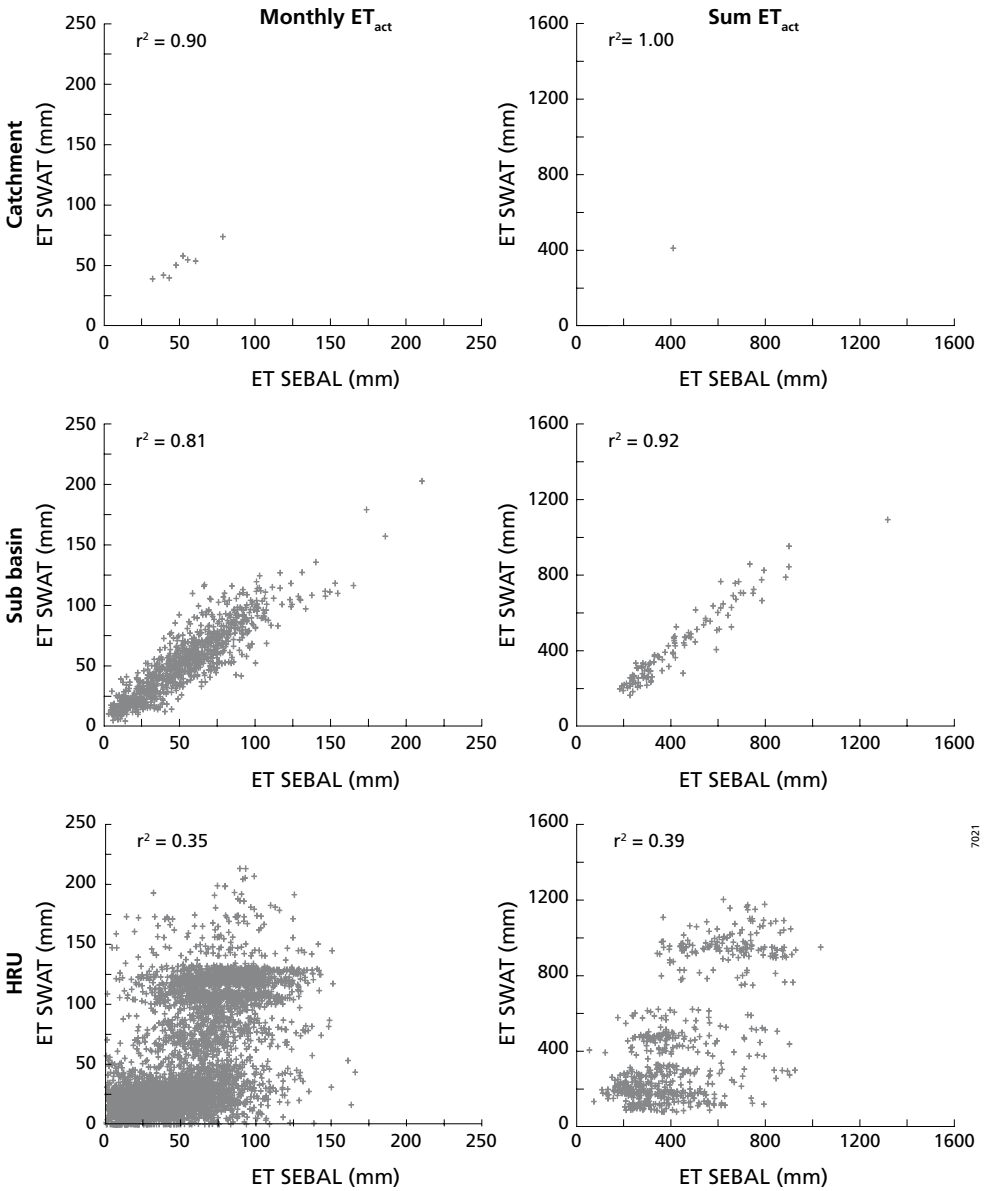

Figure 4.7 Scatter plots of SEBAL and SWAT ET_{act}. Monthly data are shown on the left side graphs and the eight month sum is shown on the right side. Spatial detail increases from top to bottom and ranges from catchment, sub basin to HRU level respectively. SWAT results relate to COM2 optimisation.

Figure 4.8 maps the eight month ET_{act} sum for SWAT and SEBAL at sub-basin and at HRU level. At sub-basin level, the spatial patterns between SWAT and SEBAL were highly consistent. At HRU level there were considerable differences. The general spatial patterns were well depicted. However, some HRUs within a sub-basin evaporated more than derived with SEBAL and some evaporated less, however aggregated over the entire sub basin these differences were levelled out. For example most sub basins with a significant area of AGR3 also contained a large

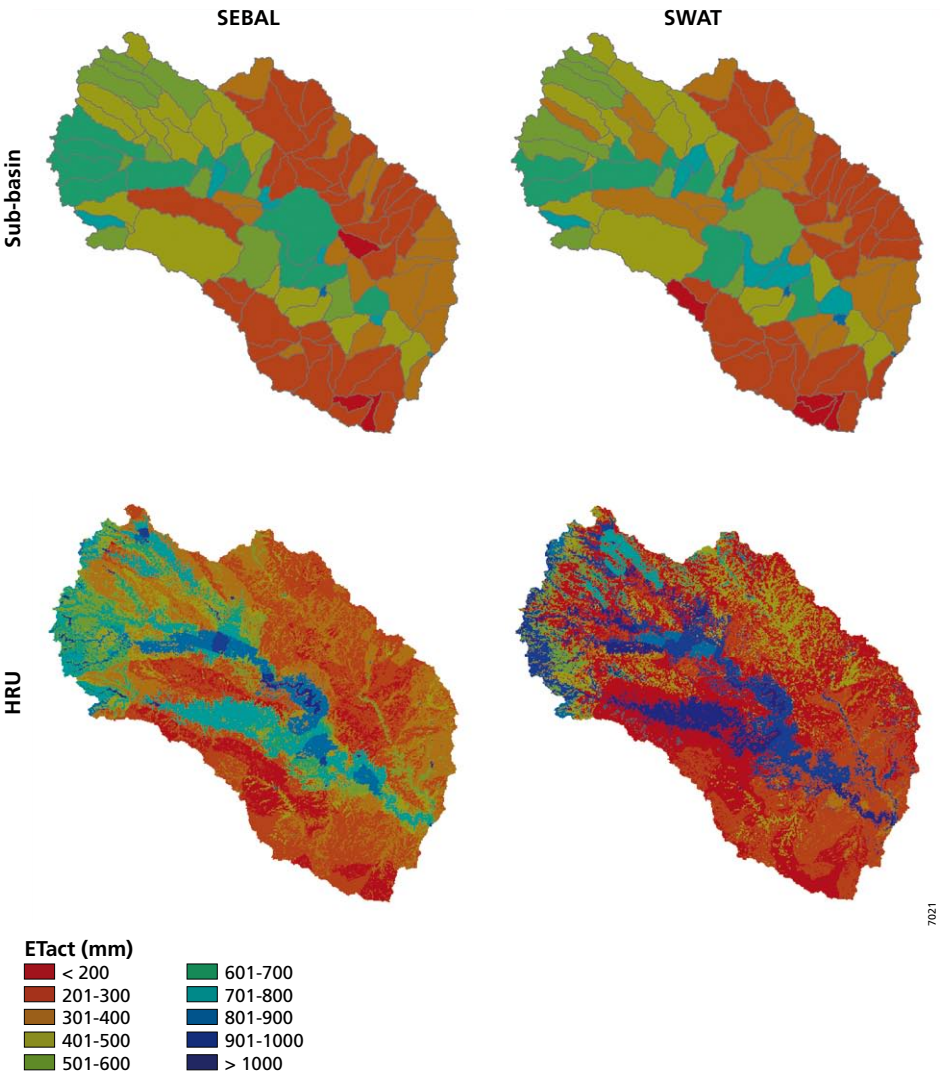

Figure 4.8 Eight month sum of ET_{act} for SWAT and SEBAL on sub basin and HRU level respectively SWAT results relate to COM2 optimisation.

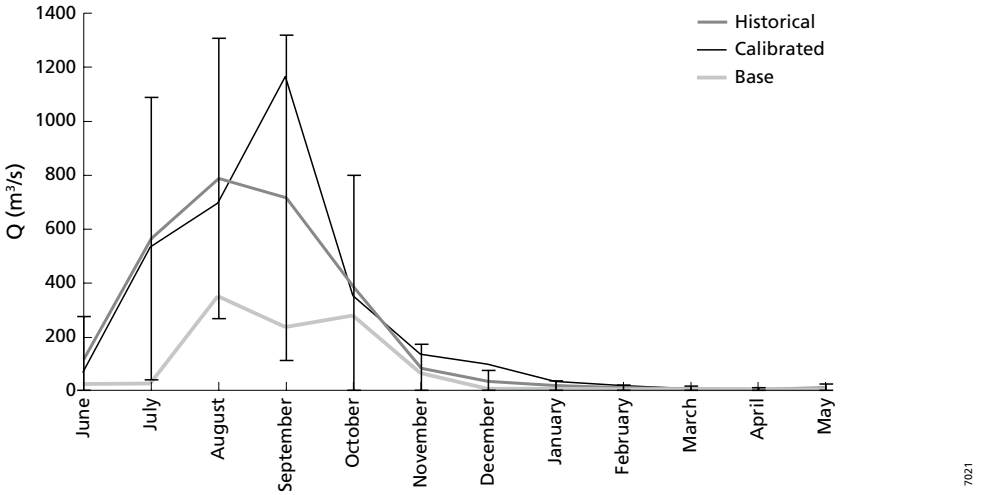

Figure 4.9 Historical observed and simulated (base and calibrated) discharges at the outlet of the catchment. Error bars around the observed historical series denote one standard deviation based on the 1970-1996 time series.

area of RNGE. ET_{act} of AGR3 seems to be overestimated and ET_{act} of RNGE seems to be underestimated. On subbasin scale these differences level out and the results are good, however the variation in SWAT ET_{act} at HRU level was larger. This was a result of the fact that PEST optimises monthly ET_{act} at sub basin level and not at HRU level.

Discharge data of the simulation period are unavailable and even if measured discharge would be available, their use in calibration would be questionable, given the fact that stream flow is completely human controlled in the catchment. A qualitative control on measured discharge was however performed using historical data from 1970 to 1996. The discharges of the entire catchment were used for comparison with the model simulations. Figure 4.9 shows the historical observed and simulated discharges for the base and calibrated models. The calibrated model mimicked the observed discharges better than the base model. The simulated calibrated discharges in 2004-2005 were well within one standard deviation of the average measured discharges between 1970 and 1996. December was an exception and modelled discharges were slightly higher. It should be noted though, that the coefficient of variation in the observed discharges were large and range from 66% in August to 160% in May. Further validation of actual discharges during the simulation period (2004-2005) is recommendable; however these data were not available.

4.5 Discussion and conclusion

This study showed that the spatially distributed hydrological model SWAT can potentially be successfully calibrated using the GML algorithm and remotely sensed derived evapotranspiration from a time series of MODIS images in a data scarce area. The best results were obtained by optimising a combination of soil, meteorological, and groundwater related parameters for an eight month time series of sub-basin actual evapotranspiration. Optimising a total of 53 variables

using 920 monthly observations increased the r^2 between SEBAL and SWAT ET_{act}, significantly, from 0.40 to 0.81. A validation with historical measured discharges revealed that the modelled discharges are well within one standard deviation of the observed data. Separate optimisation runs revealed that ET_{act} is more sensitive to the groundwater and meteorological parameters than to soil and land use parameters. On sub-basin level the ET_{act} showed least response to the land cover dependent maximum leaf area index. Furthermore, it can be concluded that at the HRU level more work is required to fine-tune the calibration procedure. The calibration was only reliable at the spatial and temporal scale on which the observations, used in the optimisation, were based. Future work should focus on calibration strategy that incorporates HRU level ET_{act} observations and discharges at a high temporal resolution in the objective function.

In this study, the gradient search GML algorithm was used in the optimisation although this method is sometimes sensitive to local minima, especially when non-linear processes are modelled. However, a time series of spatially distributed ET_{act} exhibits more linear behaviour than discharge at a limited number of locations. Moreover, it has been shown that global search algorithms require much more function calls to identify the global minimum. SWAT was recently used in the evaluation of a number of optimisation algoritms; Shuffled Complex Evolution, real-valued simple Genetic Algorithm, multi-start Simplex and Monte Carlo Sampling and a new algorithm called the Global Greedy Search algorithm (Tolson and Schoemaker, 2006). For two case studies a maximum of 2500 (6 parameters) respectively 6000 (14 parameters) SWAT model calls were required. The GML algorithm is much more efficient in this respect (Skahill and Doherty, 2006) and for the best performing optimisation (53 parameters) in this study 2987 model calls were required. We therefore conclude that PEST and the GML algorithm served our objectives best.

Traditional calibration on a limited number of discharge stations lumps all hydrological processes together and chances on the occurrence of the equifinality problem are much larger. In this study we showed that using spatially distributed ET_{act} observations with a monthly temporal resolution provide a promising alternative. The success of the approach lays in the spatial and temporal isolation of the calibration problem at hand. Information content of a time series of discharges at the outlet of a catchment is simply insufficient to attribute deviations between observation and simulation to specific processes at a specific location at a specific point in time. Using spatial data constrains the spatial distribution of fluxes, but the equifinality problem may still occur at the scale of a HRU given the large number of parameters in the SWAT model. Franks and Beven (1997, 1999) utilised the function similarity concept and use representative parameter combinations at the unit scale, which are not necessarily correct, but produce the correct output. Although it is important to consider this issue of equifinality at the HRU scale we believe that using function similarity concept compromises the understanding of hydrological processes. The approach of this study offers a basically unlimited number of observations in time and space and adding information on for example stream flows or groundwater heads to the objective function may further reduce equifinality issues without compromising parameterisation of essential hydrological processes. Adding other independent sources of information may also further substantiate the reliability of SEBAL estimates of ET_{act}. Although we have found very good results at the sub basin level on a monthly time step, further study is required to increase the reliability of the results in space (at HRU level) and time (weekly or daily).

One of the variables used in the optimisation is a monthly rainfall increment. It is generally not common practice to vary model excitations in a calibration procedure; however we believe

that in this case it was legitimate. Precipitation data used in this study was based on TRMM for two important reasons: (i) station data for the simulation period are unavailable and (ii) there is a large spatial variation in precipitation that is not captured by using a limited number of meteorological stations. However using raw TRMM data would result in unreliable absolute precipitation amounts and the TRMM precipitation is scaled with data from 11 meteorological stations within the catchment using linear regression and data between 1998 and 2004. The r^2 values between monthly TRMM and observed rainfall for these stations range from 0.29 tot 0.81 with an average of 0.59. Both TRMM as well as the observed station data are subject to error, which cannot be isolated. Considering this it was justifiable to use monthly RFINC as calibration parameter. No changes occur in the spatial distribution of rainfall and average adjustment in precipitation is only -13 mm/month with an maximum in December (21 mm) and a minimum in April (-29 mm) for the best performing optimisation.

The calibration period covers only eight months and a longer time scale would be preferable. Presently longer time series of remotely rensed ET_{act} are unavailable, but this might changes in the future. An attempt to develop a standard MODIS ET product has recently been abandoned (Running et al., 1995), but Mu et al. (in press) have recently suggested a potential globally applicable methodology based on the Penman-Monteith equation, MODIS data and global meteorology data.

The monsoon period is not covered in the calibration, because of the absence of cloud free imagery. SEBAL depends on the visible, NIR en thermal IR part of the spectrum which is hampered by clouds. A viable alternative could be to incorporate radar based soil moisture and measured discharges in a combined objective function during the monsoon months in order to appropriately calibrate the model in the monsoon season. No parameters directly related to runoff were included in the calibration. The curve number for example is normally a common parameter to included and is known to be a sensitive parameter to control runoff. The calibration period did, however, not include the monsoon and rainfall, and thus runoff are small during the calibration period, which renders it unsuitable for calibration. However runoff during the monsoon influence initial soil moisture condition and more importantly reservoir inflow. Therefore to be able to realistically model reservoir storages, erosion and nutrient loads it is recommendable to calibrated runoff in the monsoon months in addition to ET_{act} in the other months through a combined objective function.

Realistic simulations during the dry period from October to May are also more important than the monsoon period. Runoff is not a critical issue, but ET management, water shortage and irrigation are the dominant hydrological issues relevant to water managers.

Differences in space and time in ET_{ref} between SEBAL and SWAT were caused by spatial altitude dependent operations, which SEBAL performs on important parameters. The DEM was used to correct air pressure and density and thus the psychometric constant. The DEM was further used to correct the absorbed solar radiation values for slope and aspect. Southern facing terrain, due to the angle of incidence, absorbs more solar radiation per unit land than the northern facing slope. Another cause of the difference in ET_{ref} is the fact that SEBAL uses grass as a reference crop and SWAT uses alfalfa. We showed that a near perfect match between observed and measured ET_{ref} after inferring a small adjustment (average = 3.5%) of monthly radiation.

In this study it was assumed that ET derived with SEBAL provides an independent measurement of ET. Although much more closely tied to direct observations than a process based prognostic model such as SWAT, it must be acknowledged that SEBAL still is a diagnostic model.

Remotely sensed surface temperatures and vegetations characteristics are used to model ET fluxes using the energy balance as a basis. This has clear advantages as it eliminates problematic spatially distributed input data requirements. Since the basis for ET calculation in SWAT (hydrological and process based) is completely different from SEBAL (energy balance based) it is legitimate to use SEBAL ET as a data source for calibrating SWAT. It should be acknowledged though that the true test of the applicability of this calibration approach should be further investigated in the future in a catchment where natural flows are measured and used as an independent verification. Additional validation with discharge data in this case could only be based on historical data, because of lack of data. Another compromising factor is that stream flow in the catchment is mainly human controlled through a cascade of reservoirs and local water storage facilities and are therefore less suitable for validation. The key objective of this study was to introduce an innovative calibration procedure based on remotely sensed ET_{act}, especially targeted for these kinds of data scarce human controlled catchments.

In developing countries, where lack of data is an issue and the planning process needs to be supported by scientific sound measures, the innovative use of remote sensing in hydrological model calibration as presented in this study will contribute to the prevention of disasters and improve sustainable management in the long term. Recently, interest in using simulation models in ungauged or sparsely gauged basins has increased leading to some concerted actions. The most relevant is the Prediction in Ungauged Basin (PUB) initiative; an International Association for Hydrological Sciences (IAHS) initiative for the decade of 2003-2012, aimed at uncertainty reduction in hydrological practice (Sivapalani et al., 2003). PUB focuses the development of new predictive approaches that are based on "understanding" of hydrological functioning at multiple space-time scales. This study provided an ET based innovative approach at different temporal and spatial scale that fits well into the PUB science program.

5 Integrating remote sensing and a process-based hydrological model to evaluate water use and productivity in a south Indian catchment

Based on: Immerzeel, W.W., A. Gaur & S.J. Zwart (2007), Integrating remote sensing and a process-based hydrological model to evaluate water use and productivity in a south Indian catchment (in press)

Abstract

The combined use of remote sensing and a distributed hydrological model have demonstrated the improved understanding of the entire water balance in an area where data are scarcely available. Water use and crop water productivity were assessed in the Upper Bhima catchment in southern India using an innovative integration of remotely sensed evapotranspiration and a process based hydrological model. The remote sensing based Surface Energy Balance Algorithm for Land (SEBAL) was used to derive an eight month time series of observed actual evapotranspiration from October 2004 to May 2005. This dataset was then used in the calibration of the Soil and Water Assessment Tool (SWAT). This hydrological model was calibrated by changing 34 parameters to minimize the difference between simulated and observed actual evapotranspiration. The calibration efficiency was assessed with four different performance indicators. The calibrated model was used to derive a monthly basin water balance and to assess crop water productivity and crop water use for the irrigation year 2004-2005. It was found that evapotranspiration is the largest water loss in the catchment and total evaporative depletion was 38,172 Mm^3 (835 mm). Of the total evaporative depletion 42% can be considered as non-beneficial and could be diverted to other beneficial utilization. Simulated crop water productivities for sugarcane, sorghum and winter wheat are relatively high at 2.9 kg/m^3, 1.3 kg/m^3 and 1.3 kg/m^3 respectively. The frequency distributions of crop water productivity are characterised by low coefficient of variation, yielding limited scope for improvement in the agricultural areas under the current cropping systems. Further improvements in water productivity may however be achieved by shifting the crop base from sugarcane to a dual crop and introducing a fallow period from March to May or by converting non-productive rangelands to bio fuel production or other agricultural land uses.

5.1 Introduction

The Krishna River Basin (258,948 km^2) in semi-arid southern India is the fourth largest in India in terms of annual discharge, and the fifth in terms of surface area. The basin covers parts of three south-Indian states: Maharashtra (27%), Karnataka (44%), and Andhra Pradesh (29%). After independence (1947), a major national objective was the rapid harnessing of the country's water resources potential, which resulted in a surge of developments from 1960 onwards and a drastic reduction in river discharge. The massive proposed irrigation schemes promoted interstate water conflicts. The Krishna basin as a whole is now nearly a closed basin (Gaur et al., 2007).

A major part of the water available in the Krishna basin originates from the humid regions of the Western Ghat mountains where precipitation exceeds 5,000 mm. The Upper Krishna and Upper Bhima catchments served by Western Ghats are, therefore, two very important catchments out of 12 major catchments in Krishna basin. These two catchments contribute significantly to Krishna river flows for downstream use. The Upper Bhima cathment is additionally important for the state of Maharashtra in the context of serving inter-sectoral water demands including hydropower, agriculture and drinking water supplies. Following the increase in utilization, the water released to the main stem of the Krishna from the Upper Bhima catchment has declined by 59% from an average of 8,816 Mm^3 in 1970-80 to 3,615 Mm^3 during 1994-2004, and is mainly concentrated in the monsoon months June to September (Government of Maharashtra, 2005). During the last 20 years, a shift in agricultural practices towards more water consuming crops, such as sugarcane, took place. The sugarcane area, for example, has almost tripled during this period. An increased competition for water resources between agriculture and the industrial and domestic sectors may lead to a decrease in food production and to environmental degradation. The agricultural sector, being the largest consumer of water, should therefore focus on enhancing the productivity of water through (i) improving the production per unit of water consumed, or (ii) by maintaining the same production while reducing water use (Kijne et al., 2003; Rijsberman, 2006). Better knowledge on fresh water depletion and crop production patterns throughout a basin is essential for water managers and policy makers to improve water management in areas where water productivity is low. Traditional water management techniques often focus on water saving at field level by reducing irrigation water allocation to fields. However, a plot level saving may not necessarily lead to 'real' water savings at the basin scale, as excess water can be reused downstream (Keller and Keller, 1995). Water management should, therefore, focus on a reduction of water depletion by evapotranspiration and increasing water productivity, as this water is not available for reuse. Therefore, water productivity in this study is defined as the marketable crop yield over the seasonal water use by actual evapotranspiration (ET_{act}).

Remote Sensing and distributed hydrological models are indispensable tools in objectively quantifying water depletion, water balance components, agricultural yields and water productivity in areas where data is scantily available. This paper shows how the hydrological model Soil and Water Assessment Tool (SWAT) (Arnold et al., 1998; Srinivasan et al., 1998) can be applied to simulate the catchment's water balance, quantify water depletion per land use, and to analyze crop water productivity per agricultural system. Using an innovative methodology, the SWAT model is calibrated using Remotely Sensed ET_{act} based on the Surface Energy Balance Algorithm for Land (SEBAL) algorithm (Bastiaanssen et al., 1998; Bastiaanssen et al., 2005). This approach is unique in the sense that Remote Sensing is completely integrated in the calibration of a hydrological model. Traditionally hydrological models are calibrated using measured hydrographs.

Lack of data and absence of natural flows generally compromise the calibration of such models. The approach demonstrated in this paper provides an innovative methodology to assess water resources in drought prone catchments with limited data availability.

5.2 Study area

The Upper Bhima catchment has a total area of 45,678 km^2 and is located between 16.5°-19.5° N and 73.0°-76.5° E and comprises of the catchment area of the river Bhima from its source to its confluence with the Sina River. The Sina River drains the north western part of the catchment. The elevation ranges from 414 meter in the east to 1458 meter in the Western Ghat mountains, while 95% of the catchment is below 800 meter and relatively flat.

The catchment has a highly diverse climate mainly caused by the interaction between the monsoon and the Western Ghat mountain range (Gunnel, 1997). The normal annual precipitation varies from 5000 mm in the mountains in the Western Ghats to less than 500 mm in the eastern part of the catchment with an average of 642 mm. During the study period, 2004-2005, the average precipitation was 842 mm, which is 31% more than average (Figure 5.1). A total of 61% of the area received less than 750 mm and 25% more than 1,000 mm.

Figure 5.2 shows the monthly precipitation (P) and reference evapotranspiration (ET_{ref}) in the basin, as well as the minimum and maximum temperatures. The catchment has a high annual ET_{ref} (1814 mm) ranging from 224 mm/month in May to 108 mm/month in December. Over 90% of the annual precipitation occurs during the monsoon months June to September. Between October and May large precipitation deficits occur with the peak in May (211 mm) just before the onset of the monsoon. The minimum temperature ranges from 12 °C in December 2004 to 25 °C in May 2005, while the maximum temperature ranges from 30 °C in august 2004 to 40 °C in May 2005.

The large amounts of precipitation in the Western Ghat range are retained in a chain of reservoirs and excess is released to downstream areas, especially along the Bhima tributary. The reservoirs accumulate water during the monsoon season (June to September), and supply the water during the monsoon as well as throughout the irrigation season (October to May). Flows in the rivers are therefore mainly human controlled and respond less directly to variations in the climate excitations and biophysical conditions.

Agriculture in the upper Bhima catchment is characterised by a diverse cropping pattern of sugarcane, sorghum, wheat, corn, millet, groundnut, grass fodder and a variety of horticultural crops (Neena, 1998). Three main types of agricultural systems can be identified in the catchment: (i) rainfed agriculture with a single crop cultivated during the monsoon (RFA) such as maize, millet, pulses and sorghum, (ii) supplemental irrigated agriculture with one rainfed crop during the monsoon (e.g. rice, maize, sorghum) and a groundwater irrigated crop grown during winter (e.g. winter wheat, sorghum, vegetables) (SIA) and (iii) irrigated perennial crops (e.g. sugarcane, horticulture) (SIUG) (Figure 5.4). These crops are grown throughout the year the majority is irrigated the reservoirs.

The normalized difference vegetation index (NDVI) patterns of these land use classes are shown in Figure 5.3. The natural NDVI peak was just after the monsoon early October and the NDVI of the irrigated agriculture classes remained relatively high also after the wet period. The

sugarcane NDVI was still as high as 0.35 at the end of May. Other non-agricultural land covers in the catchment include rangelands, mixed forests, evergreen forests and water surfaces.

Most of the catchment lies on granite, zeonite and basalt rocks, that all contain considerable stocks of groundwater. Groundwater levels, however, vary greatly both in space and time.

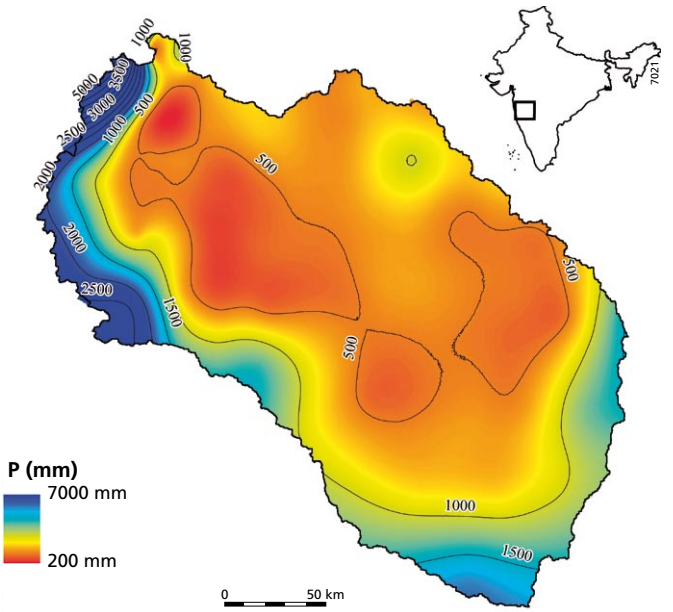

Figure 5.1 Upper Bhima catchment boundary and isohyets of total precipitation from June 2004 to May 2005

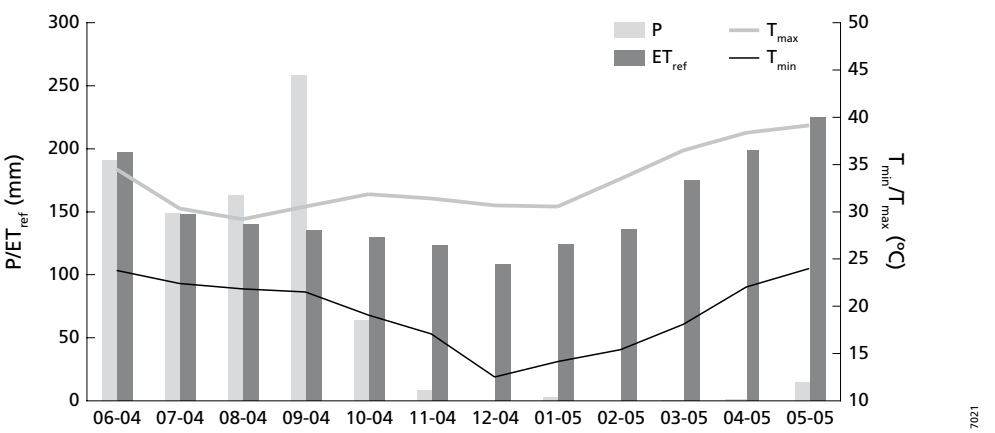

Figure 5.2 Monthly precipitation (P), reference evapotranspiration (ET_{ref}), minimum (T_{min}) and maximum temperature (T_{max}) averaged for two meteorological stations (Pune, Sholapur).

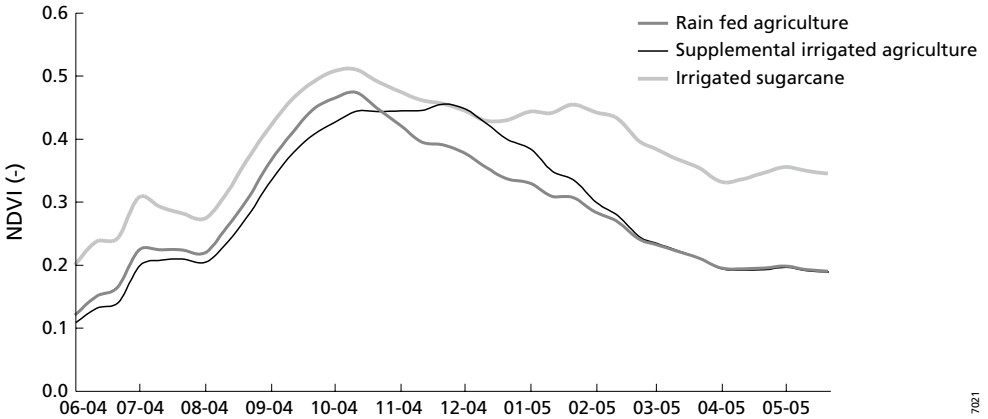

Figure 5.3 Average 10-daily NDVI patterns for the agricultural land use classes from June 2004 to May 2005, measured by the SPOT-VGT sensor.

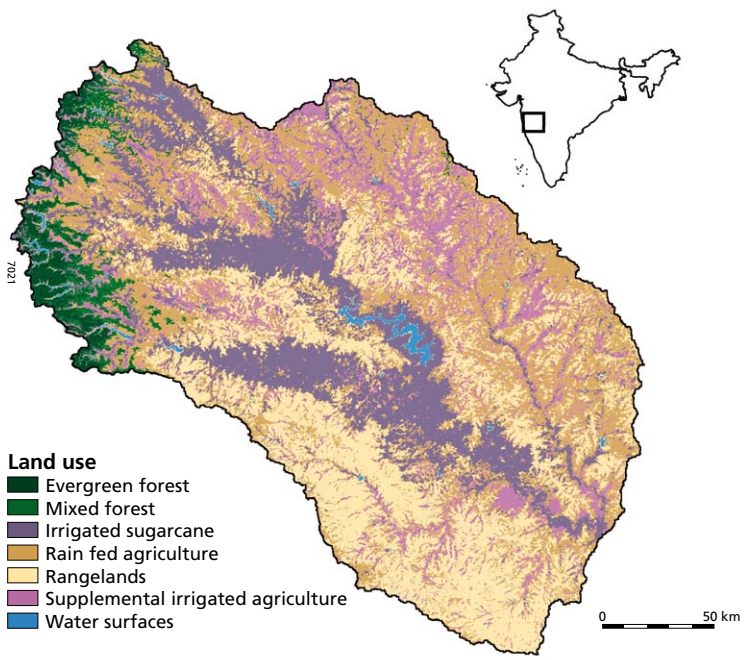

Figure 5.4 Land use based on unsupervised classification of MODIS time series of NDVI imagery with a spatial resolution of 250 meter.

Table 5.1 Soil properties of major soils in the catchment based on the digital soil map of the world (FAO, 1998). Ksat is the saturated hydraulic conductivity and AWC is the Available Water Capacity.

Soil code	Description	Layer	Depth (cm)	K_{sat} (mm/hour)	AWC (cm/cm)	Clay (%)	Silt (%)	Sand (%)
Be66-2c	Eutric Cambisols	top soil	30	0.2	0.22	22.9	37.2	39.9
		sub soil	98	0.21	0.22	22.2	34.2	43.6
Bv12-3b	Vertic Cambisols	top soil	30	0.13	0.10	48.3	21.0	30.7
		sub soil	113	0.09	0.01	49.9	20.7	29.3
Hh11-2bc	Haplic Phaeozems	top soil	30	0.17	0.22	28.0	26.2	45.8
		sub soil	107	0.14	0.07	28.3	23.1	48.6
I-Hh	Lithosols	top soil	30	0.18	0.31	21.8	23.0	55.3
		sub soil	65	0.16	0.11	20.8	20.3	58.8
Lc75-1b	Chromic Luvisols	top soil	30	0.18	0.38	25.9	19.9	54.2
		sub soil	113	0.13	0.05	30.3	21.0	48.6
Nd51-2b	Dystric Nitosols	top soil	30	0.21	0.60	25.9	17.6	56.5
		sub soil	195	0.19	0.14	35.3	18.2	46.5
Vc43-3ab	Chromic Vertisols	top soil	30	0.11	0.05	51.7	23.7	24.6
		sub soil	113	0.06	0.01	54.6	22.9	22.5
Vc44-3a	Chromic Vertisols	top soil	30	0.11	0.07	55.6	19.7	24.6
		sub soil	125	0.06	0.01	58.7	18.9	22.5
Vc45-3a	Chromic Vertisols	top soil	30	0.12	0.07	55.4	23.8	20.8
		sub soil	125	0.07	0.01	57.0	22.2	20.7
Vp42-3a	Pellic Vertisols	top soil	30	0.23	0.32	60.4	16.5	23.1
		sub soil	125	0.16	0.02	61.6	15.7	22.7

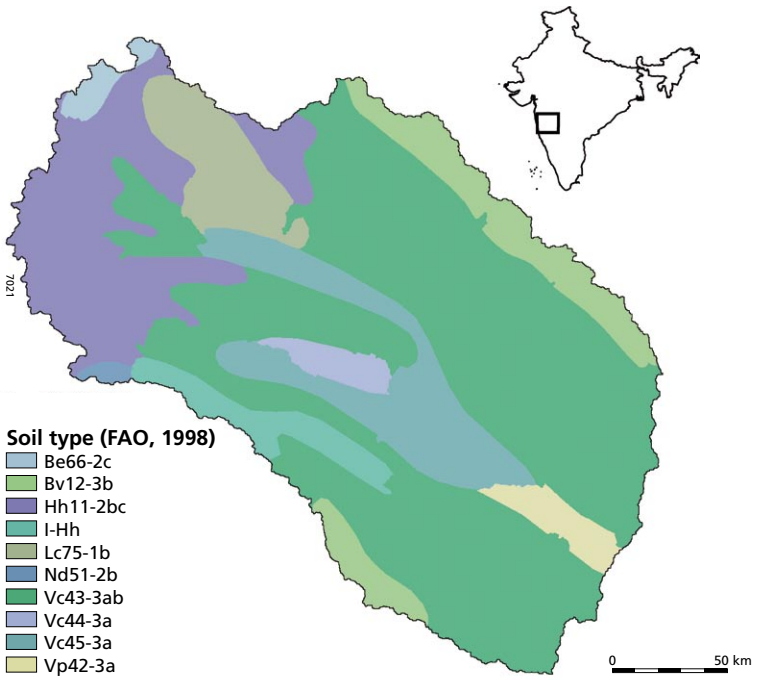

Figure 5.5 Soil types based on the digital soil map of the world (FAO, 1998)

According to the FAO digital soil map of the world (FAO, 1998) ten different soil units are identified in the catchment. The alluvial plains are predominantly characterized by vertisols, while the Western Ghats and steeper slopes by luvisols (Figure 5.5). A further description of the soil types is provided in Table 5.1.

5.3 Methodology

5.3.1 Evapotranspiration mapping

SEBAL (Bastiaanssen et al., 1998; Bastiaanssen et al., 2005) was applied to estimate total ET_{act} spatially between October 2004 and May 2005. During the monsoon period, June to September, cloudy conditions prevented the application of SEBAL. SEBAL uses satellite imagery from sensors measuring the visible, near-infrared and thermal radiation. The latent heat flux (*LE*) was computed on a pixel-by-pixel basis as a residual of the energy balance:

$$LE = R_n - G - H \quad (1)$$

Where R_n is the net radiation (W/m²), G is the soil heat flux (W/m²), and H is the sensible heat flux (W/m²). The net radiation (R_n) is the actual radiation that is available at the earth surface, which is equal to the sum of the net shortwave and longwave radiation. The former was computed as a function of the surface albedo, while the latter was computed from the difference between

Table 5.2 Acreages, crops, and growing season of different land use classes in the upper Bhima catchment

Land use class	Crops	Growing season	Area (km^2)	Area (%)
Water surfaces (WATR)	-	-	411	1
Rangelands (RNGE)	-	-	12242	27
Rain fed agriculture (RFA)	Sorghum (SGHY)	10/6 - 30/9	15348	34
Supplemental irrigated agriculture (SIA)	Sorghum (SGHY)	10/6 - 30/10	6121	13
	Winter wheat (WWHT)	15/10 - 0/2		
Irrigated sugarcane (ISUG)	Sugarcane (SUGC)	1/6 - 31/5	9090	20
Evergreen forest (FRSE)	-	-	1416	3
Mixed forest (FRST)	-	-	1051	2

incoming and outgoing longwave radiation. Incoming longwave radiation was calculated using a modified Stefan-Boltzmann equation that uses an apparent emissivity, which is coupled to an atmospheric transmissivity and a measured air temperature. The outgoing longwave radiation was calculated using the Stefan-Boltzmann equation with a calculated surface emissivity and a surface temperature measured by the satellite sensor. The soil heat flux (G) was estimated as a fraction from R_n, surface temperature and NDVI. The sensible heat flux (H) was estimated from surface temperature, surface roughness and measured wind speed. An essential step in the application of SEBAL is the solution of extreme values for H, prior to the pixel-by-pixel computations. In desert surroundings H is considered equal to R_n-G, while for water surfaces H is equal to 0.

SEBAL was applied on 16 cloud free satellite images that were recorded by the Aqua sensor onboard the Moderate Resolution Imaging Spectrometer (MODIS). Initially SEBAL solved the instantaneous surface energy balance at the moment of overpass from the satellite sensor. ET_{act} sums for 2-week periods were obtained by re-applying the SEBAL models with average meteorological measurements for the 2-week periods and by assuming certain bio-physical parameters constant throughout the period. These parameters include surface albedo, NDVI, emissivity, evaporative fraction, surface roughness and bulk surface resistance. The final maps of ET_{act} have a spatial resolution of 250 m.

5.3.2 Land use classification

A land use map was derived from remote sensing data and was based on an unsupervised land use classification using a time series of 16 MODIS derived NDVI images with a spatial resolution of 250 meter from October 2004 to May 2005. The time series used for the land use classification was similar to the SEBAL analysis. The distinction between the temporal patterns of NDVI of major land use classes provides sufficient information to derive a land use classification. Firstly, an unsupervised classification with a large number of classes (15) was performed. Secondly, using an existing land use map of low spatial resolution (500 m) in combination with limited field survey data in the upstream part of the catchment, the 15 classes were attributed to the seven main land use classes in Table 5.2. Finally the classified land use map was visually cross-checked with high resolution satellite imagery.

5.3.3 Data preparation

A digital elevation model (DEM) acquired with the shuttle radar topographic mission (Rabus et al., 2003) was used. The original spatial resolution of the DEM was 90 meter, but for model efficiency and compatibility with the land use map the DEM were resampled to a resolution of 250 meter with a similar extent as the land use map.

The digital soil map of the world (FAO, 1998) is accompanied by a database with soil properties. This database is used to parameterise the SWAT model. For this study each soil type is schematised as a representative profile consisting of a top and sub soil. A description of the top and sub soils of the ten soil types and the most important derived soil hydraulic properties are shown in Table 5.1.

Daily data on radiation, wind speed, relative humidity, and air temperature for two different meteorological stations (Pune and Sholapur) were used (Figure 5.1). These data were used to calculate reference evapotranspiration. Precipitation data were available at a more detailed spatial scale. Monthly precipitation data for 52 municipalities were collected for the period under study (June 2004 – May 2005). The precipitation was attributed to the centre point of the municipality and spatially interpolated to monthly grids with a resolution of 250 meter. These grids were then used as input in the SWAT model.

5.3.4 Application of SWAT

SWAT is a distributed hydrological model providing spatial coverage of the entire hydrological cycle including atmosphere, plants, unsaturated zone, groundwater and surface water. The model is comprehensively described in literature (Arnold et al., 1998; Srinivasan et al., 1998).

A number of key processes are described in more detail.

The Penman-Monteith method (Monteith, 1965) was used in SWAT to calculate daily ET_{ref} for alfalfa and potential plant transpiration (T_p). ET_p deviates from ET_{ref}, because actual daily crop height and leaf area index (LAI) are used to determine the aerodynamic resistances and canopy resistances respectively. Potential soil evaporation is an exponential function of ET_{ref} and the soil cover and is further reduced during periods with high plant water use. Actual soil evaporation is limited by the soil water content (θ) and is reduced exponentially when θ drops below field capacity.

To calculate actual plant transpiration the potential plant water uptake is defined by (Neitsch et al., 2002)

$$w_{p,z} = \frac{T_p}{[1 - e^{\beta_w}]} \cdot \left[1 - e^{\left(-\beta_w \cdot \frac{z}{z_{root}} \right)} \right] \qquad (2)$$

Where $w_{p,z}$ (mm H_2O) is the potential plant water uptake from the soil surface to a specified depth z (cm) from the soil surface on a given day, T_p (mm) is the maximum plant transpiration on a given day taken from a lookup table, β_w (-) is the water use distribution parameter, z is the depth from the soil surface (mm), and z_{root} is the depth of root development in the soil (mm). Actual plant water uptake equals actual plant transpiration is reduced exponentially when θ drops below field capacity, similar to soil evaporation. ET_{act} is the sum of interception, actual soil evaporation and actual plant transpiration.

For each day of simulation, potential plant growth, i.e. plant growth under ideal growing conditions, was calculated. Ideal growing conditions consist of adequate water and nutrient

supply and a favourable climate as depicted in the T_p. Firstly, the absorbed photosynthetical active radiation was computed from intercepted solar radiation as a function of LAI, followed by a Light Use Efficiency that is in SWAT essentially a function of carbon dioxide concentrations and vapor pressure deficits. Actual growth was calculated from optimal growth by inferring stress factors for extreme temperatures and water and nutrient deficiencies. The crop yield was computed as the harvestable fraction of the accumulated biomass production across the growing season.

The first step in setting up a SWAT model is the subdivision of the catchment into sub-basins and a river network based on the DEM. Based on unique combinations of soil and land use the sub-basins were further detailed into hydrological response units (HRUs), which are the fundamental units of calculation. A total of 115 sub basins and 768 HRUs were delineated in the Upper Bhima catchment. The HRUs are then further parameterized. Soil parameters were attributed to the HRUs according to the data provided in Table 5.1. The classified land use map was linked to the SWAT land use database that provided the land use parameters. The growing seasons of the agricultural classes are shown in Table 5.2. For the three agricultural classes (RFA, SIA and ISUG) specific crop management activities (fertilization and irrigation) was specified as input to the model. It is assumed that for every fertilization application urea is used at a dose of 300 kg/ha. The irrigation amounts are based on average crop water requirements during the growing season, and based on potential evapotranspiration. RFA is fertilized once on June 22. SIA consist of a dual cropping pattern. Firstly, it was assumed that sorghum is cultivated during the monsoon and is fertilized on June 10, immediately after planting, and again on August 1. Secondly, winter wheat is fertilized thrice: October 17, November 1, and February 10. Winter wheat is irrigated on November 10 (40 mm), November 20 (40 mm), December 15 (100 mm), and January 15 (100 mm). The total amount of irrigation water applied is 280 mm. SUGC is cultivated year-round and is fertilized thrice on June 1, September 1, and January 1. In total 690 mm or irrigation water is applied to all SUGC areas in 12 monthly applications. Limited amounts are applied during the monsoon (40 mm/month) and larger amounts during the dry season from March until May (100 mm/month).

The major reservoirs are mainly located along the Bhima River. In the model, the reservoirs were clustered into two reservoirs. The majority of inflow into the reservoirs occurred during the monsoon and reservoirs are generally filled by October. The stored water is used for irrigation in the remainder of the season. Irrigation water is extracted from the reservoirs and the unused excess water is released using a monthly distribution derived from historical measurements.

The model was run with a daily timestep from June 1, 2004 to May 31 2005. Outputs of the SWAT model comprise:

- Water balance components at HRU, sub basin and catchment scale
- Streamflow data of each stream in the routing network, and
- Biomass production and crop yields at HRU level

5.3.5 Model calibration and validation

The parameter estimation package (PEST) was used to calibrate the SWAT model. PEST is a non-linear optimisation software package based on the Gauss-Marquardt-Levenberg algorithm (Doherty, 2005). PEST is able to run a model as many times as it needs to while adjusting its parameters until the discrepancies between selected model outputs and a complementary set of measurements is reduced to a minimum. It calculates the optimal parameter set for which the

sum of the squared deviations between model-generated results and experimental observations is reduced to a minimum (**Φ**). Expressing this mathematically, the objective function **Φ** needs to be minimised, where **Φ** is defined by the equation:

$$\Phi = \sum_{i=1}^{n} (O_i - M_i)^2 \quad (3)$$

Where n equals the total number of observation, O_i is the observed value on timestep i, and M_i is the modelled value on timestep i. For linear models minimization can be achieved in one step, whereas for non-linear problems it is an iterative process. At the beginning of each iteration the relationship between model parameters and model-generated outputs is linearised by formulating a Taylor expansion about the currently best parameter set. Hence, the derivatives of all observations with respect to all parameters must be calculated. This linearised problem is then solved for a better parameter set, and the new parameters tested by running the model again.

In this study SWAT simulated actual evapotranspiration ($ET_{act, SWAT}$) is calibrated using monthly SEBAL derived ET_{act} ($ET_{act, SEBAL}$) using PEST. The total time series spans eight months and the spatial calibration scale is the smallest possible SWAT scale (HRU). The $ET_{act, SEBAL}$ are first aggregated per month per HRU. PEST was then used to minimize the difference between the squared deviations between $ET_{act, SEBAL}$ and $ET_{act, SWAT}$. Only HRUs from non-water surface were used (668), resulting in a total of 5344 (8 months x 668 HRUs) observations that were used in the calibration. A number of important model parameters that have a large influence on ET_{act} have been included in the calibration:

- *Available water capacity (AWC).* The AWC is defined as the difference between the field capacity of the soil and the permanent wilting point. It is defined per soil layer per soil type and determines, to a large extent, the water holding capacity of the soil. In this case one AWC was defined per soil type. Ten different soil types resulted in ten different parameters to be optimized. The AWC was bound by the range 0.05 mm/mm and 0.30 mm/mm.
- *Groundwater revap coefficient (REVAP).* Water may conceptually move from the shallow aquifer into the overlying unsaturated zone. The process of water being evaporated from the capillary fringe in dry periods is referred to as groundwater revap and in SWAT quantified by REVAP multiplied by ET_{ref}. One REVAP for each land use, except water, was defined (6 parameters) and bound by the range 0.7-1.0.
- *Maximum canopy storage (CAN).* CAN determines for a large part the interception of precipitation. Actual interception is a function of actual LAI and maximum LAI, at which CAN is defined. One CAN was defined for each non-water land use resulting in 6 parameters bound by the range 0-10 mm for non-forested land uses and 0-20 mm for forests.
- *Soil evaporation compensation factor (ESCO).* ESCO determines to what soil depth evaporation of the soil is permissible to sustain evaporative demand. As the value for ESCO is reduced, the model is able to extract more of the evaporative demand from lower levels. For each non-water land use one ESCO parameter was optimised and bound by the range 0.01-1.00.
- *Plant uptake compensation factor (EPCO).* EPCO is similar to ESCO, but for plant water uptake. As EPCO approaches 1.0, the model allows more of the water uptake demand by plants to be met by lower layers in the soil. For each land use class one EPCO parameter was optimised and bound by the range 0.01-1.00.

This definition resulted in 34 (10 x AWC+6 x REVAP+6 x CAN+6 x ESCO+6 x EPCO) parameters to be optimised. To be able to capture the spatial heterogeneity most parameters are optimized per land use class, because land use information is available at relative high level of detail compared with the soil information (Figure 5.4 and Figure 5.5). Other studies have used a similar approach (Immerzeel and Droogers, 2007).

The efficiency and performance of the SWAT model calibration was assessed according to four commonly used indicators (Hoffmann et al., 2004).

Firstly, the Pearson correlation coefficient (r) between the $ET_{act, SEBAL}$ and $ET_{act, SWAT}$ was calculated. A value of 1 yields perfect correlation, and a value of 0 indicates that $ET_{act, SEBAL}$ and $ET_{act, SWAT}$ are uncorrelated.

Secondly, the Nash-Suthcliffe model efficiency (Nash and Sutcliffe, 1970) was determined, which is given by

$$1-\sum_{i=1}^{n}(M_i-O_i)^2/\sum_{i=1}^{n}(O_i-\overline{O_i})^2 \quad (4)$$

The values range between $-\infty - 1$ and the higher the value the more efficient the calibration. A negative value indicates that the mean value of the observed values would have been a better predictor than the simulated values with the SWAT model.

Thirdly, the bias was determined, which is given by

$$\sum_{i=1}^{n}M_i \Big/ \sum_{i=1}^{n}O_i - 1 \quad (5)$$

The bias reveals to which degree the modelled value is over or underestimated.

Finally, the root mean square error (RMSE) was assessed, which is given by

$$\left(\sum_{i}^{n}(O_i-M_i)^2/n\right)^{1/2} \quad (6)$$

The RMSE provides information on the average error between the $ET_{act, SEBAL}$ and $ET_{act, SWAT}$.

The results of the calibrated SWAT model were validated using discharge measurements at the outlet of the Upper Bhima catchment. Since the flows in the rivers are mainly controlled by artificial releases from the reservoirs some caution is warranted. For this reason only total observed and modelled monthly discharge out of the catchment from June 2004 to May 2005 have been compared.

5.3.6 Water productivity analysis

In general there are three different types of crop water productivity that can be distinguished:

- Technical water productivity (kg/m^3) defined as the mass of product per unit of water consumed.
- Economic water productivity (\$/m^3) defined as net private benefits per unit of water consumed.
- Socio-economic water productivity (\$/m^3) defined as the net social benefits per unit of water consumed, which are difficult to value.

Depending on whether a system is food scarce, water scarce or whether the market is completely open, one of the above crop productivities can be optimized. Clearly, the latter two are beyond

the scope of this paper, and we have limited this study to the analysis of technical water productivities.

The crop water productivity (CWP) (kg/m^3) is defined as the ratio of the crop yield (kg/ha) and $ET_{act, SWAT}$. The crop growth module of the calibrated SWAT model was used to estimate crop yields for each of the major crop cycles of the three main agricultural land use classes (RFA, SIA, ISUG). The cropping patterns were generalized as follows. For the rainfed crops it was assumed that sorghum was cultivated (RFA, SIA). The winter crop for SIA was modelled as winter wheat (SIA), and sugarcane has been assumed as perennial crop (ISUG) (Table 5.2).

The SEBAL algorithm also derived biomass production from satellite radiances, which can be further converted to crop yields by multiplying with the crop harvest index. In combination with the $ET_{act, SEBAL}$ the SEBAL based CWP was then calculated. This SEBAL based CWP was then used to validate the SWAT results. This could only be done for winter crops, which are grown from October 15 to February 10 (Table 5.2), because SEBAL could not be applied during the monsoon due to clouds. Finally, the predicted crop yields simulated by SWAT were also compared to measured yields reported as census statistics.

5.4 Results and discussion

5.4.1 Land use mapping

Figure 5.4 shows the land use map of the catchment and Table 5.2 shows the acreages of each land use class as well as the crop cycles within the agricultural land uses. In total 67% of the area is under agriculture, 5% is forested, 27% is non-productive rangeland and 1% is covered by open water. The forested areas are located in the western part of catchments where slopes are steep and rainfall is high. The irrigated sugarcane is mainly situated along the major irrigation systems along the Bhima River branch, while the supplemental irrigated agriculture is more abundant along the Sina River. Rainfed agricultural exhibits a more capricious spatial pattern. The rangelands are predominantly found in the south western part of the catchment. The total cropped area shows great similarity to the district agricultural statistics. The area classified as ISUG (20%) seems to be overestimated when compared with district statistics (4%). There are several possible explanations: (i) this study assumes all perennial crops as sugarcane, (ii) due to the moderate resolution of the satellite images a pixel with mixed crops was classified as ISUG, or (iii) the statistics are not correct. An independent verification is recommendable for the future.

5.4.2 Model calibration and validation

The performance of the model was assessed according to four different indicators. Firstly, the Pearson correlation equalled 0.58, compared with 0.48 for the uncalibrated model. This means that the calibration resulted in an improved correlation between $ET_{act, SEBAL}$ and $ET_{act, SWAT}$. Secondly, the Nash-Suthcliffe model efficiency index was 0.28, which indicates that the calibrated model is a better predictor than the mean value of the observed $ET_{act, SEBAL}$ contrary to the uncalibrated case when the Nash-Sutcliffe criterion was -0.42. Thirdly, the bias equalled 0.03 mm/month, which is very low, indicating there is no systematically under- or over prediction of ET_{act}. For the uncalibrated model the bias was slightly higher (0.25 mm). Finally, the average error between $ET_{act, SEBAL}$ and $ET_{act, SWAT}$ (RMSE) was reduced from 36 mm/month to 26 mm/month. It is also interesting to see how the RMSE is related to the number of model calls that PEST requires

to minimize **Φ**. Figure 5.6 shows that after approximately 200 SWAT models calls **Φ** (and the RMSE) are minimized. This shows that the optimisation converged relatively quickly, given the number of parameters. Figure 5.7: Cumulative ETact from October 2004 to May 2005 derived with SEBAL (left) and simulated with SWAT (right). Both figures display aggregated data per HRU.

Figure 5.7 shows the spatial patterns of the sum of ET_{act} during the calibration period. The SWAT spatial patterns were generally in good agreement with the SEBAL results. There were however local differences and the SEBAL results show a larger within land use class variation,

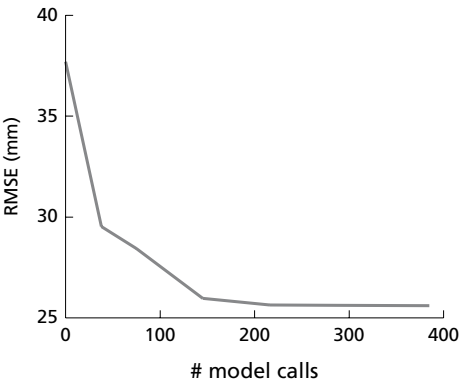

Figure 5.6 The root mean square error of modelled actual evapotranspiration (RMSE) versus the number of SWAT model calls required by PEST.

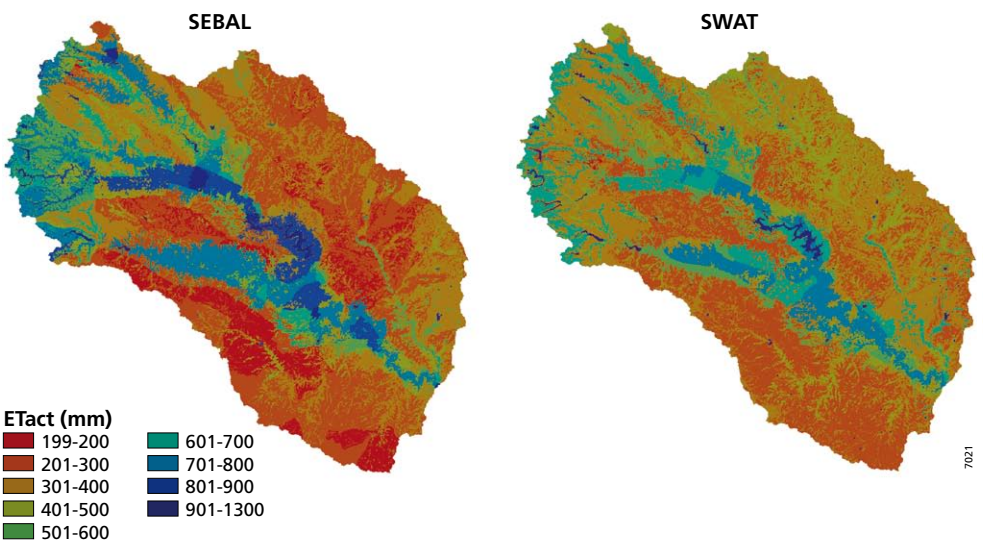

Figure 5.7 Cumulative ET_{act} from October 2004 to May 2005 derived with SEBAL (left) and simulated with SWAT (right) Both figures display aggregated data per HRU.

Table 5.3 SWAT calibration results per land use and per month; μ denotes the average ΔET_{act} and σ is the standard error, defined as the standard deviation of ΔET_{act}.

		RFA		SIA		ISUG		FRSE		FRST		RNGE		Catchment	
		μ (mm)	σ (mm)	μ (mm)	σ (mm)	μ (mm)	σ (mm)	μ (mm)	σ (mm)	μ (mm)	σ (mm)	μ (mm)	σ (mm)	μ (mm)	σ (mm)
Oct-04	base	27	23	1	30	-33	19	1	25	-7	29	17	21	5	32
	calibrated	1	22	-0	30	-15	21	10	24	5	30	12	19	0	25
Nov-04	base	21	18	-55	19	-13	33	58	45	-2	38	4	18	-6	37
	calibrated	-1	18	-20	18	-2	21	10	25	5	32	-7	17	-6	21
Dec-04	base	43	14	-19	17	34	20	80	35	42	35	28	17	25	30
	calibrated	26	13	12	12	30	15	41	22	33	26	19	15	23	16
Jan-05	base	38	17	37	15	38	15	66	22	27	23	-32	22	22	35
	calibrated	17	16	-4	13	31	13	17	20	10	19	1	15	11	20
Feb-05	base	28	22	25	22	31	21	68	21	26	18	0	27	22	27
	calibrated	7	21	13	22	22	20	16	20	8	18	3	18	11	21
Mar-05	base	15	22	11	24	-27	29	54	19	14	12	9	20	5	29
	calibrated	-12	19	-4	23	-16	25	-15	19	-11	12	-8	19	-10	22
Apr-05	base	23	23	20	25	-7	32	50	22	11	15	20	21	16	28
	calibrated	-9	21	-2	24	-22	29	-30	22	-19	15	-2	21	-9	25
May-05	base	24	28	26	34	1	39	78	24	28	19	15	28	19	34
	calibrated	-13	28	-1	32	-9	35	-13	24	-6	19	-8	28	-8	31
Total	base	27	23	6	37	3	38	57	36	17	29	8	28	14	33
	calibrated	2	24	-1	25	2	31	5	30	3	26	1	22	1	26

specifically the rangelands and irrigated sugarcane, which can be attributed to the different scales (HRU vs. pixel).

Table 5.3 provides more insight in the monthly results of the calibration per land use class. The uncalibrated results (base) are compared with the calibrated results. The calibration resulted in a considerable improvement as for all land uses, both the average monthly residual as well as the standard error, have decreased significantly. The decrease in average monthly residual between the base and calibrated model was the highest for the evergreen forests in the Western Ghat Mountains (53 mm/month). The largest decrease in standard error is found for the supplemental irrigated agriculture HRUs (12 mm/month). On a catchment scale the average residual is only 1 mm/month. It is concluded that, based on four different efficiency criteria, the calibration has clearly improved the model's capability to mimic $ET_{act, SEBAL}$.

Figure 5.8 shows the observed and modelled discharge after calibration. The observed and modelled discharges correlate very well (R^2 = 0.98) and this emphasizes the reliability of the calibration procedure. By calibrating the spatial and temporal pattern in ET_{act} using this set of parameters, the hydrogical processes related to discharge were also adequately parameterized.

5.4.3 Water balance

While remote sensing provides only information on one component of the water balance (ETact), the SWAT model is able to analyze the entire water balance as well as biomass and crop growth processes. The monthly water balance was derived from the results of the calibrated model. Figure 5.9 shows the monthly water balance for the catchment. Balance closure refers to the sum of net change in groundwater and soil storage and model inaccuracies. This storage generally decreased during the dry months and increased during the monsoon. Over the entire length of the study period there was 142 mm decrease in storage. There are many possible reasons for this large decrease in storage that could be either attributed to input data or model quality. From a data perspective there are three possible explanations. Firstly, it could be that the precipitation in the Western Ghats is underestimated. It is known that there is an extremely large increase

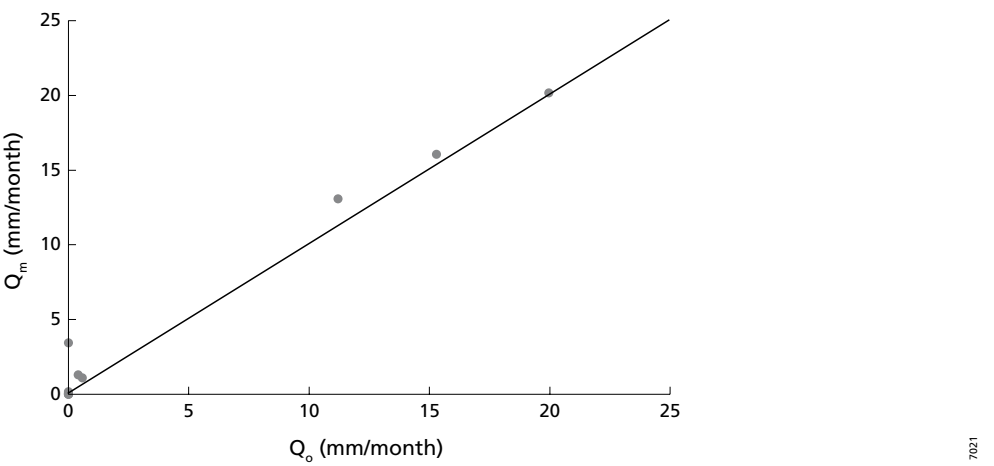

Figure 5.8 Modelled discharge at the outlet of the catchment (Q_m) versus observed discharge at the outlet of the catchment (Q_o).

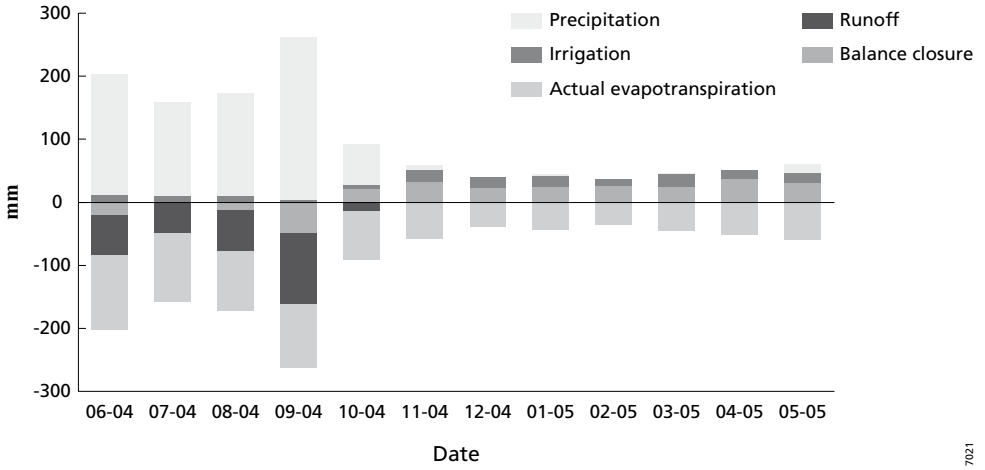

Figure 5.9 Monthly basin average water balance from June 2004 to May 2005.

in precipitation over a very short horizontal distances (Gunnel, 1997), while the density of meteorological stations is low. Secondly, there are water transfers from outside the catchment (e.g. regional groundwater fluxes) but these are not incorporated in the model. Thirdly, it could be that the ET_{act} calculated by SEBAL is too high. From a model quality perspective, it could be that the hydrogical processes related to the groundwater movement and storage are insufficiently represented and do not capture regional fluxes. This warrants further research.

The annual surface runoff coefficient (R/P) was 36% and only a slight evapotranspiration deficit was observed at catchment scale (17 mm). The runoff during the monsoon season is stored in the reservoirs and subsequently used for irrigation later in the season. There was considerable variation among monthly water balance components. The rainfall was insufficient to meet crop water requirements in the catchment from November to May and nearly all ET_{act} was met from irrigation water and storage decreases.

Discharge measurements indicate that a total of 2,167 Mm^3 (47 mm) of water was released to the main stem of the Krishna River in the irrigation year 2004-2005. This amounts to 5.6% of the total precipitation and the water was released during the monsoon months only. There was no discharge out of the catchment during the dry season. It is not possible to relate this to the simulated water balance, since there are no data on reservoir storage change available. However the dry year 2003-2004 depleted most reservoirs to dead storage levels and it is likely to assume that a considerable part of the runoff was used for increasing reservoir storage. It was not possible to isolate whether this large storage change originated from the model quality or input data.

A dynamic link with a regional groundwater model and the incorporation of reservoirs storage data could further detail the water balance and is recommendable.

Volumetric cumulative annual precipitation was 38,912 Mm^3, while annual evaporative depletion equalled 38,172 Mm^3 and ET_{act} was by far the largest water loss in the catchment. Cumulative precipitation increased mainly during the monsoon months and ET_{act} was distributed more equally throughout the year (Figure 5.10). High ET_{act} rates in the dry season were enabled by the spatial and temporal redistribution of water through the reservoir system, groundwater irrigation and depletion of soil and groundwater storage.

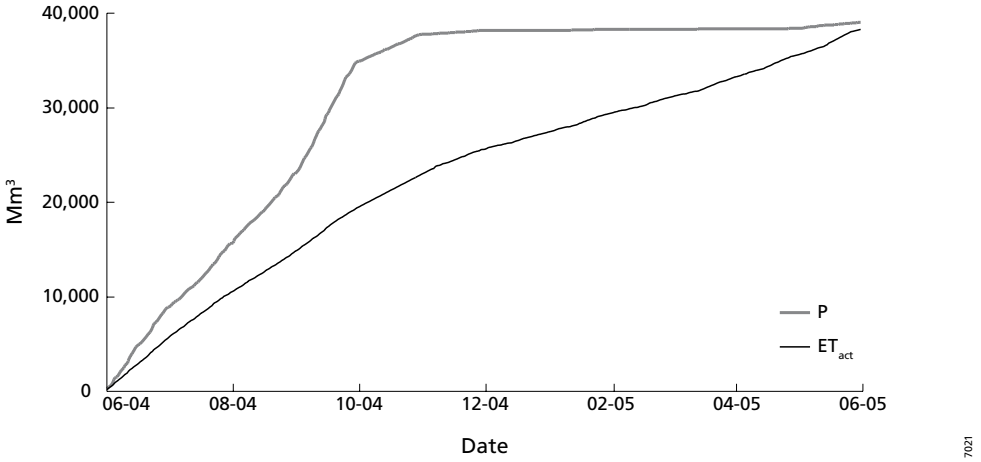

Figure 5.10 Cumulative volumetric precipitation (P) and actual evapotranspiration (ET_{act}) from June 2004 to May 2005.

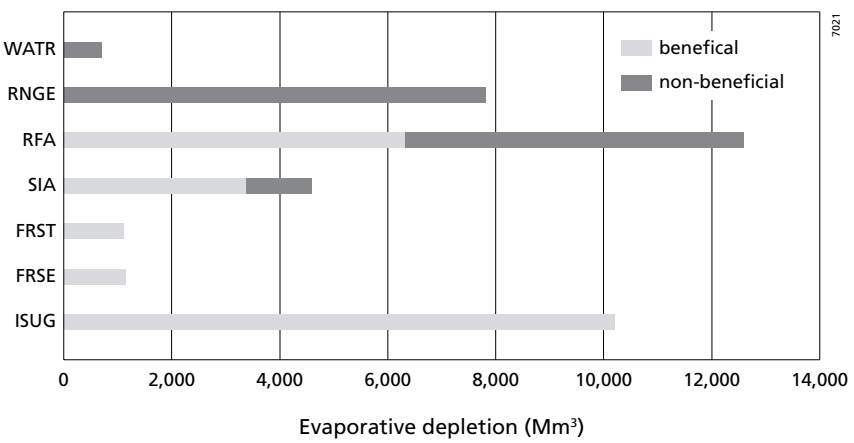

Figure 5.11 Evaporative depletion per land use from June 2004 to May 2005.

The distribution of evaporative depletion among different land uses is important to identify the opportunities for water savings or reallocation of water (Figure 5.11). A distinction between beneficial and non-beneficial evapotranspiration was made to determine whether water is productively used within the catchment. Perry (2007) recently proposed the following definitions:

- Beneficial evapotranspiration: water evaporated or transpired for the intended purpose – for example evaporation from a cooling tower, transpiration from an irrigated crop.
- Non-beneficial evapotranspiration: Water evaporated or transpired for purposes other than the intended use – for example evaporation from water surfaces, riparian vegetation, waterlogged land.

In this study ET_{act} from non-productive rangelands is also considered non-beneficial, because these are non-productive sparsely vegetated areas, from which large amounts of water are lost mainly through soil evaporation. ET_{act} resulting in growth of agricultural crops during their growing season or growth of biomass of valuable ecosystems such as forests can be considered beneficial. ET_{act} from non-productive rangelands, from agricultural lands beyond the growing season and from reservoirs can be considered non-beneficial. It is interesting that a total of 42% of total evaporative depletion was non-beneficial and non-productive rangelands were the largest contributor (20%). Of the beneficial ET_{act}, sugarcane depleted most in absolute terms (10,205 Mm^3). Forests depleted a relative small amount due to their limited area.

5.4.4 Water productivity analysis

The spatial distributions of CWP were analyzed to examine the scope of manipulation within the land use system to provide better alternatives to enhance overall crop water productivity in the catchment. Zwart and Bastiaanssen (2007) propose to use the coefficient of variation (CV) of the distribution of CWP within a system as a measure to define the scope for improvement. A high CV and a strongly negatively skewed distribution indicate a large potential, whereas a low CV indicates a homogeneity and little room for improvement. The statistical summary of CWP for the major crops is shown in Table 5.4.

The estimated CWP was found highest for sugarcane (2.9 kg/m^3). Evapotranspiration by sugarcane is the largest consumer of water, but crop water productivity is high and its distribution very narrow (CV = 1.4%), leaving limited scope for further improvement. Water consumption is very high (up to 1300 mm/year), because of the 12 months growing period; yields are however also extremely high (up to 37 ton/ha) (Table 5.4). The large sugarcane areas are all relatively flat and homogeneous and are generally not under water stress, since they are irrigated from the large reservoir based irrigation schemes. This is further clarified by Figure 5.12. Yields are shown as contours as a function of actual evaporative depletion and the sum of precipitation and irrigation. The figure shows that yields are nearly linearly related to ET_{act}, but indifferent to the annual sum of precipitation and irrigation. Only in the lower left corner of the figure water stress is a constraint to the yield. Once ET_a is higher than 900 mm/year, ET_a is not depending on precipitation or irrigation, but is rather a function of other environmental variables (e.g. soil, nutrients, slope, pests and diseases).

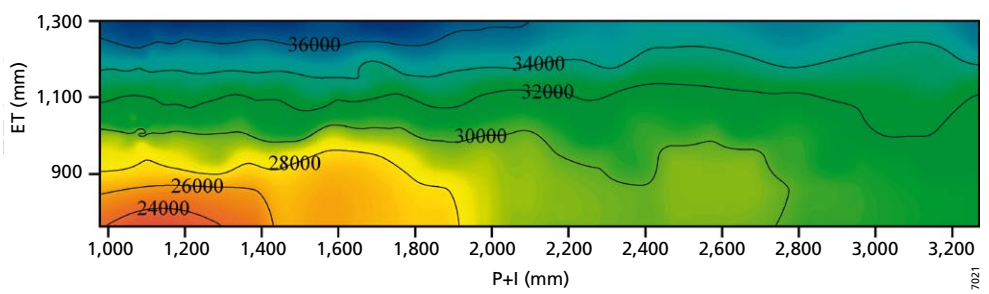

Figure 5.12 Sugar cane yield (kg/ha) as a function of annual actual evapotranspiration (ETact) and the sum of annual precipitation and irrigation (P+I).

Table 5.4 Statistical parameters of yield (Y), actual evapotranspiration (ET_{act}) and water productivity simulated by SWAT per agricultural land use (rainfed agriculture (RFA), supplemental irrigated agriculture (SIA), irrigated sugarcane (ISUG)) and per crop (sorghum (SGHY), winter wheat (WWHT), sugarcane (SUGC).

		RFA	SIA			ISUG
		SGHY	SGHY	WWHT	WWHT*	SUGC
minimum	(kg/m^3)	0.7	0.8	1.0	0.2	2.8
maximum	(kg/m^3)	1.6	1.8	2.1	1.3	3.0
average	(kg/m^3)	1.3	1.3	1.3	1.1	2.9
standard deviation	(kg/m^3)	0.1	0.2	0.2	0.1	0.0
CV	(%)	11.4	15.8	18.5	4.6	1.4
Skewness	(-)	-1.2	-0.3	1.1	-5.1	-0.1

* based on SEBAL results

Average CWP for winter wheat based on SWAT results was estimated to be 1.3 kg/m^3, which is higher than reported in a review by Zwart and Bastiaanssen (2004) as a global average value for winter wheat (1.1 kg/m^3). The CV is relatively large (18.5%), as the availability of water amongst HRUs is less uniform. Table 4 also shows the CWP results for winter wheat based on the SEBAL analysis. The average CWP computed by SEBAL for WWHT is 1.1 kg/m^3 and the CV is 4.6%, which are both smaller than the SWAT calculated values. However the SEBAL derived CWP distribution is more negatively skewed. This caused by the fact that the SEBAL estimation is pixel based and SEBAL captures the ET_{act} with more spatial detail than the SWAT model which is based on a HRUs. The fact that the CWP ranges are similar provides, however, confidence in the SWAT simulated crop yields.

Finally the CWPs of the rainfed crops, represented by sorghum within the RFA and SIA land use classes, are equal (1.3 kg/m^3). The CVs are relatively large and both distributions are negatively skewed.

The concept of using CWP to assess scope for improvement has proven to be a powerful tool, but caution is warranted and these results need to be interpreted carefully. The district agricultural statistics (Government of Maharashtra, 2007) reveal that the reported yields show large differences with the simulated yields by SWAT and SEBAL. The reported sugarcane yields are much higher (up to 200% of the simulated yield) and this requires further parameterization of the sugarcane crop in SWAT, mainly because sugarcane is a C_4 crop, with specific characteristics and a very high potential biomass production. The reported winter wheat and rain fed crop yields are much lower (up to 25% of the simulated yield) and consequently the simulated CWP were higher than in reality. The simulated CWP could be referred to as potential CWP. For the determination of actual CWP, which is also governed by other environmental stress factors and management decisions, it would be preferable to include measured field data in the analysis. By comparing gaps between actual and potential CWP in space and time, scope for improvements can then be further quantified.

5.5 Conclusions

The total simulated evaporative depletion and precipitation indicate that the upper Bhima catchment was nearly closed in 2004-2005. This was confirmed by independent discharge measurements, which show that only 5.6% of the total precipitation was released to the main stem of the Krishna River. If even a water supplying catchment, such as the Upper Bhima, is nearly closed the future for the entire Krishna basin looks grim and a structural rethinking of the planned expansion of irrigated agriculture is warranted. The water productivities are already relatively high and there seems limited scope for further improvement. Based on the analysis two ways to use or allocate water more effectively in the catchment are proposed. Firstly, a diversion from sugarcane to a dual cropping season (similar to SIA) and the introduction of a fallow period from March to May (when precipitation is absent and ET_{ref} is extremely high) are proposed. Sugarcane is grown throughout the year and its water consumption is highest of all land use classes that were distinguished. A shift towards a dual cropping systems will most likely increase the catchment's discharge. Of course some caution is warranted and social-economic considerations need to be taken into account. Secondly, by converting non-productive rangelands to rain fed agriculture, the beneficial ET will further increase on the expense of non-beneficial ET. A viable alternative could be the introduction of Jatropha curcas, that is considered to be an excellent source of bio-diesel and that can be grown in wastelands across India (Francis et al., 2005). The Governement of India is keen on reducing its dependence on coal and petroleum to meet its increasing energy demand. Promoting the cultivation of Jatropha is a crucial component of its energy policy, which should lead to energy independence by the year 2012. A conversion to other agricultural land uses could also be viable, but requires a careful land use suitability assessment.

The study faced a number of data limitations for which further improvements are recommendable. Firstly, the land use map could diversified to a larger number of crops by more elaborate ground-truthing and inclusion of more remote sensing data sources in the classification. Secondly, a more detailed soil map (including soil physical parameters) would yield more detailed results and a more efficient calibration. Thirdly, the calibration period could be extended in the monsoon season by including other datasets that do not depend on cloud cover (e.g. radar). The SEBAL algorithm depends on radiances in the visible, near-infrared and thermal infrared part of the spectrum, and measurements are hampered by clouds. The current calibration period covers eight months and a longer time series would be preferable. However, realistic simulations during the dry period from October to May are more important considering that water management issues related to evapotranspiration management, water shortage and irrigation are the dominant hydrological issues relevant to agriculture and water managers. Finally the simulation period should be extended to cover a multi-year periods covering a range of possible climate conditions.

It can be concluded that the integration of Remote Sensing in the calibration of a distributed hydrological model is highly innovative and enhances our insight in the hydrological pathways in drought prone areas with limited data availability. Catchments, such as the Upper Bhima, are difficult to model given the large number of anthropogenic disturbances, such as reservoirs, dams and irrigation canals, that render stream flow unusable for calibration. By using remotely sensed ET_{act} this problem is overcome and a detailed calibration of a hydrological model was performed and assessed by a number of efficiency indicators. The use of a hydrological model has clear advantages over using remote sensing alone. A model provides insight in the entire hydrological cycle, fluxes between the different water balance components and the crop growth cycle, while

remote sensing provides only insight in one component of the water balance at high spatial detail at a specific point in time. A calibrated model also offers opportunities to analyse future scenarios, e.g. land use change and climate change. It is the combination of the strength of both approaches that provides a wealth of possible future applications.

6 Can payments for ecosystem services secure the water tower of Tibet?

Based on: Immerzeel, W.W., J.J. Stoorvogel & J.M. Antle (2007), Can payments for ecosystem services secure the water tower of Tibet? Agricultural Systems (in press).

Abstract

Tibet can be considered as the water tower of Asia and the protection of its water resources crucial. We show that a minimum data approach to model the supply of ecosystem services can potentially be applied to water conservation in Tibet. The approach integrates the spatial heterogeneity of the biophysical environment and the economic behaviour of farmers. A spatially distributed hydrological model is used to simulate the effect of irrigation on evapotranspiration reduction and stream flow enhancement in a Tibetan agricultural catchment. The results feed into an economic model that estimates the supply curve of conserved water from the distribution of net returns between irrigated and rain-fed barley cultivation. The analysis shows that it is theoretically possible to increase discharge out of the catchment in the critical months April to June by 11% on average. Accumulated over larger areas this could provide a significant increase in total upper Brahmaputra discharge. The methodology appears to be a transparent and cost effective tool to quantify the effect of financial incentives in the conservation of water resources. Policy relevant information can be generated without the need to conduct expensive field surveys and to set up more elaborate econometric simulation models. Given the anticipated effects of climate change the potential of payments for ecosystem services to conserve water may become increasingly more important in sustaining stream flow early in the growing season.

6.1 Introduction

The Tibetan plateau (TP) is often considered to be the water tower of Asia being the source of many major Asian rivers such as the Mekong, Yangtze, Brahmaputra, Indus and the Karnali. These rivers support hundreds of millions of people downstream. Since Asia is monsoon-dominated with precipitation concentrated in just a few months, the perennial flow of the rivers largely relies on the constant flux of the glaciers in Tibet. As the pressure on Tibet's water resources is mounting because of rapid economic development, its conservation becomes ever more important. Population growth, increased incomes and urbanization have joined forces and agriculture cannot keep up with the increasing demands of this emerging, new society (Ecoregional Fund, 2005). Yields are restricted by a short growing season, large diurnal temperature ranges and above all a shortage of water. Annual precipitation is only 600 mm and is concentrated in the monsoon months July and August (Immerzeel et al., 2005). The proportion of arable land is only 0.3%

of the total land area and more than 60% of this land is arid and has a low productivity. Gaps between actual and potential yields of the main crops barley and wheat are very large and this is caused by a poorly developed irrigation infrastructure (Tashi et al., 2002). To sustain the increased demand for more and diverse agricultural products it is inevitable that the acreage of irrigated area will increase over the years (Immerzeel, 2005).

Climate change is another major threat to the future of Tibet's water resources. Widespread accelerated glacier retreat and shifts in stream flow timing, from spring to winter, are likely to be associated with climate change (IPCC, 2001). There are serious concerns about the alarming rate of retreat of Himalayan glaciers. It has been predicted that the coverage of glaciers in western China, accounting for up to 70% of the Himalayan glaciers, will decrease by 27% by 2050 (Qin, 2002). In the short run the glacier melt may increase water availability, but eventually the base flow from glaciers will cease (Barnett et al., 2005). Changes in timing and available volume of water available for irrigation will threaten agricultural productivity (IPCC, 2001) and will impact heavily upon the economy of the region (Matthews et al., 1995).

Tibet supplies an important ecosystem service in the form of fresh water to a large part of Asia. During the monsoon months the water supplied by the TP is a negligible fraction of the total river flows. However, at the end of the winter and in early spring glacial melt from the TP, is the major water source for agriculture in the downstream agricultural areas of India, Bangladesh and China during a crucial period of the growing season (Barnett et al., 2005).

The increased demand for agricultural production in Tibet, the expected climate change and the need to sustain the water supply to downstream areas challenges policy makers to make the most appropriate trade-offs between agriculture and the environment.

Globally there has been a shift from traditional subsidy and trade policies to policies that provide farmers with incentives to increase the supply of ecosystem services from agriculture. This is being referred to as payments for ecosystem services (PES). PES is emerging as a new approach to managing the valuable services derived from ecosystems. The Millenium Ecosystem Assessment (2005) describes fresh water as one of the critical provisioning services that ecosystems provide. Protection of the New York City watershed is often cited as one of the earliest uses of the concept of payments for ecosystem services, a plan implemented in 1997 (World Resources Institute, 2000). Since then, there has been an increasing number of efforts to protect water quantity and quality by paying land owners to use practices that protect water resources, mostly through forest protection and re-forestation (FAO, 2007). In water conservation policies the focus has been primarily on the development of water pricing instruments (Dinar, 2000). The concept of payments for ecosystem services applied in this study can be interpreted as a way to implement an efficient water pricing policy wherein farmers are assigned the initial rights to use irrigation water and downstream users (or governments) pay farmers to reduce water use. The analysis presented here combines analysis of bio-physical potential for water conservation, which, together with economic analysis of farmers' willingness to change management practices, simulates a water supply curve to downstream users. This water supply curve can be used by policy decision makers to assess how much water farmers are willing to supply at a given price per unit of water. Combined with an assessment of how much water is worth to down-stream water users, an efficient water policy can then be implemented.

Recently a number of researchers have utilised site-specific data and models to assess the potential for ecosystem service payments (Pautsch et al., 2001; Antle et al., 2003; Wu et al., 2004; Lubowski et al., 2005). These studies utilize highly detailed data such as the National Resources

Inventory in the United States or specialized longitudinal farm surveys. However, in most cases neither time nor resources are available to collect such detailed data. In this paper we show how a less data-intensive "minimum data" economic model can be used in combination with a hydrological and production model to assess whether it would be technically and economically feasible to pay farmers to reduce water consumption by changing from irrigated to rain-fed crop production and thus secure the water tower of Tibet.

6.2 Materials and methods

6.2.1 Study area

The elevation of the TP ranges from 400 metres above sea level (m.a.s.l.) to the summit of Mt. Everest (8848 m.a.s.l) with an average altitude of over 4000 metres. The TP covers an area of 1.2 million km^2. This paper focuses on a sub catchment located between 27.47-29.33° N and between 88.51-90.20° E in the central southern part of the Tibetan plateau within the province of ü-Tsang. This province has developed as Tibet's cultural and political heartland and is commonly known as the grain bowl of Tibet. This is mainly caused by the fact that ü-Tsang provides broad U-shaped valleys for agriculture below the upper limit of cultivation of approximately 4500 m.a.s.l. (Ryavec, 2001). The Nyangchu River drains the catchment, with a total contributing area of 14271 km^2 into the Yarlung Tsampo River, which is further downstream more commonly known as the Brahmaputra River as it descends down into India and Bangladesh. The catchment is located in Shigatse prefecture and overlaps with the Shigatse, Gyantse and Panam counties. Shigatse, which is the second largest city of Tibet, is located at the confluence of the Nyangchu and the Yarlung Tsampo rivers. Further upstream the Nyangchu River traverses the third largest town Gyantse. The altitude in the catchment ranges from 3827 to 6989 m.a.s.l with an average altitude of 4737 m.a.s.l. Irrigated agriculture is found below 4500 m.a.s.l. and 37134 ha. of the catchment (2.6%) is classified as irrigated cropland. The main crop is spring barley, which has been Tibet's staple food crop for centuries. Over 80% of the catchment consists of extensive grasslands used for yak herding. The remainder of the catchment is comprised of bare soils at extreme altitudes (14.7%), urban areas (0.1%) and a number of large lakes (2.4%). The catchment receives on average 560 mm of precipitation annually with more than 70% of the annual rainfall concentrated in the months June, July, August and September. Annual potential evapotranspiration is relatively high and varies around 1500 mm due to low relative humidity, high solar radiation, and high wind speeds on the plains. Temperatures are lowest in January and highest in July with average temperatures of -8.3 °C and 8.9 °C respectively with extremely large diurnal ranges and spatial variation due to the high (variation in) altitude. Soils in the catchment are of sandy texture (50% sand) with a depth generally less than 0.65 m., except for the agricultural areas in the valleys where soil depths reach 1.5 m.

6.2.2 SWAT

The physically based distributed hydrological model Soil and Water Assessment Tool (SWAT) is used to simulate the hydrological processes as well as the crop growth in the catchment. SWAT represents all the components of the hydrological cycle including rainfall, snow, interception storage, surface runoff, soil storage, infiltration, evaporation, transpiration, lateral flow, percolation, pond and reservoir water balances, shallow and deep aquifers and channel routing. It also includes

land use management such as irrigation, fertilization and tillage. The model is comprehensively described in the literature (Arnold et al., 1998; Srinivasan et al., 1998).

SWAT simulates crop growth on the basis of daily temperature sum and water availability. For each day of simulation, potential plant growth, i.e. plant growth under ideal growing conditions (adequate water and nutrient supply) is calculated according to Monteith (1977). First, the photosynthetically active radiation, is computed from intercepted solar radiation as a function of Leaf Area Index (LAI). The radiation use efficiency (RUE), defined as the amount of dry biomass produced per unit intercepted solar radiation; is used to calculate the maximum daily plant growth. The RUE is essentially a function of carbon dioxide concentrations and vapour pressure deficits. Actual plant growth is then calculated and inhibited by temperature, water, and nutrient stress. The crop yield is computed as the harvestable fraction of the accumulated biomass production during the growing season.

To avoid water stress irrigation water is applied automatically based on a specified water stress criterion. Water stress is 0.0 under optimal water conditions and approaches 1.0 as the soil water conditions vary from the optimal. Water stress is simulated according to:

$$wstrs = 1 - \frac{E_{t,act}}{E_t} = 1 - \frac{w_{actualup}}{E_t} \quad (1)$$

where *wstrs* is the water stress for a given day, E_t is the potential plant transpiration on a given day (mm H_2O), $E_{t,act}$ is the actual amount of transpiration on a given day (mm H_2O) and $w_{actualup}$ is the total plant water uptake for the day (mm H_2O).

The catchment is partitioned into a number of sub-watersheds or sub-basins. The sub-basin delineation is performed on the basis of the catchments' topographic features derived from a 90m resolution digital elevation model (DEM) acquired with the Shuttle Radar Topography Mission (SRTM) (Werner, 2001). The sub-basins (78) are further subdivided into hydrological response units (HRUs), which are unique combinations of soil and land use. A detailed land use map, based on aerial photograph interpretation, is provided by the Tibetan Bureau of Meteorology. This land use map was reclassified to land uses in the SWAT database. Soil variation is derived from the FAO soil map of the world with some local adaptations (FAO, 1995). By overlaying the sub-basins with the reclassified land use and soil map a total of 181 HRUs are delineated. The HRU is the smallest unit of calculation for the land phase of the model. Each sub-basin is linked to a single reach and all HRUs in a sub-basin drain their water into that reach by surface runoff, drainage and ground water flow. Subsequently the water is routed through the catchment from upstream to downstream. Water used for irrigation is extracted from the surface water and applied to the respective HRUs.

Monthly data on precipitation, temperature and relative humidity are extracted from the CRU TS 2.1 database (Mitchell and Jones, 2005). The CRU TS 2.1 is a set of monthly climate grids which are constructed for nine climate variables and interpolated onto a 0.5° grid and provide best estimates of month-by month variations. Data from the Tibetan Bureau of Meteorology for Shigatse from 1971-1998 are used to scale the temperature and precipitation data to the local situation. Monthly cloud cover and wind speeds are derived from the IWMI climate atlas (New et al., 2002). The SWAT model is run for 20 years from 1983-2002. The most detailed spatial level on which meteorological data can be defined in SWAT is at sub-basin level. The monthly climate data derived from the CRU TS 2.1 database and the IWMI climate atlas are therefore first averaged per sub-basin and then converted to daily values using the inbuilt weather generator.

Spring barley is cultivated on all HRUs classified as irrigated agriculture. The spring barley is planted on April 15 and harvested on October 1 making full use of the short summer and monsoon rains. A total of 24 HRUs are cultivated with barley ranging in area from 108 ha to 3080 ha, with an average area of 1547 ha. The barley is fertilized with 300 kg/ha of urea in April and August. Two practices are simulated: (a) irrigated barley using auto-irrigation with a water stress criterion of 0.95., and (b) rain-fed barley. The SWAT model is used to determine how reductions in the use of irrigation water reduce crop transpiration and how this eventually affects discharge out of the catchment. For both practices the 20 year average crop yield as well average annual crop evapotranspiration reduction of each HRU are input to the MD model which simulates the water supply curve based on economic features of each scenario.

SWAT simulates the 20 year period with a daily time step, but the output is stored on a monthly basis. Monthly water balances are stored at sub-basin, HRU and reach level, while biomass, crop yields, water and nutrient stress are stored at HRU level with a monthly time step. The monthly data at HRU level are input to the economic model. For a detailed overview of SWAT outputs reference is made to Arnold et al. (1998).

There are no hydrological data available for the catchment to validate the results of SWAT. In Tibet scientific research in this field is in its infancy, caused by the remoteness of the terrain and Tibet's status as an outlying region, remote from the centre of power, and its limited capacity for local research (Bouma et al., 2007). It is stressed that this study is explorative in nature and the major objective is to show whether PES could potentially work to conserve water. However, to be able to validate the results on their plausibility we have used two sources of information.

Firstly, stream flow data of the nearest gauge in the Brahmaputra River at Yangcun (29.28°N, 91.88°E) extracted from a database compiled by the global runoff data centre (Fekete et al., 2000) were analyzed and compared with the simulated average monthly discharge in the catchment.

Secondly, a subset of monthly latent heat fluxes from 1983-2002, produced by the National Centre for Environmental Prediction (NCEP) and the National Centre for Atmospheric Research (NCAR) through their reanalysis project (Kalnay et al., 1996), has been processed and converted to actual evapotranspiration rates for the catchment. The monthly average evapotranspiration has been compared with the simulated evapotranspiration for the entire simulation period.

6.2.3 MD model for analysis of ecosystem service supply

To implement the economic analysis, we use the minimum-data (MD) approach developed by Antle and Valdivia (2006) to model the supply of ecosystem services from agriculture. Whereas other studies of agriculture-environment processes have used highly complex, data-intensive models (e.g., Antle et al., 2003; Wu et al., 2004), the MD approach exploits the structure of the PES problem to obtain an approximation to the ecosystem service supply curve using relatively simple secondary data. The MD model assumes farmers take land-use and management decision to maximize their perceived economic well being. When the farmers are not provided with any incentives there is an initial equilibrium supply of ecosystem service. This provision of this ecosystem service is driven by the farmer's economic motivation and ignores the demand for that ecosystem service, e.g. other downstream water users. To increase the supply of water above this initial equilibrium the downstream demanders must provide the farmers with financial incentives stimulating farmers to change their land use management. For each barley HRU in the catchment we consider the two practices a, *i.e.* irrigation, and b, *i.e.* rain-fed, as competing land uses. An amount of $e(s)$ ($(m^3/ha)/yr$) of ecosystem service is produced at site s when practice

b is adopted and *e(s)* equals zero when practice *a* is adopted. Here *e(s)* is defined as the difference in evapotranspiration between the two practices. A farmer will receive a payment of p_e for each m^3 that is produced. The amount of *e(s)* at a specific site within a HRU is however not known beforehand, but since the objective is to obtain a total quantity for the entire HRU payments can be based on an expected average rate of supply generated by the SWAT model.

A farmer will decide to adopt rain-fed barley if

$$\omega(p,s) = v(p,s,a) - v(p,s,b) \leq p_e e \text{ (s)} \tag{2}$$

where *v* is the net return, *p* is a vector of input and output prices, *s* indexes the site and *a*,*b* indicate the practice at the site. Thus $\omega(p, s)$ can be interpreted as the opportunity cost of changing from practice *a* to practice *b*. This equation implies that farmers are willing to change practices to receive the payment if $\omega/e \leq p_e$, i.e. if the opportunity cost per unit of water conserved is less than the price paid for the water. If we order all the sites *s* for a given *p* within an HRU in increasing order of $\omega(p, s)$ we can define the spatial distribution of opportunity cost per unit of ecosystem *e*, $\phi(\omega/e)$. The fraction of the total number of farmers who adopt practice *b* without payment is given by

$$r(p) = \int_{-\infty}^{0} \varphi(\omega/e)d(\omega/e) \tag{3}$$

The initial equilibrium supply of water before farmers are given payments is then given by

$$S(p) = r(p)He \tag{4}$$

where H is the total area of the HRU. Similarly by integrating $\phi(\omega/e)$ between zero and p_e the fraction of the total number of farmers is found who change from practice a to b given p_e, $r(p,p_e)$. The supply of ecosystem services in that case equals

$$S(p, p_e) = S(p) + r(p, p_e)He \tag{5}$$

To model the supply of water per HRU we use the MD approach to parameterize the spatial distribution of opportunity cost by estimating the mean net returns of each practice and their variances and covariance. The opportunity cost per hectare can be calculated according to:

$$\omega = p \cdot (Y_a - Y_b) - c_a + c_b \tag{6}$$

where *p* is local market price for barley, c_a and c_b are the average local cost of production per hectare and Y_a and Y_b are the yields of practice a and b respectively.

Antle and Capalbo (2001) found that cost functions for barley production exhibited costs of production with approximately unitary output elasticities. Therefore, it can be plausibly assumed that cost of production is proportional to its yield, and that the coefficient of variation in net returns (CV) across land units in a region (at a point in time) can be estimated by the spatial CV for yield. Previous work showed that this approach provides an approximation that is well within an order of magnitude (Antle and Capalbo, 2001). The MD approach implemented in this study

utilizes these assumptions. The 20 year average crop yields are calculated using the SWAT model for both practices and the coefficient of variance in yield for practice *b* (CV_b) has initially been assumed to be equal to the CV of field slope, e.g. if the variation in slopes within a HRU is high the variance in yields will be high, mainly because water cannot be retained in the soil. The CV of practice *a* (CV_a) is assumed to be 20% of CV_b, because irrigation water is available and the effect of steep slopes will be much less. In order to estimate the covariance between yields, the correlation between the yields of irrigated and non-irrigated crops is assumed to be positive but less than unity. In many cases the correlation between the yields of different practices is likely to be high, but not perfect (Antle and Valdivia, 2006). Since this correlation is not readily observed, sensitivity analysis is used to assess the impact of alternative values. The opportunity cost is assumed to be normally distributed and its variance is calculated according to the following set of equations

$$\sigma^2_{\omega} = \sigma^2_{a} + \sigma^2_{b} - 2\sigma_{ab} \tag{7}$$

$$\sigma^2_{a} = CV_a^2 \cdot v_a^2 \tag{8}$$

$$\sigma^2_{b} = CV_b^2 \cdot v_b^2 \tag{9}$$

$$\sigma_{ab} = CV_a \cdot v_a \cdot CV_b \cdot v_b \cdot \rho_{ab} \tag{10}$$

where σ^2_a and σ^2_b are the variances in net returns of practice a and b respectively, ν_a and ν_b are mean yields, and σ_{ab} and ρ_{ab} are the covariance and spatial correlation coefficient in net returns between practice *a* and *b*. The MD model constructs this distribution per HRU and by sampling this distribution at different p_e the supply curve of fresh water for each HRU is calculated.

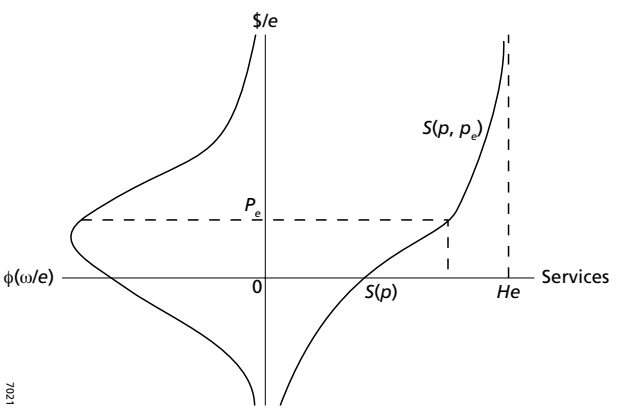

Figure 6.1 Derivation of the supply of ecosystem services from the spatial distribution of opportunity cost per unit of ecosystem services (Antle and Valdivia, 2006) e = ecosystem service rate, p_e = price per unit of ecosystem service, $\phi(\omega/e)$ = opportunity cost per unit of ecosystem service, H = total area, p = vector of input and output prices, and S = total supply of ecosystem service.

The model aggregates the supply curves for each HRU to obtain a supply curve for the entire catchment.

Figure 6.1 shows how the supply of water is derived from the spatial distribution of opportunity costs for changing practices. Figure 6.1 actually contains two graphs. The left side of the graph shows the spatial distribution of opportunity cost per unit of ecosystem service. The price per unit of *e*, *Pe*, is shown on the vertical axis and the density function $\phi(\omega/e)$ is shown on the horizontal axis. The area under this curve in the price range from $-\infty$ to 0 is the initial equilibrium supply of fresh water. The shape of the distribution is estimated by equations 7 to 10. The right side of the graph shows the supply curve. The horizontal axis shows the supply of fresh water as a function of the price per unit *e* on the vertical axis. The supply curve crosses the horizontal axis at the initial equilibrium and logically further increases as P_e increases. The rate of increase (slope of the supply curve) depends on the shape of the distribution of opportunity costs. The supply curve approaches a vertical asymptote equal to the maximum amount of ecosystem service ($H\,e$) that can be produced when every HRU switches to activity *b*.

6.3 Results

6.3.1 Hydrological modelling

Figure 6.2 shows the average annual water balance for the 20 year period 1983-2002 for the entire catchment. The catchment receives an average annual precipitation of 563 mm of which, on average 418 mm (73%) evaporates. Given a potential evapotranspiration of 1457 mm/year it is evident the catchment is under severe water stress. Around 15% of the incoming water is returned as stream flow through direct runoff. The remainder infiltrates in the soil and exits the catchment as sub-surface flow or ground water flow. Only a very small proportion is lost from the catchment through percolation to the deep aquifer (1 mm/year). On a catchment scale, the amount of irrigation water applied is limited due to the relatively small proportion of irrigated agriculture. However, it is, as will be shown subsequently, a very important and manageable proportion. Based on this analysis it is concluded that water conservation in the catchment should be sought in the reduction of evapotranspiration.

Figure 6.3 shows the results of the validation. The average monthly discharge in mm/month shows good agreement. Some caution is warranted as the Yangcun gauge is located in the Brahmaputra downstream of the study catchment and drains a much larger area (153,191 km^2) that includes the catchment. The drainage areas is however relatively homogeneous and the comparison of area weighted discharges shows that SWAT simulates plausible monthly discharges. The comparison of actual evapotranspiration further supports this finding. The NCEP/NCAR and modelled actual evapotranspiration are in a similar range. The NCEP/NCAR data are generally higher than SWAT in the summer. A possible explanation could be that the NCEP/NCAR dataset is grid based with a spatial resolution of 2 degrees and the selected grid cell includes an area north of the catchment, which, due to the wide Brahmaputra floodplain, includes a large wetted surface resulting in a higher evapotranspiration rate.

To gain insight into how to achieve the largest water savings, the analysis of monthly partitioning into precipitation, irrigation and actual evapotranspiration (ET_{act}) for irrigated barley is useful. Figure 6.4 shows these components for practice *a* and *b* respectively. The left figure shows that irrigation amounts are highest in the months April and June and decrease later

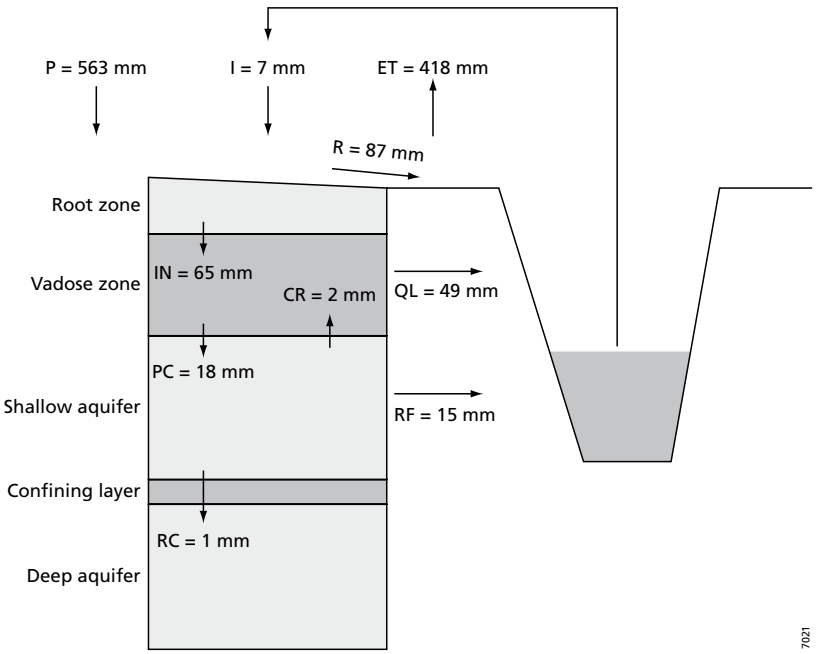

Figure 6.2 Average annual water balance from 1983 to 2002 (P = Precipitation, I = Irrigation, ET = Actual evapotranspiration, R = Surface runoff, IN = Infiltration, CR = Capillary rise, PC = Percolation, QL = Subsurface flow, RF = Return flow, RC = Recharge to deep aquifer)

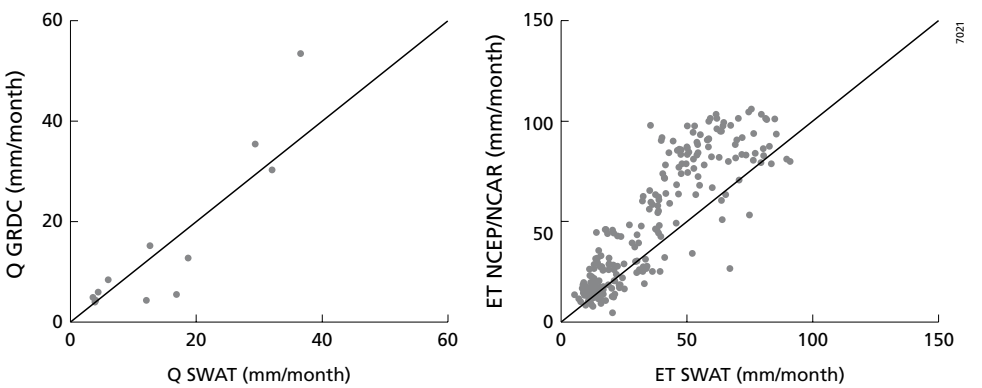

Figure 6.3 SWAT validation results: (i) Modelled discharges at the catchments' outlet vs average monthly measured discharges at Yangcun (left figure), (ii) Modelled monthly actual evapotranspiration vs. monthly NCEP/NCAR derived actual evapotranspiration from 1983-2002 (right figure).

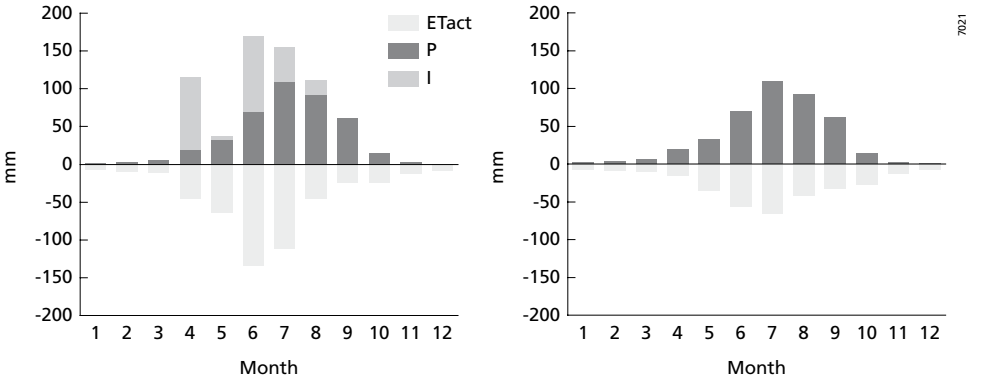

Figure 6.4 Monthly average precipitation (P), irrigation (I) and actual evapotranspiration (ET_{act}) from 1983-2003 for irrigated (left figure) and rain fed (right figure) barley.

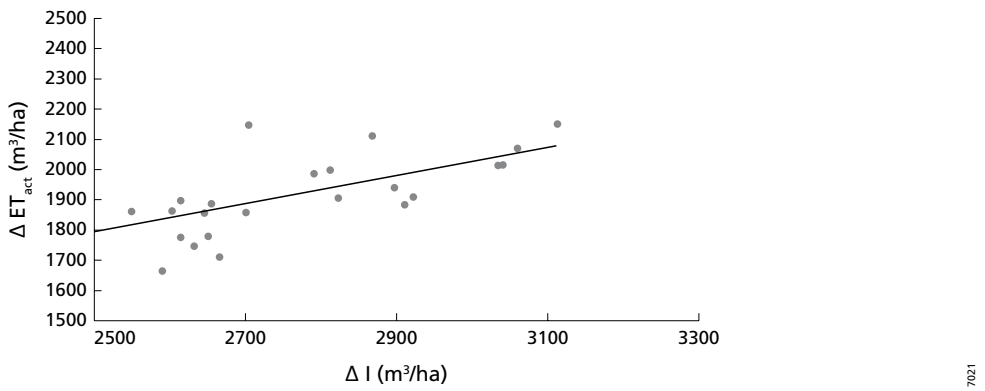

Figure 6.5 Relation between the reduction in irrigation (ΔI) and the reduction in actual evapotranspiration (ΔET_{act}) per HRU based on 20 year averages.

in the growing season when the monsoon rains provide sufficient water to sustain crop water requirements. In April the soil water content is replenished to field capacity and sufficient to sustain the relatively low crop water requirements in April and May. The months April-June are critical months for the downstream agricultural areas and water conservation efforts should focus on increasing discharge out of the catchment in the early months of the growing season.

An increase in discharge can be achieved by reducing irrigation and thus ET_{act}. However the response of ET_{act} to changes in irrigation amounts is governed by the biophysical conditions of the system. Figure 6.5 shows, for each agricultural HRU, the relation between a reduction in irrigation (ΔI) and a reduction in ET_{act} (ΔET_{act}). The relation can be approximated by linear regression (intercept = 630, slope = 0.5, R^2 = 0.4). The figure shows (i) that a decrease in irrigation leads to a decrease in ET_{act}, (ii) the decrease in ETact is always less than the decrease in irrigation, and (iii) there are large differences between the various HRUs. These differences are mainly explained by the fact that different HRUs receive different amounts of precipitation and by the

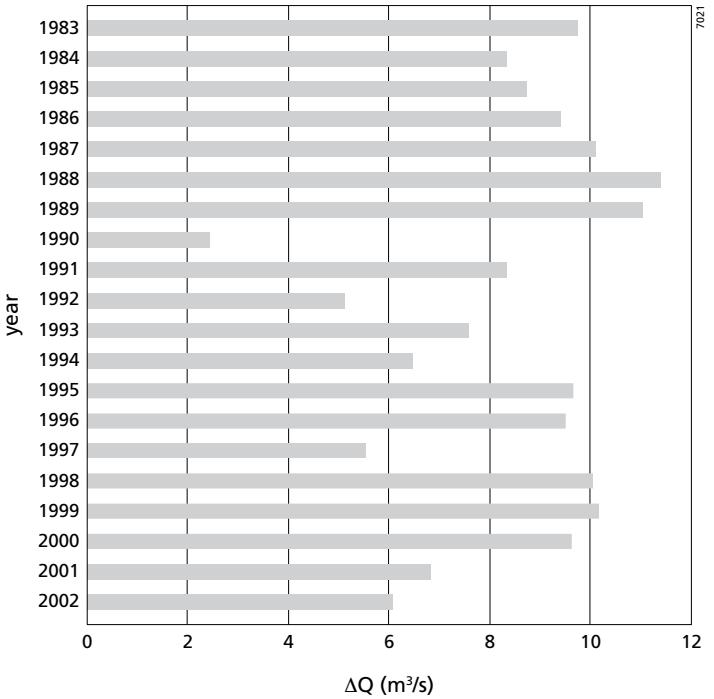

Figure 6.6 Average annual difference in discharge between the rain fed and irrigated scenario from 1983-2002 in the months April-June at the catchment outlet.

differences in soil type. Deeper soils with a high water retaining capacity respond less directly to reduction in irrigation.

A reduction in ET_{act}, assuming that the irrigation water originates from within the catchment, will yield an increase in discharge at the outlet of the catchment. Figure 6.6 shows the increase in discharge (m^3/s) from April to June at the outlet of the catchment when all agricultural HRUs shift from irrigated to rain-fed barley. The simulated average total discharge in these months is 87 m^3/s (16 mm/month). This means that discharge can potentially be increased in these critical months between 2% and 30% with an average of 11%. These are very considerable amounts especially when considering only 2.6% of the total catchment area is irrigated agriculture.

6.3.2 Economic model

Table 6.1 shows the inputs for the MD model. The average yield in the irrigated case is 4404 kg/ha and this is in good agreement with barley yields reported in literature (Tashi et al., 2002). The yields in the rain-fed case are on average 1646 kg/ha (37% of the irrigated case) and the average rate of ecosystem service (reduction in actual evapotranspiration) is 191 mm. The ecosystem service rates are based on crop water requirements and biophysical conditions within the HRUs. The average amount of required reduction in irrigation water to achieve this ecosystem service rate is 276 mm per growing season. The average barley market price in 2005 in Tibet's capital Lhasa ranges between 0.18 $/kg and 0.20 $/kg. For both case *a* and *b* an average of 0.19 $/kg is

Table 6.1 Inputs for the economic analysis per Hydrological Response Unit (HRU); Y_a = average yield of irrigated barley, CV_a is the coefficient of variation in the net returns of irrigated barley, Y_b = yield of rain-fed barley, CV_b = coefficient of variation in the net returns of rain-fed barley, C_b = cost of production of rain-fed barley, e = ecosystem service rate.

HRU	Area (ha)	Y_a (kg/ha)	CV_a (%)	Y_b (kg/ha)	CV_b (%)	C_b ($/ha)	e (m^3/ha)
1	1755	4217	23	1720	117	130	1857
2	2754	4253	31	1722	154	129	1862
3	2305	4211	18	1712	89	130	1900
4	920	4284	30	1651	148	123	1664
5	467	4287	13	1735	63	129	1776
6	918	4659	22	1653	111	113	2150
7	2249	4661	39	1678	194	115	2111
8	2530	4280	32	1746	161	130	1887
9	2782	4621	30	1632	152	113	2148
10	1690	4297	28	1691	141	126	1856
11	3077	4507	41	1654	207	117	1863
12	1640	4255	38	1651	191	124	1746
13	3080	4601	42	1673	211	116	1998
14	1225	4480	22	1665	112	118	2015
15	756	4460	34	1704	171	122	1940
16	413	4493	21	1700	106	120	2013
17	1022	4564	38	1621	191	113	2071
18	231	4468	46	1679	231	120	1909
19	1556	4640	39	1648	193	113	1986
20	1036	4311	29	1717	143	127	1897
21	1530	4547	34	1422	168	100	1906
22	1886	4563	21	1713	103	119	1884
23	1206	4224	25	1353	127	102	1779
24	108	3824	24	1362	120	114	1711

used. The local cost of production is 330 $ ha^{-1} yr^{-1} for the irrigated case (personal communication 1/8/2006; Dr. Quimei) and the gross income for the irrigated case is on average 837 $/ha. The cost of production is assumed to be proportional to yield, and the cost of the rain-fed case was estimated accordingly. In addition, the rain-fed cost was further reduced because no water fees for irrigation water are required. A water fee of 0.004 $ m^{-3} irrigation water (Loeve et al., 2001) is multiplied by the required amounts of irrigation water and deducted from the production costs for case *a*. Irrigation costs are on average only 3% of total production costs. Average cost of production for the rain-fed case averages 119 $/ha, while the average gross income for the rain-fed case equals 313 $/ha.

Figure 6.7 shows the results of the economic simulation for a single year of HRU 1. The left side of the graph shows the distribution of the difference in net returns between case a (irrigated) and case b (rain-fed) per unit ecosystem service (ΔET_{act}). The initial distribution (solid line) reveals that the centre of the distribution is located around a P_e of 0.15 $/$m^3$. The tail of the distribution approaches zero at $P_e \approx$ -0.09 $/$m^3$ at the left side and at a $P_e \approx$ 0.37 $/$m^3$ at the right side (nearly all farmers change from practice a to b). In case a there is therefore a limited

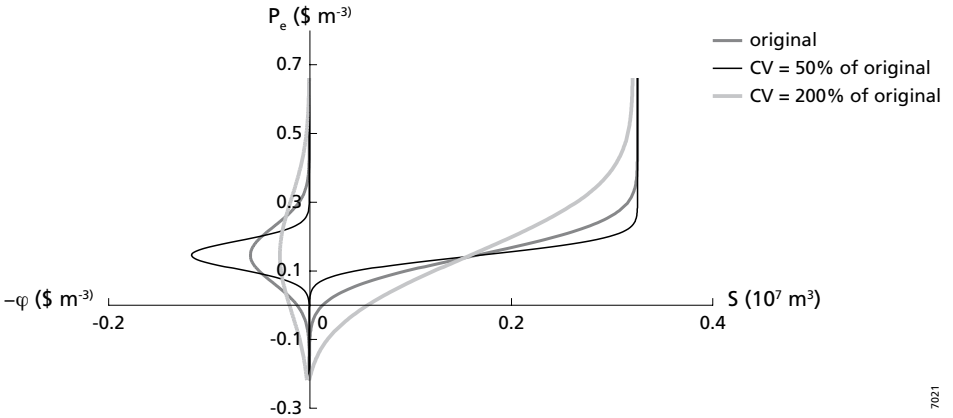

Figure 6.7 The spatial distribution of opportunity cost per unit of ecosystem service (left side) and the derived supply curves (right side) for three different variances in net returns of the two practices for HRU 1.

equilibrium supply of water (S(p)). This means that a number of farmers adopt practice *b* even if no additional financial incentives are provided, because their yields are low and irrigation is costly, i.e. they are better off without irrigation.

The right side of the graph shows the associated supply curve. At the right side of the graph the supply curve approaches the vertical asymptote equal to 1755 ha x 1857 m^3/ha ≈ 3.3 10^6 m^3. The slope of the supply curve is least steep at the centre of the distribution. The figure also shows the effect of the CV on the shape of the distribution of opportunity cost and the supply curve. An increase in CV widens the opportunity cost distribution and increases the slope of the supply curve. A decrease in CV causes the opposite.

It is interesting to note that with a CV of 200% of the initial CV the left tail of the distribution is now located at a $P_e \approx$ -0.2 $/m^3$. This means that the equilibrium supply of fresh water has increased considerably due to the relative large spatial variation in yields between the two cases.

Figure 6.8 shows the accumulated results for the entire catchment over a period of 20 years. The slope of the supply curve is smallest at a price of 0.15 $/m^3$. At that point approximately 50% of the farmers enter into a contract. The maximum achievable amount of evapotranspiration reduction accumulated over the 20 years roughly equals 1.4 10^9 m^3 (= 7.0 10^7 m^3/year), which will result in very significant increases in April-June discharge (2-30%). Besides conservation of water, there is considerable additional income generated by the farmers as is shown in the lower half of Figure 6.8.

6.3.3 Sensitivity analysis

The model has been parameterized with model simulations, expert judgements and statistics available from literature and personal communications. However there are no long-term locally measured data available to calibrate the results. It was shown that the output of the hydrological model is plausible and subsequently a sensitivity analysis was performed for the most important physical and economic parameters in the economic model to indicate the range in which realistic results may be expected. Three parameters have been chosen which are governed by the local

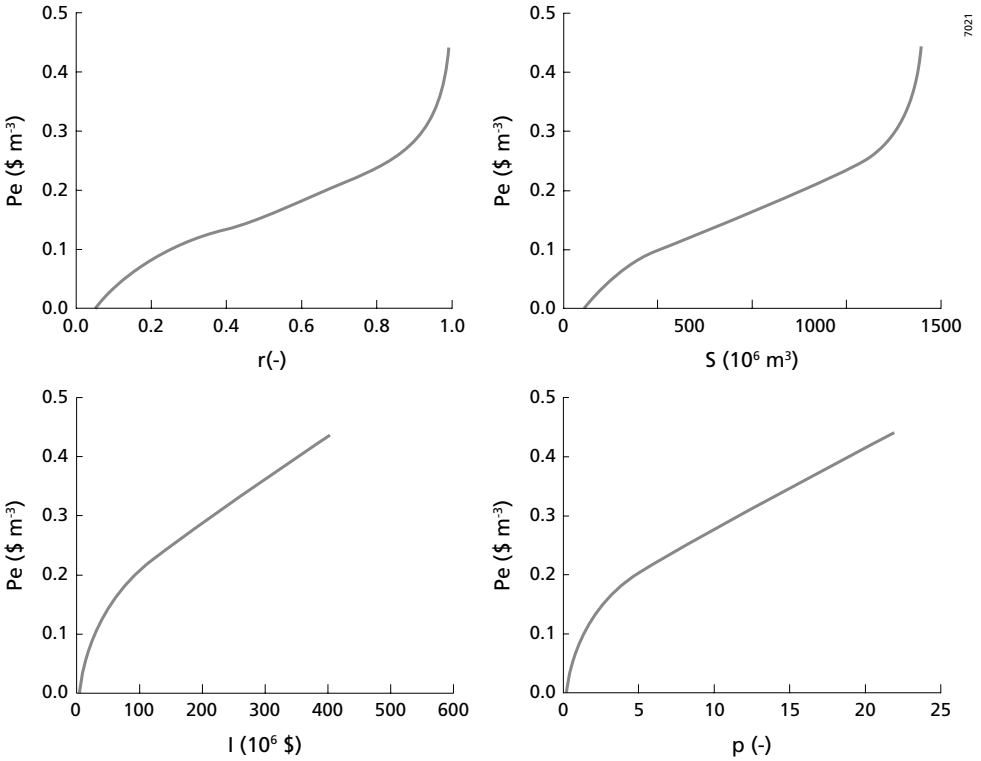

Figure 6.8 Catchment results for the base model: The price of ecosystem service (P_e) as a function of fraction of farmers participating in a contract (r), the total amount of ecosystem service produced in 20 years (S), the total additional income (I) and relative income compared to the base scenario (p).

biophysical conditions (CV_a, CV_b and e) and three parameters have been chosen that relate to the economic model (P, C_a and C_b). The sensitivity analysis was performed at a fixed P_e level (0.15 $/m^3$), which equals the centre of the distribution of the base model. All parameters were increased and decreased by 30% respectively and the effects on the total catchment supply, the slope of the supply curve and the number of farmers entering into a contract are shown in Table 6.2. The CV, which is the parameter which is least known, does not have a large influence on S, $\Delta S/\Delta P_e$ and r. In other words we may reasonably accurately simulate the supply of ecosystem service at catchment level without accurate knowledge of the CVs. The supply of ecosystem service is however very sensitive to e. An increase of 30% in e results in a near doubling of the total amount of ecosystem service produced. A decrease in e also considerably reduces the slope of the supply curve. An increase in market prices causes fewer farmers to shift from case a to b; e.g. a higher financial incentive is required to compensate the larger difference in net returns. An increase of costs of the irrigated barley system will reduce the difference in net returns between the two practices and more farmers will adopt rain-fed barley production at the same P_e. The opposite is true for the costs of rain-fed agriculture.

Table 6.2 Sensitivity of the total supply of ecosystem service (S), the slope of the supply curve (ΔS/ΔPe) and the fraction of farmers participating in a contract (r) at a fixed P_e of 0.15 $ m^{-3}.

			S (10^6 m^3)	$\Delta S/\Delta P_e$ (10^9 m^3 $\$^{-1}$)	r (-)
	Base		716	2.9	0.50
Physical parameters	CV_a	+30%	711	3.2	0.50
	CV_a	-30%	716	2.7	0.50
	CV_b	+30%	717	2.1	0.50
	CV_b	-30%	699	4.8	0.49
	e	+30%	1232	4.2	0.67
	e	-30%	306	1.2	0.29
Economic parameters	P	+30%	396	2.1	0.26
	P	-30%	1326	1.5	0.93
	Ca	+30%	963	2.3	0.68
	Ca	-30%	381	2.8	0.25
	Cb	+30%	559	4.3	0.38
	Cb	-30%	792	2.3	0.55

6.4 Discussion and conclusion

Providing payments for ecosystem services has the potential to contribute to the preservation of Tibet's water tower. We have shown that when farmers are provided with a sufficiently high economic incentive the river discharge in the critical pre-monsoon period can be increased significantly even if the percentage of irrigated lands is relatively low. This approach could yield substantial water savings at a critical period of the growing season, if sufficient economic incentives are provided to farmers to change practices. The concept was showcased for a relatively small catchment on the Tibetan plateau; however the presented methodology could be applied to the entire Tibetan plateau. Depending on the physical characteristics (e.g. soil, slope and land use) and the agricultural water use, implementation of the approach at a larger scale may yield significant water savings in critical periods of the year at basin scale.

The methodology presented above, which combines biophysical simulation models with an economic approach, appears to be a transparent and cost effective tool to quantify the effect of financial incentives in the conservation of water resources. Policy relevant information can now be generated without the need to conduct expensive field surveys and set up more elaborate econometric simulation models for which there is generally no time in a political context. As argued by Antle and Valdivia (2006) the MD approach is motivated by the fact that policy makers demand timely, quantitative information with sufficient level of detail, which needs to be accurate within an order of magnitude.

This study was intended to be a proof-of-concept, and the objective was to show that the PES concept can be applied for the conservation of water in data scarce areas. The purpose of the analysis is to have an assessment of economic feasibility of payments for the ecosystem service with readily available data that can be carried out in a timely matter to support policy decision making. It is not intended to be a full-blown assessment of all the possible factors that might affect farmers' decision making (e.g., risk aversion, other institutional constraints). The point of the MD analysis is to get a first-order approximation to the supply curve without

taking a long time to do detailed surveys and understand farmers' decision processes. We have used the combination of the SWAT and MD model in an area where limited data is available and a fully-fledged validation of both the economic and hydrological results was impossible. However using secondary sources of information we have shown that SWAT simulates plausible hydrological outputs and the explorative sensitivity analysis revealed the range in which results may be expected. This validation issue will always remain, particularly because PES contracts are generally signed for a multi-year period in the future based on plausible ranges from the past. The strength of the tools presented lies in the ability to provide these plausible ranges. This contract is also important in forcing the farmers' decision to adopt the prescribed water conserving practice, i.e. rain-fed barley cultivation. The farmers enter a contract with the buyer of water and it defines at least the amount of ecosystem service to be supplied, the alternative practice and the financial compensation.

We have used a process based hydrological model in an ungauged basin. This is an issue many scientists face and recently, interest in using simulation models in ungauged or sparsely gauged basins has increased, leading to some concerted actions. The most relevant is the Prediction in Ungauged Basin (PUB) initiative; an International Association for Hydrological Sciences (IAHS) initiative for the decade of 2003-2012, aimed at uncertainty reduction in hydrological practice (Sivapalani et al., 2003). PUB focuses on the development of new predictive approaches that are based on "understanding" of hydrological functioning at multiple space-time scales. SWAT is such a process based model that comprehensively covers all components of the hydrological cycle, and which has been applied in numerous studies around the world (Arnold and Fohrer, 2005).

For the economic input a number of important assumptions were made. This is legitimate, since no regional data are available as will often be the case in these types of studies, but some caution is required. Two important assumptions were made, which directly affect the output of the MD model. Firstly, it was assumed that the CV of rain-fed barley yield was equal to the CV in slope, because slope is important in characterising the HRUs potential to retain water. This approach is preferred over using a constant CV for all HRUs. The sensitivity analysis showed that the influence of the CV in characterising the potential of the HRU to retain water is limited. More research into the estimation of the CV in yield based on biophysical properties is however recommendable. Secondly, it was assumed that the CV in net returns can be estimated by the CV in yield, because data from a variety of studies show that cost of production tends to be proportional to yield (Antle and Capalbo 2001). However, the CV of net returns may be higher than the CV of yields when yield is highly variable (as in this case of rain-fed barley) and farmers apply inputs in fixed proportions per hectare. Note that this tendency will be mitigated in semi-subsistence systems with low use of variable inputs, as illustrated by the data in Table 6.1. Sensitivity analysis to the assumption of a substantially lower or higher CV shows that the results are not highly sensitive to the CV in any case (Figure 6.7).

Conservation of water is not straightforward. We have shown that through the reduction of evapotranspiration, discharges can be enhanced during the dry season. A possible way to reduce evaporation is the reduction of irrigation and the associated change in land cover. In this study we have compared rain-fed agriculture with irrigated agriculture. However there may be other crops which transpire less than spring barley, which may provide additional savings. Rain-fed agriculture still consumes a considerable amount of water. It might also be a viable option to pay farmers to leave their fields partially fallow.

Water is a common property resource, and there are always two issues to consider, efficiency and equity. For efficiency in the TP case the general principle that is pursued with PES is to create an incentive for farmers to use water efficiently from a social point of view. In TP the argument is that water may be worth much more to downstream users (agriculture, urban or hydropower) than to crop producers in the highlands. In this context, PES has been applied as a way to implement water pricing. An efficient outcome can be obtained in two equivalent ways: farmers using irrigation can be made to pay a positive price per unit of water consumed; or farmers can be paid a positive price per unit of water not used. The opportunity cost calculation is exactly the same in both cases. In other words, "taxing" water-using farmers per unit of water consumers, or "subsidizing" farmers per unit of water not consumed, are equivalent ways to achieve the same outcome. For equity, the question is, who has the rights to the water? If downstream users have the rights, then farmers should pay for using the water; and if farmers have the rights, then downstream users should pay farmers not to use water. So in this case the PES concept of paying farmers not to use water implies they have the rights to the water. The key policy questions that remain to be addressed are how much the water is worth, and who should pay for it. The PES analysis has shown how much water will be delivered at various water prices, but does not provide conclusive answers on which price is the "right" or socially efficient price. The challenge for policy makers thus is to choose the appropriate level for P_e and P_e should be set equal to the marginal social value of the water downstream. The payment will not be higher due to transaction costs; rather, the net price received will be lower.

The concept of payments for ecosystem service for the conservation of water resources may prove to become increasingly important in light of the pending impacts of climate change. A recent study (Immerzeel, 2007) has shown that the Tibetan Plateau is highly sensitive to climate change. Glacial melt will increase river discharge in the decades ahead, but once the glaciers have melted away completely river discharges will decline rapidly. Water conservation through agricultural adaptation may be one of few viable alternatives.

7 Synthesis

7.1 Introduction

Water is the most essential substance on earth and adequate access to water is of paramount societal importance and strongly influences the economic potential. More than a quarter of the world's population or a third of the population in developing countries live in regions experiencing severe water scarcity (Seckler et al., 1999). Water is cycled through the earth's system and it is a resource that is constantly recharged. Water resources assessment should therefore focus on the flow of water between different compartments. The circulation rate of renewable fresh water resources is limited by the climate system. Although the current withdrawal rate of these resources is well below the physical limit, there are more than two billion people living under highly water stressed conditions, due to the uneven distribution in time and space of the water resources. Climate change is expected to further accelerate hydrological circulation rates. This could be beneficial to the reduction of water scarcity, however, shifts in the temporal distribution and projected increases in extreme droughts and excessive rainfall could yield the opposite (Oki and Kanae, 2006).

Figure 7.1 provides an overview of the global circulation on the earth's land surface. In total 110,000 km^3 of precipitation is falling on the land surface and a distinction is made between green water (soil moisture) and blue water (rivers, wetlands, lakes and groundwater). Of the total annual water resources 39% is blue water and 61% is green water. Of the total precipitation 63% is eventually used for evapotranspiration, either by natural surfaces (56%), agriculture (6%), or

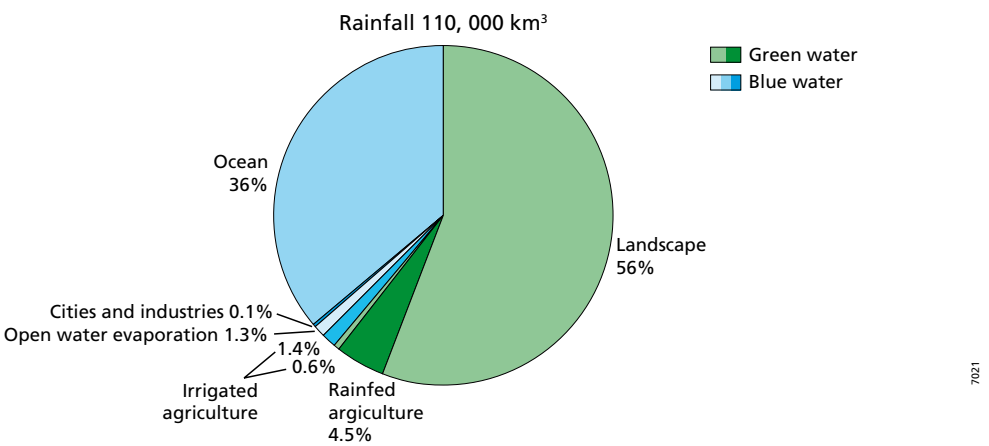

Figure 7.1 Global water use (source Comprehensive Assessment of Water Management in Agriculture, 2007)

open water evaporation (1.3%). Water use by cities and industries comprise a negligible fraction of the total precipitation (0.1%). The spatial and temporal variation in this circulation is enormous (Comprehensive Assessment of Water Management in Agriculture, 2007).

In mountain areas the hydrological cycle is even more intense and diverse, because of orographic effects, low relative humidities, and a high variance in land covers across small horizontal distances. Mountain ranges are also more vulnerable to climate change, because the land surface hydrology is for many areas determined by snow and ice melt. The hydrological cycle at the land surface in mountains includes the processes of snow/ice accumulation and melting as well as the impact these processes will have on regional changes in evaporative depletion and runoff. The circulation in mountain areas is therefore more susceptible to changes in temperature. At the same time mountain ranges play an important role in supplying fresh water resources that sustain the livelihoods of the people downstream in critical periods during the year. The Himalaya, which is the focus of this study, is the water tower of Asia and rivers originating here flow into various regions in Asia. The Mekong, the Yellow river, the Yangthze, the Yarlung Tsampo (Brahmaputra), the Indus and the Karnali all originate in the Himalaya's or on the Tibetan plateau, and support hundreds of millions of people downstream. Since Asia is monsoon dominated, with precipitation concentrated in just a few months, the perennial flow of the rivers largely relies on the constant flux of the snow and ice melt.

The knowledge on the global water cycle certainly has been enriched over the last forty years. Great advancements have been made in measuring and modelling the hydrological cycle at increasing spatial and temporal resolution supported by remote sensing and simulation models (Oki and Kanae, 2006). The future of this type of research also requires improved communication between scientists and policy makers to ensure that scientific finding are related to political actions. A systems approach that integrated all aspects of the interaction between the hydrological cycle, climate change and agriculture in mountain areas is however largely lacking. Research on these components has been performed in the past but the integration is severely hampered by the lack of systematic data and/or tools in many cases. A central concept in this thesis has been the transition from data to information, and from information to knowledge, and from knowledge to support decision makers. Each transition of this chain has been covered in varying degrees of detail. Although each part is a field of science this thesis covers the entire range of this continuum, because this is key to the sustainable development of mountain catchments.

The systems approach is best described by the diagram in Figure 7.2. To prevent external pressures from threatening the important values of mountain catchments we need to understand the past to be able to change the future. The combined analysis using statistics, observations, remote sensing and a combination of different types of models has led to an improved understanding of hydrological processes, insight in spatial and temporal distribution of important hydrological variables, and showed the linkage between upstream events and downstream effects. In particular the remote sensing derivatives are input to simulation models that can then be used to evaluate scenarios for the future. The hydrological assessment of different future scenarios in combination with an economic approach provides clear and transparent information for decision makers. In other words; from past to future and from data to information to knowledge to policies.

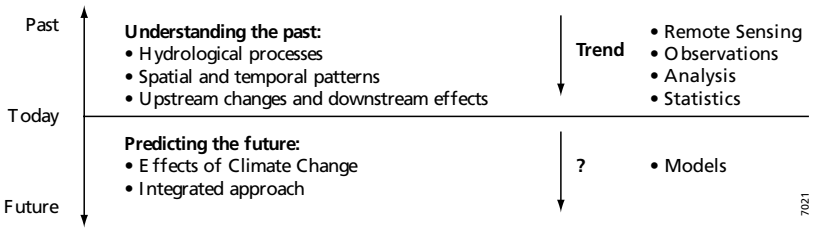

Figure 7.2 Schematic representation of the systems approach

Three knowledge gaps have been identified which impede a successful implementation of a systems approach: (i) lack of fundamental data (e.g. meteorological, hydrological and economic datasets) and knowledge about the spatial heterogeneity of climate variables in mountains, (ii) absence of a straightforward technique to calibrate simulation models in data scarce areas and (iii) the missing link between outputs of simulation models and policy changes. Given this background the overall objective of this study was:

The development of a systems approach for mountain river basins leading to a better understanding of the hydrological functioning and to the development of tools supportive to decision makers

This objective was further detailed through four different research questions:

1. How can remote sensing support the quantification of processes of the hydrological balance in highly diverse topographic terrain?
2. Is it possible to make a reliable assessment of climate change and its effects at river basin scale in mountain areas?
3. Is it feasible to develop a methodology to reliably calibrate hydrological models in ungauged basins on the basis of remote sensing derived hydrological parameters?
4. Is it possible to integrate economic and hydrological modelling and if yes, what incentives and economic instruments can best be applied to conserve water in upstream areas of water scarce river basins?

The four research questions covered a continuum from physical based research into deriving hydrological parameters from remote sensing to the provision of science based information to decision makers based on hydrological and economic models. Each research question has resulted in a peer reviewed paper as presented in previous chapters. This chapter aims at putting the individual topics in a wider context and to provide direction for future developments in this scientific field.

7.2 Mapping precipitation using remote sensing

The use of remote sensing in hydrology has taken a leap forward in the past decades for several reasons; an increased number of satellites and types of sensors, improved data accessibility, and an accelerated development of scientific algorithms to retrieve relevant hydrological information

from satellite radiances. The advantage of having access to spatial temporal patterns of major water balance constituents (e.g. precipitation, evapotranspiration, soil moisture, and ground water storage) is evident; knowledge on the variation in time and space of these constituents yields an enormous amount of information, which can never be met by traditional point based hydro-meteorological monitoring programs.

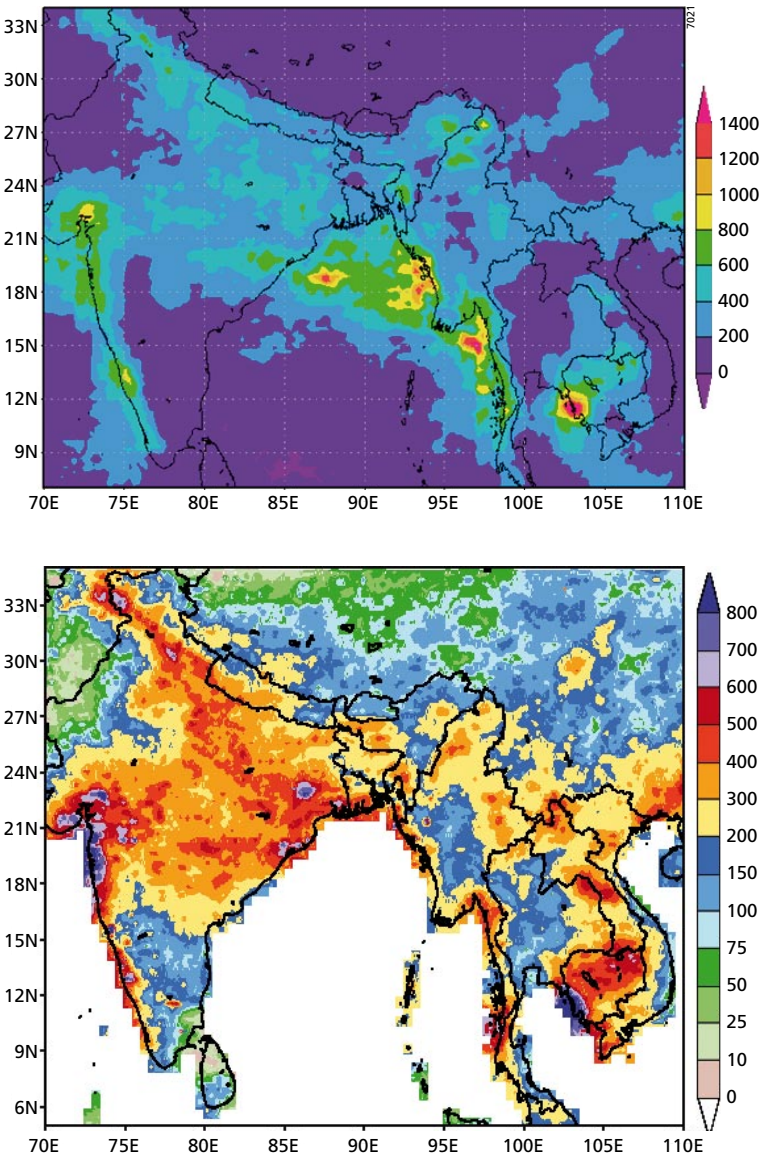

Figure 7.3 Two examples of satellite based remotely sensed precipitation (mm) in July 2006. The top figure shows the TRMM 3B43 product and the bottom figure shows the NOAA RFE 2.0 product.

It is beyond the scope of this thesis to provide a complete overview of remote sensing application in hydrology and in this study the focus has been on understanding precipitation patterns using remote sensing. An indirect approach was used and the behaviour of the vegetation on the Tibetan plateau was analyzed using Fourier analysis to further understand spatial and temporal variation in precipitation (Chapter 2). In recent years a number of remote sensing derived precipitation products, which utilizes a combination of more direct measurements, became accessible. There are two relevant products that are important to mention in this context:

Firstly, the products derived from the Tropical Radar Monitoring Mission (TRMM) (NASA, 2007). The TRMM satellite was launched in 1997 and the mission was recently extended to 2009. The satellite is in a non-sun-synchronous orbit, has a latitudinal range of 50° S-50° N and a revisit time of around 15 hours. The TRMM satellite carries three rain measuring instruments: (i) the TRMM Microwave Imager (TMI), which provides information on the integrated column precipitation content, (ii) the Visible Infrared Scanner (VIRS), which provides high resolution observations on cloud coverage, cloud type and cloud top temperatures, and (iii) the Precipitation Radar (PR) that measure 3-D rainfall distribution. TRMM products are derived from many algorithms, but the most recent and best estimates of precipitations is provided by the 3B42 (3 hourly) and 3B43 products (monthly) (Hufmann et al., 2007). These level 3 products combine information from the three TRMM instruments with information of other satellites calibrated with precipitation gauge data from the Global Precipitation Climatology Project (GPCP) network (Adler et al., 2003). The resulting products are global grids at a spatial resolution of 0.25° (~25 km). An example of the 3B43 monthly precipitation across Asia in July 2006 is shown in Figure 7.3.

Secondly, the Rainfall Estimates (RFE 2.0) provided by the NOAA Climate Prediction Centre (NOAA, 2007). The data are provided for south-east Asia, Africa, Central America, and the area surrounding the Indian Ocean. Daily rainfall estimates are provided at a spatial resolution of 0.1° (~10 km). Four kinds of observation-based data sets are used as inputs to construct the merged analysis of daily precipitation; (i) analysis derived from WMO Global Telecommunication System (GTS) gauge observations of daily precipitation; 2) the GOES Precipitation Index (GPI, Arkin and Meisner 1987) inferred from full resolution IR data from geostationary satellites (Janowiak et al., 2001), (iii) estimates derived from microwave observations of SSM/I (Ferraro and Marks 1995) and (iv) from AMSU-B (Zhao et al., 2001). An example of the merged precipitation product is shown in Figure 7.3.

Inherent to the methodology these satellite derived precipitation products still show relatively large uncertainties and are best used by averaging over larger areas (Hufmann et al., 2007). This will be particularly true for mountain areas where precipitation shows large variation and where the number of precipitation gauges required for removing biases is often limited. In this study an innovative approach has therefore been adopted to explore precipitation patterns. In chapter 2 the response of vegetation to precipitation was used to explain precipitation patterns and land use interaction on the Tibetan plateau. A time series of Normalized Difference Vegetation Index (NDVI) images from 1998 to 2003, observed by the VEGETATION instrument aboard the SPOT 4 and SPOT 5 satellites, was analyzed. This dataset has a ground resolution of 1 km and a frequency of 10 days.

To derive useful information from the NDVI time series a Fourier or harmonic analysis was applied. The analysis unravelled the NDVI signals into a number of sine and cosine waves, each characterized by a specific amplitude and phase angle. The thus manipulated time series revealed a number of interesting findings:

- By using only the first two harmonic terms over 90% of the variation in the NDVI signal was explained.
- There is considerable difference in NDVI patterns between land uses. The irrigated lands and forests show an NDVI peak early November and less intra-annual variation is observed. Other land uses (e.g. grasslands, shrub lands and tundra) respond much more direct on the monsoon precipitation and peak in early august.
- Direct comparison with average precipitation data shows that for all station there is a direct positive NDVI response after the first rains in April. The cropland grassland mosaic land use has the most pronounced response to rainfall. Shrubland show very limited reponse. The needleleaf forest has the largest net increase in NDVI integrated over the whole growing season, e.g. the largest increase in biomass.
- Regression analysis with 15 meteorological stations revealed that precipitation during the growing season shows strong correlation ($r^2 = 0.72$) with the amplitudes of the first two harmonic terms of the Fourier series.
- The Fourier manipulated time series can well be used to derive the onset and length of the growing season.

In this study access to measured precipitation was limited, and there is scope to further extend this interesting methodology. Future work in mountain areas should integrate standard precipitation products, such as TRMM and NOAA RFE 2.0, with time series analysis of NDVI observations. On 1 km pixel resolution spatial patterns of the amplitudes of the Fourier terms could easily be derived based on the developed methodology. The spatial amplitude information in combination with local precipitation gauge data could then be used to downscale the TRMM and/or RFE2.0 datasets to a more accurate precipitation product at a higher spatial detail for mountainous areas.

Another interesting avenue to explore would be the use of other techniques to analyze time series of NDVI. The application of the wavelet transform is promising in this respect. The wavelet transform has some clear advantages over the use of the Fourier transform; most importantly it allows the detection of changes in frequency and amplitude in the signal over time. The discrete wavelet transform decomposes a signal iteratively into approximations (A) and details (D) contained in the signal using a set of high and low pass filters. Approximations relate to the high scale, low frequency components of the signal and the details to the low scale, high frequency components. After the first iteration the approximated sample is down sampled by a factor two, and subsequently the high and low pass filters are applied again. This process is repeated until the final approximation only contains one sample. Both the approximation and details still show changes over time, whereas the Fourier analysis only reveals frequencies, which are abundant in the entire signal.

There are two important aspects that are relevant to the analysis of precipitation patterns using time series of NDVI. Firstly, it is expected that the approximated NDVI signal at a certain decomposition level is related to the same approximated level of the precipitation signal. There

will also be a certain lag time between the two signals, because vegetation responds generally only after a precipitation event has occurred. This lag time can easily be determined using the developed Fourier approach and inferred on the approximated NDVI signal. The NDVI signal is available for each pixel in a remotely sensed image and by superimposing the detailed part of the precipitation signal of the nearest meteorological signal on the approximated signal of each pixel. Using this approach significant improvement in deriving spatial precipitations patterns can be achieved. Secondly, because the temporal changes in frequency and amplitude can be detected, it is possible to use the approximated NDVI signal at the correct level of decomposition to detect trends in precipitation; e.g. trends in intensity (amplitude) and seasonal shifts (frequency). This is an entire new field to be explored, especially since the application of wavelets in remote sensing has been limited to the spatial domain (e.g. data reduction and pattern recognition) (Zhu and Yang, 1998, Carvalho, 2001, Epinat et al., 2001) and to a lesser extent to the temporal domain on a pixel basis.

7.3 Hydrological implications of climate change in large scale mountainous catchments

The recently published fourth assessment paper of the International Panel on Climate Change (IPCC 4AR) (IPCC, 2007) concludes that warming of the global climate system is unequivocal, as is now evident from observations of increases in global average air and ocean temperatures, widespread melting of snow and ice, and rising global average sea level. At continental, regional, and ocean basin scales, numerous long-term changes in climate have been observed. These include changes in Arctic temperatures and ice, widespread changes in precipitation amounts, ocean salinity, wind patterns and aspects of extreme weather including droughts, heavy precipitation, heat waves and the intensity of tropical cyclones. Based on a large number of simulations from a wide variety of atmosphere ocean general circulation models (AOGCM) the report also presents the analysis of possible futures for the period 2000-2100 following the scenarios defined in the IPCC special report on emission scenarios (SRES) (IPCC, 2000).

Figure 7.4 shows the multi-model surface warming prediction for six different SRES scenarios, as well as a scenario where the year 2000 concentration of greenhouse gases has been kept constant. The solid lines are multi-model global averages of surface warming (relative to 1980-99) for the scenarios A2, A1B and B1, shown as continuations of the 20th century simulations. Shading denotes the plus/minus one standard deviation range of individual model annual averages. The orange line is for the experiment where concentrations were held constant at year 2000 values. The gray bars at the right indicate the best estimate (solid line within each bar) and the likely range assessed for the six SRES marker scenarios. The assessment of the best estimate and likely ranges in the gray bars includes the AOGCMs in the left part of the figure, as well as results from a hierarchy of independent models and observational constraints. (IPCC, 2007).

The figure show that irrespective of the scenario the average global temperature is very likely to increase between 1.8 °C and 4 °C by the year 2100. Even the year 2000 constant composition will result in a temperature increase between 0.3 °C and 0.9 °C. The report further concludes that the warming is expected to be greatest over land and at most high northern latitudes, snow cover is projected to contract and that it is very likely that hot extremes, heat waves, and heavy precipitation events will continue to become more frequent.

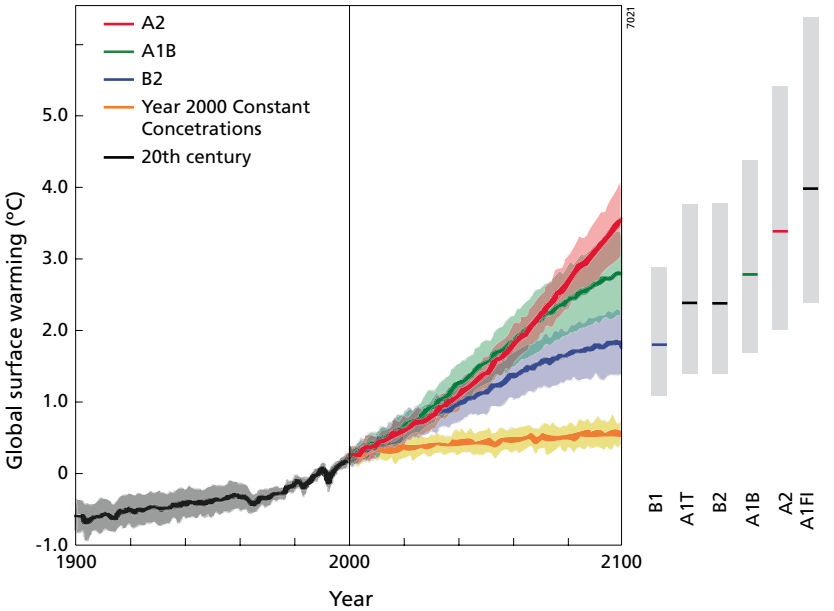

Figure 7.4 Projected global surface warming (source IPCC, 2007)

The spatial variation in observed and projected climate change is large and mountain ranges and their downstream areas are particularly vulnerable for several reasons:

- Firstly, the rate of warming in the lower troposphere increases with altitude, i.e. temperatures will rise more in high mountains than at low altitudes (Bradley et al., 2004).
- Secondly, there is a large high natural variation in climates because of the large difference in altitudes over small horizontal distances. This renders mountain areas more susceptible to climate change (Beniston et al., 1997).
- Thirdly, and probably most important, is the role mountains play in the water supply to downstream areas. More than one sixth of the global population depends on water supplied by mountains and changes in hydrology and water availability are expected to be large in mountain basins (Barnett et al., 2005). Climate Change is expected to intensify the hydrological cycle, e.g. more precipitation and more evapotranspiration. Snow and ice accumulation in mountain areas determine for a large part the surface hydrology and the temporal distribution of the availability of water. This will change significantly when surface air temperatures rise. Especially the diminishing role of snow and ice as a natural delay proves in supplying water will have a tremendous impact.

Despite its relevance, few studies have been conducted on the hydrological effects of climate change at basin scale in the Himalayas. Barnett et al., 2005 in a global assessment of the impact of global warming on snow dominated region indicate that the Himalaya – Hindu Kush area is perhaps the most critical area, where vanishing glaciers will negatively affect water supply in the next few decades, because of the region's huge population. The ice mass over this mountainous region is the third-largest on earth, after the Arctic/Greenland and Antarctic regions. The

hydrological cycle of the region is complicated by the Asian monsoon, but there is little doubt that melting glaciers provide a key source of water for the region in the summer months.

In chapter 3 an innovative approach to analyze climate change for a large Himalayan basin (Brahmaputra, 530,000 km^2) is presented and focus was on three components; (i) analysis of historical trends in precipitation and temperature, (ii) future trends in precipitation and temperature, and (iii) the impact of climate change on hydrology.

Based on the most accurate monthly observational global dataset available an assessment was made of temperature and precipitation patterns from 1900-2002 in the three physiographic zones of the basin, the Tibetan plateau, the Himalayas, and the floodplains. Warming was in general consistent with global warming patterns for the northern hemisphere (0.006 °C/year), with the largest increase in all three zones in spring. Notably a critical period concerning snow and ice melt. Monsoon dynamics govern precipitation and no obvious trends could be identified. However, multiple regression analysis between precipitation and the El Niño Southern Oscillation (ENSO) teleconnection and the air temperature difference between the plateau and the floodplains yielded interesting findings. Firstly, no significant relation was found between monsoon precipitation and ENSO indicators, which is contradictory to earlier studies. Secondly, a significant relation between the air temperature difference between the plateau and the floodplains and precipitation was found. This temperature difference is related to the tropospheric temperature gradient between the plateau and the Indian Ocean, known to positively related to the strength of the monsoon. The troposphere above the plateau is among the warmest on earth, because warming of the plateau is directly related to tropospheric temperatures due to the high elevation. Then, the question arises which processes determine the heating of the air above the plateau? A number of conspiring effects of snow on the surface energy balance seem to play a crucial role here; snow increases the albedo and net energy is reduced, snow also causes a significant part of the net energy being consumed by sublimation and finally melting of snow results in a wetted surface which results in high latent heat fluxes on the expense of the sensible heat flux.

By statistical downscaling outputs from 2000-2100 of six different AOGCMs to spatial resolution of the observed grids a basin wide assessment of two SRES scenario of anticipated changes in precipitation and temperature was made. The analysis showed that the warming rate in this century is increasing and that the temperature increase is largest on the Tibetan plateau. Contradictory to the historical analysis clear future trends in precipitation are anticipated.

A simple stochastic rainfall runoff model based on multiple regression was calibrated using a monthly stream flow data set of a downstream gauge for the period 1956-1993. The model was fed by the downscaled AOGCM projection to provide insight in future changes in average and extreme stream flow per season. The temporal patterns of water availability will change significantly. Average summer discharge is expected to show the largest increase (20-30% in 2100), which will likely have a similar effect on peak discharges. The combination of increase peak discharges in combination with rising sea levels could have far fetching effects in Bangladesh, which is already extremely vulnerable to floods.

There are several directions which are extremely interesting to further investigate in the future:

- There is a large variation in how the combination of climate and snow and ice melt influence river flow in the Himalayas. In summer months, the monsoon from the Bay of Bengal produces heavy precipitation, intensified on windward slopes, predominantly in the

southeast of the region. The monsoon weakens from east to west, rarely penetrating as far as the Karakoram, so that summer precipitation declines in the same direction. Although westerly winds bring precipitation in the west (and at higher elevations throughout the Himalaya) in winter, the total annual precipitation generally increases from west to east. Arid conditions exist at lower elevations in the west; hence, melt water from glacierized mountains remains the major component of runoff for great distances downstream, whereas monsoonal precipitation in the more humid east contributes much of the flow at all elevations. Glaciers experience winter accumulation and summer ablation in the west, but there is predominantly synchronous summer accumulation and summer melt in the east (Rees and Collins, 2006). Further (quantified) insight in this regional difference is very relevant. This could be achieved by combining remote sensing of snow cover, precipitation, and surface temperatures.

- As discussed snow cover extent and depth play an important role in the monsoon regulation in the area. A long term assessment of historical changes in snow extent based on remote sensing would provide an improved understanding of the system. Using a combination of visual interpretation, passive microwave, and snow spectral indices it is currently possible to construct a time series with a length of approximately 40 years. In combinations with long term regional observations of precipitation and temperature, the proposed interaction between snow cover, troposheric temperature gradient and monsoon precipitation could be further validated.
- The basin wide approach has provided interesting new insights; however a global database was used with a number of disadvantages, the most important one being the scarce amount of meteorological stations in these inaccessible areas, specifically at high altitudes. Also, a simple rainfall runoff model was used to predict stream flow at a single location while more advanced distributed process based hydrological models are available, which quantify the complete water balance with high spatial and temporal detail, as presented in chapter 4. Using these types of models assimilated or calibrated with high resolution information based on remote sensing (e.g. precipitation (chapter 2) and evapotranspiration (chapter 4 and 5) could drastically improve knowledge on the functioning of mountains as water tower in large basins and the effects of climate change.

Chapter 3 describes one of the rare analyses for an area where millions of people depend on for their water supply. More research efforts to improve the understanding are therefore fully justified.

7.4 Calibrating hydrological models using Remote Sensing

Data on spatial and temporal patterns of key hydrological variables is essential to assess the current conditions of water resources and to evaluate trends in the past. However, to explore options for the future, tools are required that enable the evaluation of the impact of future trends and how we can adapt to these in the most sustainable way. A model is defined here as *a computer based mathematical representation of dynamic processes*. Simulation models are the appropriate tools to do these analyses and there are three major motivations to use models: (i) formalizing our knowledge in mathematical representation, (ii) understanding processes and (iii) scenarios analyses.

Understanding processes is something that starts right from the beginning during model development. In order to build our models we must have a clear picture on how processes in the real world function and how we can mimic these in our models. The main challenge is not in trying to build in all processes we understand, which is in fact impossible, but lies in our capabilities to simplify things and concentrate on the most relevant processes of the model under construction. The main reason for the success of models in understanding processes is that models can provide output over an unlimited time-scale, in an unlimited spatial resolution, and for sub-processes, which are difficult to observe. These are the weak points in experimental analysis, but at the same time crucial components in sustainable water resources management.

The most important virtue of simulation models is its use in exploration of different scenarios. These scenarios refer to aspects that cannot directly be influenced, such as land use changes, population growth and climate change, often referred to as projections. Complementary to these projections are the so called management scenarios where water managers and policy makers can make decisions that will have a direct impact. Examples are changes in reservoir operations, water allocation and agricultural/irrigation practices. In other words: models enable to change focus from a re-active towards a pro-active approach.

A huge number of hydrological models exits, applications are growing rapidly and a relevant question for hydrological model studies is therefore related to appropriate model selection. An important issue to consider here is the continuum between physical detail and spatial scale. In general it can be stated that the larger the spatial scale the less physical detail is included. Figure 7.5 illustrates this concept and positions a number of commonly used models.

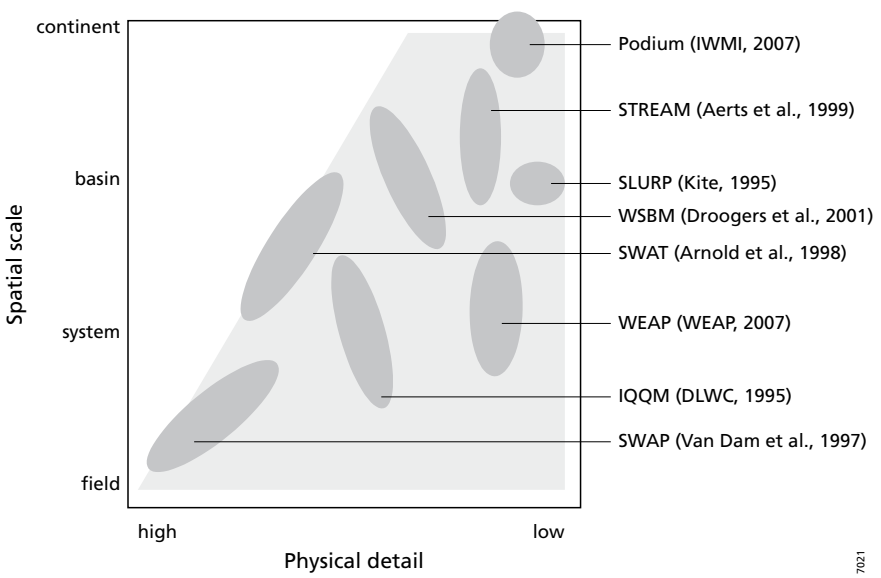

Figure 7.5 Spatial and physical detail of hydrological models

Besides these important considerations there are a number of other factors influencing the choice of the model such as the availability of source code, documentation, support, user friendliness, and inclusion of crucial processes relevant to a particular research topic. For this study (chapter 4, chapter 5 and chapter 6) extensive use was made of the SWAT model (Arnold et al., 1998, Srinivasan et al., 1998). Main reasons for using SWAT can be summarized as: (i) The model adopts a water balance approach and includes atmospheric, land surface, soil, groundwater and stream flow processes, (ii) Model parameterization is facilitated by a user-friendly GIS interface, (iii) SWAT includes high physical detail in relation to the spatial scale it can be applied on, (iv) The source code and interface are in the public domain and an active user community exists with application cases in many countries in the world.

Hydrological models use input data that have, by definition, inaccuracies. These input data or parameters must be estimated for a given catchment and for each computational segment of the model. They must be estimated either by some relationship with physical characteristics or by tuning the parameters so that model response approximates observed response, a process known as calibration. The process of model calibration is quite complex because of limitations of the models, limitations of the input and output data, imperfect knowledge of basin characteristics, mathematical structure of the models and limitations in our ability to express quantitatively our preferences for how best to fit the models to the data. As a result of these limitations, it is even not clear that a unique set of values exists for the model parameters for a given watershed.

The use of remote sensing in hydrological modelling is a growing field and proves to be highly relevant, especially in areas where data are scarce, unreliable or unusable. This situation is regularly encountered in many areas across the world, specifically in mountain catchment and developing countries. Remote sensing provides objective and continuous information on relevant variables and could provide a solution for this issue. As far as the link with models is concerned a distinction should be made in applications aimed at model parameterisation and in applications aiming at model calibration. Remotely sensed parameterization is more common, and could for example include land cover classification, inclusion of digital elevation model in catchment delineation, use of vegetation indices to derive surface roughness and the use of precipitation radar data as

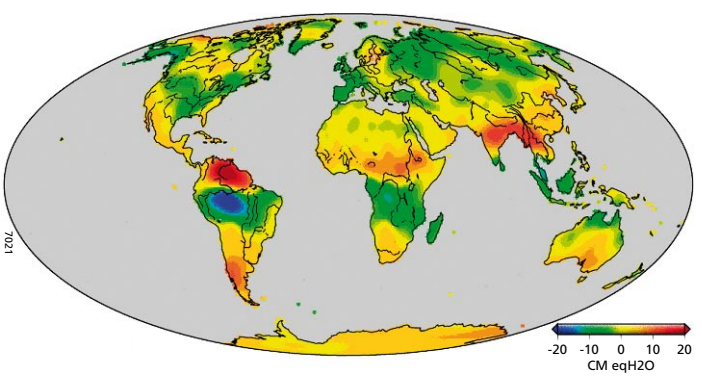

Figure 7.6 Example of global mass balance changes during august 2005 (cm of water equivalent) (Source: GRACE, 2007)

input to a model. Remotely sensed calibration is however a novel field with limited published work, but is applied in this study.

In chapter 4 a methodology was presented that deploys remotely sensed actual evapotranspiration based on the SEBAL algorithm (Bastiaanssen et al., 1998) in the auto-calibration of SWAT.

SEBAL converts satellite radiances into land surface characteristics such as surface albedo, leaf area index, vegetation index, and surface temperature, which are used in solving the instantaneous energy budget equation. In combination with observed meteorological data daily data on actual evapotranspiration is determined.

SWAT is a distributed hydrological model providing spatial coverage of the integral hydrological cycle including atmosphere, plants, unsaturated zone, groundwater, and surface water. The model is comprehensively described in literature (Arnold et al., 1998; Srinivasan et al., 1998).

The study area is a mountainous catchment in Southern India (Upper Bhima catchment in the Krishna basin), which is highly diverse in terms of climatology, where natural flows are non-existent because of a large number of interlinked man made reservoirs and dams, and where data availability is severely hampered by an interstate dispute on water allocation. This renders the catchment extremely suitable for the used approach. Traditionally hydrological model calibration is based on a limited number of discharge stations. Major disadvantage of using a small number of stations, usually near the outlet of a catchment, is that all hydrological processes are lumped together and chances on different parameter combinations that lead to similar results are much larger (equifinality). The presented methodology showed that this can be partly constrained by using spatially distributed observations with a monthly temporal resolution. A time series of 16 bi-weekly actual evapotranspiration maps from October 2004 to May 2005 with a spatial resolution was used to calibrate the SWAT model. The Parameter ESTimation (PEST) (Doherty, 2005) was used for this purpose. PEST is a model independent calibration tool that deploys the gradient based Gauss-Marquardt-Levenberg algorithm and minimizes the sum of the squared deviations between SWAT simulated and SEBAL observed actual evapotranspiration. The calibration was performed at sub basin level at a monthly time step. Several combinations of parameters were calibrated and evaluated and the best performing run improved the r^2 between SWAT and SEBAL derived actual evapotranspiration from 0.40 to 0.81.

The strength of the theoretical approach as developed and described in chapter 4 has been demonstrated in a more applied study in chapter 5, In the same catchment the calibration procedure was further (spatially) refined and applied at the level below the sub basin; the hydrological response unit. The final monthly average evapotranspiration residual between SWAT and SEBAL was 1 mm, while the monthly standard error equalled 26 mm. The calibrated SWAT model was then applied to evaluate water use and productivity in the catchment. Water balance analysis revealed that by far the majority of water is lost from the catchment through evaporative depletion. In total 42% of this evaporation can be considered as non-beneficial (open water, idle rangeland, and fallow periods of agricultural lands). Estimated water productivities are relative high and spatial variation is small, leaving limited scope for improvement for agriculture. It was concluded that major water savings could be achieved (i) by diverting from sugarcane to a dual crop and introducing a fallow period during the extremely dry period from February to May and (ii) by converting non-beneficial evaporation to beneficial transpiration by for example converting

idle rangelands to bio-fuel plantations. In this applied part of the study the combination of remote sensing and SWAT appeared to be an extremely useful tool.

In Chapter 4 and 5 it was shown that there is great scope for the use of remote sensing in the calibration of hydrological models and future work could focus on the assimilation of more diversified remote sensing products for hydrological modelling projects. Three relevant extensions can be identified in this context:

- In this study actual evapotranspiration based on the SEBAL algorithm were used, however the same algorithm also produces other relevant data sets, that could well be integrated in the calibration procedure such as soil moisture and biomass production.
- The remote sensing based precipitation products (e.g. TRMM and RFE 2.0) should be further integrated to be able to better capture spatial heterogeneity inherent to precipitation in mountain catchments.
- Changes in groundwater storage can be quantified by gravity measurements. Currently these data are operational through the Gravity Recovery and Climate Experiment (GRACE 2007). The GRACE twin satellites, launched in March 2002, are making detailed measurements of Earth's gravity field. An example is shown in Figure 7.6. The poor spatial resolution (~ 100 km) is a considerable disadvantage and it is expected that next generation gravity satellites (e.g. ESA GOCE mission) will have an improved spatial resolution.

7.5 Integrating hydrological and economic modelling to support policy making

In Chapter 6 the "minimum data approach" (MD) is used to model the supply of ecosystem services from agriculture. The approach used finds its origins in the trade-off analysis model (TOA) (Stoorvogel et al., 2004) that integrates bio-physical and economic modelling of agricultural production systems.

A trade-off is a fundamental economic concept based on the assumption that resources are scarce. The increase of one scarce good inevitably leads to giving up an amount of another scarce good and this is referred to as opportunity costs by economists. The TOA uses this principle to derive information about the sustainability of agricultural production systems by comparing environmental and production indicators through trade-off curves derived by the analysis of bio-physical processes and the economic behaviour of farmers. These curves are used to communicate information to decision makers and embody the principle of opportunity cost in production systems and are constructed by varying parameters in the production system that affect the economic incentives perceived by farmers in their land use and input use decisions. As farmers respond to changing economic incentives through changes in land use and input use, the sustainability properties of the production systems change. Tradeoff analysis integrates a suite of models, e.g. production models, environmental process models and econometric models and extensive data is required on the bio-physical characteristics, economic behaviour of farmers and experimental data for calibration of the models. (Stoorvogel et al., 2004).

Time constraints often inhibit the implementation of a complete TOA, because collection of the required data is laborious and time consuming, while policy makers require timely information and are often prepared to give up a certain degree of accuracy for this. In addition, in many areas, such as mountain catchments in developing countries, data are simply not available. For this reason Antle and Valdivia (2006) developed a minimum data (MD) approach to model the supply of ecosystem services from agriculture. The central concept in this approach is that the supply of ecosystem service can be modelled by quantifying the opportunity costs between two (or more) competing land use alternatives. One alternative is usually more environmental friendly than the other (produces more ecosystem service), but economically less attractive. By providing a farmer with financial incentives he will shift to the environmental friendly practice if the net return of this practice is higher. By modelling the spatial distribution of opportunity costs in a region, the supply of ecosystem service at different levels of financial compensation can be quantified. Antle and Valdivia (2006) propose an approach that uses mainly secondary data and sensitivity analysis, to parameterise directly the spatial distribution of net returns to competing activities. Often secondary data are available for 'average' or 'representative' costs and returns for a geographical region such as a county or agro-ecozone. The TOA and MD have been previously applied in the field of pesticide leaching (Stoorvogel et al., 2004), soil conservation (Antle et al., 2005) and carbon sequestration (Diagana et al., 2007).

The MD approach is also extremely suitable to model the supply of fresh water from agriculture in data scarce mountain catchments. In chapter 6 it was shown that the concept of payments for ecosystem services has the potential to contribute to water conservation in Tibet. The Tibetan plateau can be considered the water tower of Asia and the conservation of its water resources is of unprecedented importance. For this study a specific agricultural catchment was selected and the hydrological (and production) model SWAT was use to evaluate the hydrological effects of two competing land use practices; rain fed and irrigated barley cultivation. The model outputs were linked to the MD model that estimated the supply curve of fresh water from the spatial distribution of the difference in net return between the two practices. The results showed that during a critical period in the growing season, significant enhancements of stream flow can be achieved. In anticipation of the projected climate change for this region (Chapter 3), this approach could, implemented over larger areas, yield an effective adaptive strategy.

The purpose of the work presented in chapter 6 was a proof-of-concept and to show that payments for ecosystem services could potentially be a viable tool to conserve water. However besides some plausibility checks, no full fledged calibration of model outputs was performed. For future applications the use of remotely sensed datasets to calibrate the model (chapter 4 and 5) in combinations with the downscaled climate change projection (chapter 3) could take the approach a step further as adaptive strategy to climate change.

7.6 Conclusions

The aim of this study was the development of a systems approach that leads to a better understanding of the hydrological functioning in mountain basins and at the same time has a societal relevance and contributes to development of tools that support decision making. The

four research questions cover a continuum from deriving hydrological parameters from remote sensing to the provision of science based information to decision makers based on hydrological and economic models. The main conclusions can be summarized as:

- The results of the systems approach are unique, specifically because there is so little scientific attention for this field, while 20% of the global population depends on fresh water provided by the rivers originating in the Himalayas.
- Using the temporal behaviour of vegetation in understanding precipitation patterns in complex topographic terrain is a promising methodology.
- The effects of climate change on the hydrology in large mountainous basins can be assessed using a straightforward approach. Identified hotspots can then be further analyzed using detailed modelling.
- Remote sensing has been used innovatively in the calibration of a distributed hydrological model.
- The combination of a hydrological model with an economic approach has proven to be a potential powerful tool to support decision making in water conservation in water scarce areas.

References

Adler RF, Huffman GJ, Chang A, Ferraro R, Xie P, Janowiak J, Rudolf B, Schneider U, Curtis S, Bolvin D, Gruber A, Susskind J, Arkin P. (2003), The Version 2 Global Precipitation Climatology Project (GPCP) Monthly Precipitation Analysis (1979-Present). Journal of Hydrometeorology 4: 1147-1167.

Aerts JCJH. Kriek M. Schepel M. (1999), STREAM (Spatial tools for river basins and environment and analysis of management options): 'set up and requirements'. Physics and Chemistry of the Earth, Part B: Hydrology, Oceans and Atmosphere 24: 591-595.

Agam N, Kustas WP, Anderson MC, Li F, Neale CMU. (2007), A vegetation index based technique for spatial sharpening of thermal imagery. Remote Sensing of Environment 107: 545-558.

Agam NWP, Kustas WP, Anderson MC, Li F, Colaizzi PD. (2007b), Utility of thermal sharpening over Texas high plains irrigated agricultural fields, Journal of Geophysical Research. doi:10.1029/2007JD008407. (in press)

Anderton S, Latron J, Gallart F. (2002), Sensitivity analysis and multi-response, multi-criteria evaluation of a physical based distributed model. Hydrological Processes 16: 333-353.

Antle JM, Valdivia RO. (2006), Modeling the Supply of Ecosystem Services from Agriculture: A Minimum Data Approach. Australian Journal of Agricultural and Resource Economics 50: 1-15.

Antle JM, Stoorvogel JJ. (2006), Incorporating Systems Dynamics and Spatial Heterogeneity in Integrated Assessment of Agricultural Production Systems. Environment and Development Economics 11: 39-58.

Antle JM, Valdivia RO, Crissman C, Stoorvogel JJ, Yanggen D. (2005), Spatial Heterogeneity and Adoption of Soil Conservation Investments: Integrated Assessment of Slow Formation Terraces in the Andes. Journal of International Agricultural Trade and Development 1: 29-53.

Antle JM, Capalbo SM (2001), Econometric-process models for integrated assessment of agricultural production systems. American Journal of Agricultural Economics 83: 389-401.

Antle JM, Capalbo SM, Mooney S, Elliott ET, Paustian KH. (2003), Spatial Heterogeneity, Contract Design, and the Efficiency of Carbon Sequestration Policies for Agriculture. Journal of Environmental Economics and Management 46: 231-250.

Arkin PA, Meisner BN. (1987), The relationship between large-scale convective rainfall and cold cloud over the western hemisphere during 1982-1984. Monthly Weather Review 115: 51-74.

Arnell NW. (1999), Climate Change and global water resources. Global Environmental Change 9: 31-49.

Arnold JG, Fohrer N. (2005), SWAT2000: current capabilities and research opportunities in applied watershed modeling. Hydrological Processes 19: 563-572.

Arnold JG, Srinivasan P, Muttiah RS, Williams JR. (1998), Large area hydrologic modeling and assessment. Part I. Model development. Journal of the American Water Resources Association 34:73-89.

Azzali S, Menenti M. (2000), Mapping vegetation-soil-climate complexes in southern Africa using temporal Fourier analysis of NOAA-AVHRR NDVI data. International Journal of Remote Sensing 21: 973-996.

Barnett TP, Adam JC, Lettenmaier DP. (2005), Potential impacts of a warming climate on water availability in snow-dominated regions. Nature 438: 303-309. DOI 10.1038/nature04141

Barnett TP, Dumenil L, Schlese U, Roeckner E, Latif M. (1989). The effect of Eurasian snow cover on regional and global climate variations. Journal of Atmospheric Science 46: 661-685.

Bastiaanssen WGM, Pelgrum H, Wang J, Ma Y, Moreno J, Roerink GJ, van der Wal T. (1998b), The Surface Energy Balance Algorithm for Land (SEBAL): Part 2 validation. Journal of Hydrology 212-213: 213-229.

Bastiaanssen WGM, Menenti M, Feddes RA, Holtslag AAM. (1998), The Surface Energy Balance Algorithm for Land (SEBAL): Part 1 formulation, Journal of Hydrology 212-213: 198-212

Bastiaanssen WGM, Noordman EJM, Pelgrum H, Davids G, Allen RG. (2005),. SEBAL for spatially distributed ET under actual management and growing conditions. Journal of Irrigation and Drainage Engineering 131: 85-93.

Bastiaanssen, WGM, Bandara KMPS. (2001), Evaporative depletion assessments for irrigated watersheds in Sri Lanka. Irrigation Science 21: 1-15

Beniston M, Diaz HF, Bradley RS. (1997), Climatic Change at high elevation sites: an overview. Climatic Change 36: 233-251.

Beniston M. (2003), Climatic Change in mountain regions: a review of possible impacts. Climatic Change 59: 5-31.

Beven K. (1979), A sensitivity analysis of the Penman-Monteith actual evapotranspiration estimates. Journal of Hydrology 44: 169-190.

Beven K. (2006), A manifesto for the equifinality thesis. Journal of Hydrology 320: 18-36

Beven KJ, Freer J. (2001), Equifinality, data assimilation, and uncertainty estimation in mechanistic modelling of complexenvironmental systems. Journal of Hydrology 249: 11-29

Beven KJ. (1993), Prophecy, reality and uncertainty in distributed hydrological modeling. Advances in Water Resources 16: 41-51.

Beven KJ. (2000), Uniqueness of place and process representations in hydrological modelling. Hydrology and Earth System Sciences 4: 203-213

Beven KJ. (2001), How far can we go in distributed hydrological modelling? Hydrology and Earth System Science 5: 1-12.

Boegh E, Thorsen M, Butts MB, Hansen S, Christiansen JS, Abrahamsen P, Hasager CB, Jensen N, Van der Keur P, Refsgaard JC, Schelde K, Soegaard H. Thomsen A. (2004), Incorporating remote sensing data in physically based distributed agro-hydrological modeling. Journal of Hydrology 287: 279-299

Bouma J, Stoorvogel JJ, Quiroz R, Staal S, Herrero M, Immerzeel WW, Roetter RP, Bosch van den R, Sterk G, Rabbinge R, Chater S. (2006), Ecoregional Research for Development. Advances in Agronomy 93: 257-311

Bouwer LM, Aerts JCJH, Coterlet van de GM, Giesen van de N, Gieske A, Mannaerts C. (2004), Evaluating Downscaling Methods for preparing Global Circulation Model (GCM) Data for Hydrological Impact Modelling. In: Aerts JCJH, Droogers P (eds). (2004), Climate Change in Contrasting River Basins. Wallingford: CABI publishing.

Bradley SB, Vuille M, Diaz HF, Vergara W. (2006), Threats to water supplies in the tropical Andes. Science 312: 1755-1756. DOI 10.1126/science.1128087

Bradley, RS, Keimig F'T, Diaz HF. (2004), Projected temperature changes along the American Cordillera and the planned GCOS network. Geophysical Research Letters 3: L16210.

Brutsaert W, Sugita M. (1992), Application of self-preservation in the diurnal evolution of the surface energy balance budget to determine daily evaporation, Journal of Geophysical Research 97(D17): 18377-18382.

Campo L, Caparrini F, Castelli F. (2006), Use of multi-platform, multi-temporal remote-sensing data for calibration of a distributed hydrological model: an application in the Arno basin, Italy. Hydrological Processes 20: 2693:2712.

Carvalho de LMT. (2001), Mapping and monitoring forest remnants: A multiscale analysis of spatio-temporal data. PhD thesis. Wageningen: Wageningen University.

Comprehensive Assessment of Water Management in Agriculture. (2007), Water for Food, Water for Life: A Comprehensive Assessment of Water Management in Agriculture. London: Earthscan and Colombo: International Water Management Institute.

Crago RD. (1996), Comparison of the evaporative fraction and the Priestley-Taylor a for parameterizing daytime evaporation. Water Resources Research 32: 1403- 1409.

Davenport ML, Nicholson S. (1993), On the relationship between rainfall and the Normalized Difference Vegetation Index for diverse vegetation types of East Africa. International Journal of Remote Sensing 14:2369-2389.

Davis JC. (1986), Statistics and Data Analysis in Geology second edition. New York: Wiley.

Diagana B, Antle JM, Stoorvogel JJ, Gray KM. (2007), Economic Potential for Soil Carbon Sequestration in the Nioro Region of Senegal's Peanut Basin. Agricultural Systems 94:26-37.

Dinar, A., (2000), The Political Economy of Water Pricing Reforms. New York: Oxford University Press.

DLWC. (1995), Integrated Quantity-Quality Model (IQQM): Reference Manual. DLWC Report No. TS94.048. Parramatta.

Doherty J. (2005), PEST: Model Independent Parameter Estimation. fifth edition of user manual. Brisbane: Watermark Numerical Computing.

Droogers P, Seckler D, Makin I. (2001), Estimating the potential of rainfed agriculture. IWMI Working Paper 20. Colombo: International Water Management Institute.

Droogers P, Salemi HR, Mamanpoush AR. (2001), Exploring basin scale salinity problems using a simplified water accounting model: the example of Zayandeh Rud Basin, Iran. Irrigation and Drainage 50: 335-348.

Duan Q, Sorooshian S, Gupta HV, Rousseau A, Turcotte R (eds). (2003), Advances in Calibration of Watershed Models. AGU Monograph Series. Water Science and Application 6. Washington DC: American Geophysical Union.

Ecoregional Fund, (2005), More method in our madness: Towards a Toolbox for Ecoregional Research. The Hague: Price Waterhouse Coopers.

Epinat V, Stein A, Jong de SM, Bouma J. (2001), A wavelet characterization of high-resolution NDVI patterns for precision agriculture. Journal of Applied Earth Observation and Geoinformation 3: 121-132.

FAO, (1995), FAO-Unesco digital Soil Map of the World and derived soil properties, 1:5,000,000. Unesco, Paris.

FAO, 2007 (in press). The State of Food and Agriculture 2007.

Fekete BM, Vörösmarty CJ, Grabs W. (2000), Global, composite runoff fields based on ob-served river discharge and simulated water balances. Koblenz: Federal Institute of Hydrology.

Ferraro RR, Marks GF. (1995), The development of SSM/I rain rate retrieval algorithms using ground-based radar measurements. Journal of Atmospheric and Oceanic Technology 12: 755-770.

Francis G, Edinger R, Becker K. (2005), A concept for simultaneous wasteland reclamation, fuel production, and socio-economic development in degraded areas in India: Need, potential and perspectives of Jatropha plantations. Natural Resources Forum 29, 12-24.

Franke R. (1982), Smooth Interpolation of Scattered Data by Local Thin Plate Splines. Computers and Mathematics with Applications 8: 237-281.

Franks SW, Beven KJ. (1997), Estimation of evapotranspiration at the landscape scale: A fuzzy disaggregation approach. Water Resources Research 33: 2929- 2938.

Franks SW, Beven KJ, Quinn PF, Wright IR. (1997), On the sensitivity of soil-vegetation-atmosphere transfer (SVAT) schemes: equifinality and the problem of robust calibration. Agriculture and Forest Meteorology 86: 63-75.

Franks, SW, Beven KJ. (1999), Conditioning a multiple-patch SVAT model using uncertain time-space estimates of latent heat fluxes as inferred from remotely sensed data. Water Resources Research 35: 2751-2762.

Fu C, Fletcher JO. (1985), The relationship between Tibet tropical ocean thermal contrast and the interannual variability of Indian monsoon rainfall. Journal of Climate and Applied Meteorology 24: 841-847.

Gaur A, McCornick PG, Turral H, Acharya S. (2007), Squeezed Dry: Implications of Drought and Water Regulation in the Krishna basin, India (in press).

Government of Maharashtra. (2005), Report on water audit of irrigation projects in Maharashtra 2004-05. Mumbai: Water Resources Department.

Government of Maharashtra. (2007), Census Agricultural Statistics for Districts. [1 August 2007] <http://agri.mah.nic.in/agri/stat/aspstat/mainframeagristat.htm>.

GRACE. (2007), Gravity Recovery and Climate Experience. [14 may 2007[<http://grace.jpl.nasa.gov/>

Groten SME, Ocatre R. (2002), Monitoring the length of the growing season with NOAA. International Journal of Remote Sensing 23: 2797-2815.

Gunnel Y. (1997), Relief and climate in South Asia: the influence of the Western Ghats on the current climate pattern of Peninsular India. International Journal of Climatology 17: 1169-1182.

Gupta VK, Sorooshian S, Yapo PO. (1998), Towards improved calibration of hydrologic model: multiple and noncommensurable measures of information. Water Resources Research 34: 751-763.

Gurgel HC, Ferreira NJ. (2003), Annual and interannual variability in Brazil and its connections with climate. International Journal of Remote Sensing 24: 3595-3609.

Hall FG, Huemmrich KF, Goetz SJ, Sellers PJ, Nickelson JE. (1992), Satellite remote sensing of surface energy balance: Success, failures, and unresolved issues in FIFE. Journal of Geophysical Research 97(D17): 19061-19089.

Hill MJ, Donald GE. (2003), Estimating spatio-temporal patterns of agricultural productivity in fragmented landscapes using AVHRR NDVI time series. Remote Sensing of Environment 84: 367-384.

Hoffmann, L, El Idrissi, A, Pfister, L, Hingray, B, Guex, F, Musy, A, Humbert, J, Drogue, G, Leviandier, T. (2004), Development of regionalized hydrological models in an area with short hydrological observation series. River Research and Applications 20: 243-254.

Houser PR, Shuttleworth WJ, Famiglietti JS, Gupta HV, Syed KH, Goodrich DC. (1998), Integration of soil moisture remote sensing and hydrological modeling using data assimilation. Water Resources Research 34: 3405-3420

Huffman GJ, Adler RF, Bolvin DT, Gu G, Nelkin EJ, Bowman KP, Hong Y, Stocker EF, Wolff DB. (2007), The TRMM Multisatellite Precipitation Analysis (TMPA): Quasi-Global, Multiyear, Combined-Sensor Precipitation Estimates at Fine Scales. Journal of Hydrometeorology 8: 38-55

Ichii K, Kawabata A, Yamaguchi Y. (2002), Global correlation analysis for NDVI and climatic variables and NDVI trends: 1982-1990. International Journal of Remote Sensing 23: 3873-3878.

Immerzeel W. (2005), The Water Tower Function of Tibet; case study report. Ecoregional fund, PriceWaterHouseCoopers, The Hague, The Netherlands (www.ecoregionalfund.com)

Immerzeel WW, Droogers P. (2007), Calibration of a distributed hydrological model based on satellite evapotranspiration. Journal of Hydrology (in press).

Immerzeel WW, Gaur A, Zwart SJ. (2007a), Integrating remote sensing and a process-based hydrological model to evaluate water use and productivity in a south Indian catchment (in press).

Immerzeel WW, Quiroz RA, Jong de SM. (2005), Understanding complex spatiotemporal weather patterns and land use interaction in the Tibetan Autonomous Region using harmonic analysis of SPOT VGT-S10 NDVI time series, International Journal of Remote Sensing 11 26: 2281-2296.

Immerzeel WW, Stoorvogel J, Antle J. (2007b), Can payments for environmental services save the water tower of Tibet? Agricultural Systems (in press).

Immerzeel WW. (2007), Historical trends and future predictions of climate variability in the Brahmaputra basin. International Journal of Climatology (in press).
IPCC. (2000), Special Report on Emission Scenarios. Cambridge: Cambridge University Press.
IPCC. (2001), Climate Change 2001: The Scientific Basis. Cambridge: Cambridge University Press.
IPCC. (2007), Climate Change 2007: The Scientific Basis. Cambridge: Cambridge University Press.
IWMI. (2007), PODIUM, The Policy Dialogue Model. [1 May 2007] <http://www.iwmi.cgiar.org/tools/podium.htm>
Jakubauskas ME, Legates DR, Kastens JH. (2001), Harmonic analysis of timeseries AVHRR NDVI data. Photogrammetric Engineering and Remote Sensing 67: 461-470.
Jakubauskas ME, Legates DR, Kastens JH. (2002), Crop identification using harmonic analysis of time-series AVHRR NDVI data. Computers and Electronics in Agriculture 37: 127-139.
Janowiak JE, Joyce RJ, Yarosh Y. (2001), A realtime global half-hourly pixel-resolution infrared data set and its applications. Bulletin of the American Meteorological Society 82: 205-217.
Kalnay E, Kanamitsu M, Kistler R, Collins W, Deaven D, Gandin L, Iredell M, Saha S, White G, Woollen J, Zhu Y, Leetmaa A, Reynolds B, Chelliah M, Ebisuzaki W, Higgins W, Janowiak J, Mo KC, Ropelewski C, Wang J, Jenne R, Joseph D. (1996), The NCEP/NCAR 40-year reanalysis project. Bulletin of the American Meteorological Society 77: 437-472.
Karnielli A, Dall'Olmo G. (2003), Remote-sensing monitoring of desertification, phenology and droughts. Management of Environmental Quality 14: 22-38.
Keller A, Keller J. (1995), Effective efficiency: a water use concept for allocating freshwater resources. Resources and Irrigation Division Discussion paper 22. Arlington: Winrock International.
Kijne JW, Barker R, Molden D. (2003), Water productivity in agriculture: limits and opportunities for improvement. Wallingford:CAB International.
Kite GW, Droogers P. (2000), Comparing evapotranspiration estimates from satellites, hydrological models and field data. Journal of Hydrology 229: 3-18.
Kite GW, Pietroniro A, (1996), Remote sensing applications in hydrology. Hydrological Sciences 41: 563-592.
Kite GW. (1995), Manual for the SLURP hydrological model. Saskatoon: NHRI.
Klemes V. (1988), Foreword in Molnar, L. (ed) Hydrology of Mountainous Areas, IAHS publication 190:7
Können GP, Jones PD, Kaltofen MH, Allan RJ. (1998), Pre-1866 extensions of the Southern Oscillation Index using early Indonesian and Tahitian meteorological readings. Journal of Climate 11: 2325-2339.
Kripalani RH, Kulkarni S, Sabade S. (2004), Western Himalayan snow cover and Indian monsoon rainfall: A re-examination with INSAT and NCEP/NCAR data. Theoretical and Applied Climatology 74: 1-18.
Krishna Kumar K, Rajagopalan B, Cane MA. (1999), On the weakening relationship between the Indian monsoon and ENSO. Science 284: 2156-2159.
Kuczera G. (1997), Efficient subspace probabilistic parameter optimization for catchment models. Water Resources Research 33: 177-185.
Kummerow C, Barnes W, Kozu T, Shiue J, Simpson J. (1998), The tropical rainfall measuring mission (TRMM) sensor package. Journal of Atmospheric and Oceanic Technology 15: 808-816
Kustas WP, Perry PE, Doraiswamy PC, Moran MS. (1994), Using satellite remote sensing to extrapolate evapotranspiration estimates in time and space over a semiarid rangeland basin. Remote Sensing of Environment 49: 275-286.
Lau KM, Kim MK, Kim KM. (2006), Asian summer monsoon anomalies induced by aerosol direct forcing: the role of the Tibetan Plateau. Climate Dynamics 26: 855-864.
Leber D, Holawe F, Haüsler H. (1995), Climate classification of the Tibet autonomous region using multivariate statistical methods. GeoJournal 37: 433-454.

Levenberg K. (1944), A method for the solution of certain non-linear problems in least squares. The Quarterly Journal of Mechanics and Applied Mathematics. 2: 164-168.

Li B, Tao S, Dawson RW. (2002), Relations between AVHRR NDVI and ecoclimatic parameters in China. International Journal of Remote Sensing 23: 989-999.

Liu WT, Negron Juarez RI. (2001), ENSO drought onset prediction in northeast Brazil using NDVI. International Journal of Remote Sensing 22: 3483-3501.

Liu X, Chen B. (2000), Climatic Warming in the Tibetan Plateau during recent decades, International journal of Climatology 202: 1729-1742.

Loeve R, Dong B, Zhao JH, Zhang SJ, Molden D. (2001), Operation of the Zhanghe Irrigation System. In: Barker, R.; Loeve, R.; Li, Y.H.; Tuong, T.P. (Eds). 2001. Water-Saving Irrigation for Rice: Proceedings of an International Workshop held in Wuhan, China 23-35 March 2001. pp. 25-53. Colombo: International Water Management Institute.

Lubowski RN, Plantinga AJ, Stavins RN. (2005), Land-use change and carbon sinks: econometric estimation of the carbon sequestration supply function. Faculty Research Working Paper Series RP-2005-01. John F. Kennedy School of Government, Regulatory Policy Program. Cambridge: Harvard University.

Malo A., Nicholson SE. (1994), A study of rainfall and vegetation dynamics in the African Sahel using Normalized Difference Vegetation Index. Journal of Arid Environment 19:1-24.

Marquardt DW. (1963), An algorithm for least-squares estimation of nonlinear parameters. Journal of the Society of Industrial and Applied Mathematics 11: 431-441.

Matthews RB, Kropff MJ, Bachelet D, Van Laar HH. (1995), Modeling the Impact of Climate Change on Rice Production in Asia. Wallingford: IRRI and CABI.

Messerli B, Hofer T. (2006), Floods in Bangladesh: History, Dynamics and Rethinking the Role of the Himalayas. Tokyo: United Nations University Press.

Millennium Ecosystem Assessment. (2005), Ecosystems and Human Well-being: Synthesis. Washington DC: Island Press.

Mirza MMQ.(2003), Three Recent Extreme Floods in Bangladesh: A Hydro-Meteorological Analysis. Natural Hazards 28: 35-64.

Mitchell TD, Jones PD. (2005), An improved method of constructing a database of monthly climate observations and associated high-resolution grids. International Journal of Climatology 25: 693-612. DOI 10.1002/joc.1181

Monteith JL. (1965), Evaporation and environment. Symposia of the Society for Experimental Biology 19: 205-234.

Monteith, JL. (1977), Climate and the efficiency of crop production in Britain. Philosphical Transactions of the Royal Society of London Series B 281: 277-329.

Moody A, Johnson DM. (2001), Land-surface phonologies from AVHRR using discrete Fourier transform. Remote Sensing of Environment 75: 305-323.

Mu Q, Heinsch FA, Zhao M, Running SW. (2007), Development of a global evapotranspiration algorithm based on MODIS and global meteorology data (in press). Remote Sensing of Environment.

NASA. (2007), Tropical Rainfall Monitoring Mission. TRMM website [24 May 2007] <http://trmm.gsfc.nasa.gov>

Nash JE, Sutcliffe JV. (1970), River flow forecasting through conceptual models, part I – a discussion of principles. Journal of Hydrology 10: 282-290.

Neena D. (1998), Inter-state variation in cropping pattern in India. Indian Journal of Regional Science 30: 57-69.

Neitsch SL, Arnold, JG, Kiniri JR, Williams JR. (2001), Soil and Water Assessment Tool Theoretical Documentation Version 2000. Texas: Grassland, Soil and Water research Laboratory and Blackland Research Center.

Nelder AJ, Mead R. (1965), A simplex method for function minimization. Computer Journal 7: 308-313.

New M, Hulme M, Jones P. (2000), Representing Twentieth-Century Space-Time Climate Variability. Part II: Development of 1901-96 Monthly Grids of Terrestrial Surface Climate. Journal of Climate 13: 2217-2238

New M, Lister D, Hulme M, Makin I. (2002), A high-resolution data set of surface climate over global land areas, Climate Research 2: 1-25.

Nicols WE., Cuenca. (1993), Evaluation of the evaporative fraction for parameterization of the surface energy balance, Water Resources Research 29: 3681-3690.

Nijssen B, O'Donnel GM, Lettenmaier DP, Lohmann S, Wood EF. (2000), Predicting discharge of global rivers. Journal of Climate 14: 3307-3322.

NOAA. (2007), South Asia Rainfall Estimate. FEWS-NET [24 May 2007] <http://www.cpc.ncep.noaa.gov/products/fews/SASIA/rfe.shtml>

Oki T, Kanae S. (2006), Global Hydrological Cycles and World Water Resources, Science 313 (5790): 1068-72.

Parry M. (2002), Scenarios for climate impact and adaptation assessment. Global Environmental Change 12: 149-153.

Pautsch GR, Kurkalova LA, Babcock BA, Kling CL. (2001), The efficiency of sequestering carbon in agricultural soils, Contemporary Economic Policy 19:123-134.

Perry, C. (2007), Efficient irrigation; inefficient communication; flawed recommendations. Irrigation and Drainage 56: 367-378.

Peterson TC, Easterling DR, Karl TR, Groisman P, Nicholls N, Plummer N, Torok S, Auer I, Boehm R, Gullett D, Vincent L, Heino R, Tuomenvirta H, Mestre O, Szentimrey T, Salinger J, Forland E, Hanssen-Bauer I, Alexandersson H, Jones P, Parker D. (1998), Homogeneity adjustments of in situ atmospheric climate data: a review. International Journal of Climatology 18: 1493-1517.

Pipes LA, Harvill LR. (1971), Applied Mathematics for Engineers and Physicists 3rd edition. Singapore: McGraw-Hill.

Prasad L, Iyengar SS. (1997), Wavelet Analysis with Applications to Image Processing (Boca Raton, FL: CRC).

Prince SD. (1991), A model of regional primary production for use with coarse-resolution satellite data. International Journal of Remote Sensing 12: 1313-1330.

Qin DH. (2002), Future trends of glacier change in west China. Integrated Assessment of Environmental Evolution in Western China, Science Press, Beijing (in Chinese).

Quimei J. (2003), Systems approaches for the development of yak-based systems in Tibet. PhD thesis. Beijing: Chinese Academy of Sciences.

Rabus B, Eineder M, Roth A, Bamler R. (2003), The shuttle radar topography mission – a new class of digital elevation models acquired by spaceborne radar. Photogrammetric Engineering and Remote Sensing 57, 241-262.

Ramanathan V, Chung C, Kim D, Bettge T, Buja L, Kiehl JT, Washington WM, Fu Q, Sikka DR, Wild M. (2005), Atmospheric brown clouds: Impacts on S. Asian climate and hydrological cycle. Proceedings of the National Academy of Sciences (PNAS) 102: 5325-5333. DOI: 10.1073/pnas.0500656102.

Ramanathan V, Chung C. (2006), Weakening of North Indian SST Gradients and the Monsoon Rainfall in India and the Sahel. Journal of Climate 19: 2036-2045.

Rayner NA, Parker DE, Horton EB, Folland CK, Alexander LV, Rowell DP, Kent EC, Kaplan A. (2003), Global analyses of sea surface temperature, sea ice, and night marine air temperature since the late nineteenth century. J. Geophys. Res.108 (D14): 4407. DOI:10.1029/2002JD002670

Rees HG, Collins DN. (2006), Regional differences in response of flow in glacier-fed Himalayan rivers to climatic warming. Hydrological processes 20: 2157-2169.

Rijsberman FR. (2006), Water scarcity: fact or fiction? Agricultural Water Management 80: 5-22.

Robinson DA. (1997), Hemispheric snow cover and surface albedo for model validation. Annals of Glaciology 25: 241-245.

Robinson DA. (1999), Northern Hemisphere snow cover during the satellite era. Proceedings of the Fifth Conference on Polar Meteorology and Oceanography. Dallas. 255-260.

Roerink GJ, Menenti M, Soepboer W, Su Z. (2003), Assessment of climate impact on vegetation dynamics by using vegetation. Physics and Chemistry of the Earth 28: 103-109.

Roerink GJ, Menenti M. (2000), Reconstructing cloudfree NDVI composites using Fourier analysis of time series. International Journal of Remote Sensing 21: 1911-1917.

Ropeleweksi CF, Halpert MS. (1989), Precipitation patterns associated with the high index phase of the Southern Oscillation. Journal of Climate 2: 268-284.

Running SW, Justice CO, Salomonson V, Hall D, Barker J., Kaufman YJ, Strahler AH, Huete AR, Muller JP, Vanderbilt V, Wan ZM, Teillet P, Carneggie D. (1995), Terrestrial remote sensing science and algorithms planned for EOS/MODIS. International Journal of Remote Sensing 15: 3587-3620.

Ryavec KE. (2001), Land use/cover changes in central Tibet, c. 1830-1990:devising a GIS methodology to study a historical Tibetan land decree. The Geography Journal 167: 342-357

Scepan J. (1999), Thematic validation of high-resolution global land-cover data sets. Photogrammetric Engineering and Remote Sensing 65: 1051-1060.

Seckler D, Barker R, Amarasinghe U. (1999), Water Scarcity in the Twenty-first Century. Water Resources Development 15: 29-42.

Shaman J, Cane M and Kaplan A. (2005), The relationship between Tibetan snow depth, ENSO, river discharge and the monsoon of Bangladesh. International Journal of Remote Sensing 26: 3735-3748. DOI 10.1080/01431160500185599

Shaman J, Tziperman E. (2005), The effects of ENSO on Tibetan Plateau Snow depth: A sationary Wave Teleconnection Mechanism and Implication for the South Asian Monsoons. Journal of Climate 18: 2067-2079.

Shuttleworth J. (1998), Combining remotely sensed data using aggregation algorithms. Hydrology and Earth System Sciences 2: 149-158.

Shuttleworth WJ, Gurney RJ, Hsu AY, Ormsby JP. (1989), FIFE: The variation in energy partitioning at surface flux sites, remote sensing and large scale global processes. Oxfordshire: IAHS redbook 186: 67-74,

Singh P, Bengtsson L. (2004), Impact of warmer climate on melt and evaporation for the rainfed, snowfed and glacierfed basins in the Himalayan region. Journal of Hydrology 300: 140-155.

Singh VP, Woolhiser DA. (2002), Mathematical Modeling of Watershed Hydrology. Journal of Hydrological Engineering 7:270-292.

Sivapalani M, Takeuchi K, Frank SW, Gupta VK, Karambiris H, Lakshmi V, Liang X, McDonell JJ, Mendiondo, EM, O'Conell PE, Oki T, Pomeroy JW, Schertzer D, Uhlenbrook S, Zehe E. (2003), IAHS Decade on Predictions in Ungauged Basins (PUB), 2003-2012: Shaping an exciting future for the hydrological sciences. Hydrological Sciences 48: 857-880

Skahill BE, Doherty J. (2006), Efficient accommodation of local minima in watershed model calibration. Journal of Hydrology 329:122-139.

Sorooshian S, Gupta VK. (1995), Model calibration. In Computer Models of Watershed Hydrology, Singh VP (eds.). Colorado: WaterResources Publications 23-68.

Srinivasan R, Ramanarayanan TS, Arnold JG, Bednarz ST. (1998), Large area hydrologic modeling and assessment part II: model application. Journal of American Water Resource Association 34: 91-101.

Srivastava SK, Jayaraman V, Nageswara Rao PP, Manikiam B, Chadrasekhar MG. (1997), Interlinkages of NOAA/AVHRR derived integrated NDVI to seasonal precipitation and transpiration in dryland tropics. International Journal of Remote Sensing 18: 2931-2952.

Stoorvogel JJ, Antle JM, Crissman CC, Bowen W. (2004), The Tradeoff Analysis Model: Integrated Bio-Physical and Economic Modeling of Agricultural Production Systems. Agricultural Systems 80: 43-66.

Stoorvogel JJ, Antle JM, Crissman CC. (2004), Trade-off Analysis in the Northern Andes to Study the Dynamics in Agricultural Land Use. Journal of Environmental Management 72:23-33.

Su Z. (2000), Remote sensing of land use and vegetation for mesoscale hydrological studies. International Journal of Remote Sensing 21: 213-233

Su Z. (2002), The surface energy balance system (SEBS) for estimation of turbulent heat fluxes. Hydrology and Earth System Sciences 6: 85-99.

Tashi N, Yanhua L, Partap T. (2002), Making Tibet Food Secure: Assessment of Scenarios. Kathmandu: International Centre for Integrated Mountain Development.

Tolson BA., Schoemaker CA. (2005), Comparison of optimization algorithms for the automatic calibration of SWAT2000. In: 3rd International SWAT Conference July 11-15 2005, Abbaspour K, Srinivasan R (eds.). Zürich.

Tucker CJ. (1979), Red and photographic infrared linear combination for monitoring vegetation. Remote Sensing of Environment 8: 127-150.

Van Dam JC, Huygen J, Wesseling JG, Feddes RA, Kabat P, Van Walsum PEV, Groenendijk P, Van Diepen CA. (1997), Theory of SWAP version 2.0. Technical Document 45. Wageningen: Wageningen Agricultural University and DLO Winand Staring Centre.

Walker GT. (1924), Correlation in seasonal variations of weather. IV. A further study of world weather. Memoirs of the Indian Meteorological Department 24: 275-332.

Wang J, Price KP, Rich PM. (2001), Spatial patterns of NDVI in response to precipitation and temperature in the central Great Plains. International Journal of Remote Sensing 22: 3827-3844.

Wang QJ. (1991), The genetic algorithm and its application to calibrating conceptual rainfall-runoff models. Water Resources Research 27:2467-2471.

Warrick RA, Bhuiya AH, Mirza MQ. (1996), The Greenhouse Effect and Climate Change. In Warrick, R.A. and Ahmad, Q.K. (Editors). The implications of Climate and Sea-Level Change for Bangladesh. Dordrecht: Kluwer Academic Publishers.

WEAP. (2007), Water Evaluation and Planning Tool. [14 may 2007] <http://www.weap21.org>

Webster PJ, Moore AM, Loschnigg JP, Leben RR. (1999), Coupled ocean-atmosphere dynamics in the Indian ocean during 1997-98. Nature 401: 356-360.

Werner M. (2001). Shuttle Radar Topography Mission (SRTM), mission overview. Frequenz 55: 75-79.

Wilby RL, Wigley TML, Conway D, Jones PD, Hewitson BC, Main J, Wilks DS. (1998), Statistical downscaling of General Circulation Model output: a comparison of methods. Water Resources Research 34: 2995-3008.

Wolfe WL, Zissis GJ (Eds). (1993), The Infrared Handbook. Ann Arbor: Environmental Research Institute of Michigan.

Wood EF. (1995), Scaling behaviour of hydrological fluxes and variables: empirical studies using a hydrological model and remote sensing data. Hydrological Processes 9: 331-346.

World Resources Institute. (2000), People and Ecosystems: The Fraying Web of Life. Washington DC.

Wu J, Adams RM, Kling CL, Tanaka K. (2004). From Microlevel Decisions to Landscape Changes: An Assessment of Agricultural Conservation Policies. American Journal of Agricultural Economics 86:26-41.

Zhao L, Weng F, Ferraro R. (2001), A physically based algorithm to derive surface rainfall rate using Advanced Microwave Sounding Unit-B (AMSU-B) measurements. 11th Conference on Satellite Meteorology and Oceanography, Madison.

Zhong Q, Li YH. (1988), Satellite observation of surface albedo over the Qinghai-Xizang plateau region. Advanced Atmospheric Science 5: 57-65.

Zhu C, Yang X. (1998), Study of remote sensing image texture analysis and classification using wavelets. International Journal of Remote Sensing 19: 3179-3203.

Zwart SJ, Bastiaanssen WGM. (2004), Review of measured crop water productivity values for irrigated wheat, rice, cotton and maize. Agricultural Water Management 69: 115-133.

Zwart SJ, Bastiaanssen WGM. (2007), SEBAL for detecting spatial variation of water productivity and scope for improvement in eight irrigated wheat systems. Agricultural Water Management 89: 287-296.

Summary

Water is the most essential substance on earth and a changing climate has an important impact on the temporal and spatial distribution of water availability. It is anticipated that climate change will accelerate the hydrological circulation rates, and this would lead to an increase in extreme droughts and excessive rainfall. Mountain ranges, specifically, play an important role in regulating the earth's water balance. They provide an important 'water tower' function and, for example, over 20% of the global population depends on fresh water resources provided by the Himalayan range in critical periods of the year. Due to orographic effects, climatic conditions and spatial heterogeneity, the hydrological cycle is more intense in mountains. At the same time mountains are more vulnerable to climate change due the dependence of the surface hydrology on snow and ice melt, which directly responds to temperature increases.

Although great advances have been made over the last decades in measuring and modelling the hydrological cycle at increasing temporal and spatial resolutions, scientific work in this field in mountain areas has however lacked behind. This study has taken a systems approach to the interaction between the hydrological cycle, climate change and agriculture in mountain catchments by contributing to thee major knowledge gaps. Firstly, the lack of fundamental data and knowledge about the spatial heterogeneity of climate variables in mountains. Secondly, the absence of a straightforward technique to calibrate simulation models in data scarce areas, and thirdly, the missing link between complex outputs of simulation models and straightforward information to decision makers. This study covered a continuum from physical based research into deriving hydrological parameters from remote sensing to the provision of science based information to decision makers based on hydrological and economic models through four major topics.

For the first topic, based on the behaviour of vegetation, knowledge on the spatial and temporal precipitation patterns across different land uses on the Tibetan plateau was enhanced. A time series of normalized difference vegetation index (NDVI), derived from the VGT sensor aboard the SPOT satellites, and was manipulated using a Fast Fourier transformation. The manipulated signal proved to yield interesting information about the interaction between vegetation and precipitation and the absolute amounts of precipitation. It also provides an improved method for determining the length of the growing season. Building on this approach promising future research topics have been identified: link with other satellite derived precipitation products and the use of the wavelet approach to further extract useful information from raw time series of satellite imagery.

The second topic focused on the assessment of the effects of climate change for the Brahmaputra basin (530,000 km^2). The historical trends in precipitation and temperature from 1900 onwards were analyzed. This revealed that temperature trends are consistent with global warming with the largest temperature increase in spring in all physiographic zones in the basin. Regression analysis of historical precipitation showed an interesting significant relationship between monsoon precipitation and the temperature difference between the Tibetan plateau and

the low-lying floodplains. A possible explanation has been sought in the link between monsoon strength, troposheric temperature gradient between the Indian Ocean and the Tibetan plateau, and a set of conspiring thermodynamical processes on the Tibetan plateau. Outputs of general circulation models were statistically and spatially downscaled and ensemble averages revealed accelerated increases in precipitation and temperature that seemed to be positively related to altitude. Multiple regression analysis revealed that the downstream summer discharge is subject to a steep increase, with will most likely result in an increase in flooding in the low lying plains of Bangladesh.

For the third topic an innovative methodology was developed to calibrate the process based semi-distributed hydrological model SWAT. Instead of the traditional way of using stream flow gauge data, remotely sensed actual evapotranspiration was used for the calibration. The use of a time series of ET with high spatial detail constrains issues of equifinality, e.g. different sets of parameter combinations leading to similar model output. To derive the ET imagery from satellite data, the globally applied and validated SEBAL algorithm was used. Different sets of soil, land use, and meteorological parameters were optimised using the non-linear parameter optimisation package PEST. The thus calibrated SWAT model was then used to evaluate water use and water productivity in the Upper-Bhima catchment in southern India. Since the catchment is drought prone as well as highly diverse in climate and natural flows are non-existent due to an intricate set of linked reservoirs, the approach proved to be very useful. Future extension of the methodology could include other remote sensing datasets such as precipitation and groundwater.

The final component adds a completely new dimension to the study: a link was made between biophysical and economic modelling and the provision of timely, quantitative information with sufficient level of detail to decision makers. The "payments for ecosystem service" concept to conserve water was implemented in an agricultural catchment on the Tibetan plateau, which has an important water supplying role for downstream areas. It was shown that by providing farmers with financial incentives they may shift from irrigated to rain-fed agriculture as long as the compensation is high enough. This would lead to an increased outflow out of the catchment to downstream users, who will provide the financial compensation. The SWAT model was used to evaluate how much water could potentially be saved, and an economic model revealed what level of payment for ecosystem service would result in which portion of the total farmers to shift to the water saving alternative.

The study has covered a wide range of topics and a number of relevant issues of hydrology, climate change and agriculture in mountain areas have been extensively covered. This integrated approach has shown fascinating results, has clearly added value and opened many new scientific avenues for the future to be explored.

Samenvatting

Ruimtelijk modelleren van bergachtige stroomgebieden
Een integrale analyse van de hydrologische cyclus, klimaatverandering en landbouw

Water is van levensbelang op aarde en het veranderende klimaat heeft een belangrijke invloed op de ruimtelijke en temporele verdeling van de waterbeschikbaarheid. Het wordt verwacht dat klimaatverandering de hydrologische circulatie verder zal versnellen en dat dit zal leiden tot een toename in extreme droogten en regenval. Bergenketens in het bijzonder spelen een vooraanstaande rol in het reguleren van de waterbalans van de aarde. Zij hebben een belangrijke 'watertoren' functie en de Himalayas, bijvoorbeeld, voorzien meer dan 20% van de wereldbevolking van schoon water tijdens kritische perioden van het jaar. In berggebieden is de hydrologische cyclus nog intenser, vanwege orografische effecten, klimatologische omstandigheden, en ruimtelijke heterogeniteit. Daarnaast zijn berggebieden extra kwetsbaar voor klimaatverandering vanwege de afhankelijkheid van de oppervlakte hydrologie van het smelten van sneeuw en ijs, welke onder directe invloed staan van temperatuurstijging.

De afgelopen decaden is er grote vooruitgang geboekt in het meten en modelleren van de hydrologische cyclus met steeds hogere ruimtelijke en temporele resoluties. In berggebieden is wetenschappelijk werk in dit veld echter achter gebleven. Deze studie heeft een systeembenadering toegepast op de relatie tussen de hydrologische cyclus, klimaatverandering en landbouw en heeft bijgedragen aan het opvullen van drie grote kennis hiaten. Ten eerste het gebrek aan fundamentele gegevens over de ruimtelijke heterogeniteit van klimaat variabelen in berggebieden. Ten tweede het gebrek aan een techniek om hydrologische modellen te kalibreren in gebieden met weinig gegevens en ten derde het ontbreken van een verband tussen de complexe uitvoer van simulatie modellen en duidelijke informatievoorziening aan beleidmakers. Deze studie beslaat een continuüm van fysisch onderzoek naar het afleiden van hydrologische parameters uit remote sensing tot wetenschappelijke informatievoorziening aan beleidsmakers gebaseerd op hydrologische en economische modellen aan de hand van vier hoofdonderwerpen.

Voor het eerste onderwerp is, gebaseerd op het gedrag van vegetatie, de kennis met betrekking tot ruimtelijke en temporale neerslagpatronen op het Tibetaanse plateau verbeterd. Een tijdserie van de normalized difference vegetation index (NDVI), afgeleid van de VGT sensor aan boord van de SPOT satelliet, is geanalyseerd met behulp van een Fast Fourier transformatie. Deze getransformeerde tijdserie bevatte interessante informatie over de interactie tussen vegetatie en neerslag en absolute hoeveelheden neerslag. Daarnaast werd een verbeterde methode ontwikkeld om de lengte van het groeiseizoen te bepalen. Op basis van deze aanpak zijn interessante veelbelovende onderzoeksmogelijkheden voor de toekomst geïdentificeerd; integratie met andere op satelliet waarnemingen gebaseerde neerslag producten en het gebruik van de wavelet benadering om meer nuttige informatie uit de ruwe tijdseries van satellietbeelden te extraheren.

Het tweede onderwerp richtte zich op de beoordeling van de effecten van klimaatverandering in het stroomgebied van de Brahmaputra (530,000 km^2). De historische trends in neerslag en

temperaturen zijn geanalyseerd vanaf 1900. Deze analyse liet zien dat de temperatuur stijging grote overeenkomst vertoont met de wereldwijde temperatuurstijging en dat deze het grootste is in het voorjaar in alle fysiografische zones van het stroomgebied. Regressie analyse van historische neerslag patronen bracht een interessant significant verband aan het licht tussen de monsoon neerslag en het temperatuurverschil tussen het Tibetaanse plateau en de laaggelegen vlakten. Een mogelijke verklaring is gezocht in het verband tussen de sterkte van de monsoon, de troposferische temperatuurgradiënt tussen de Indische oceaan en het Tibetaan plateau, en een aantal thermodynamische processen op het Tibetaanse plateau. Uitvoer van een aan grootschalige klimaat modellen zijn statistisch en ruimtelijke neergeschaald en het ensemble gemiddelde laat een versnelde toename in temperatuur en neerslag zien, die lijkt te zijn gecorreleerd met hoogte. Meervoudige regressie analyse toonde aan dat de toekomstige benedenstrooms afvoer in de zomer sterk zal toenemen. Dit zal hoogst waarschijnlijk leiden tot een toename van overstromingen in de laag gelegen vlakten van Bangladesh.

Vervolgens is voor het volgende hoofdonderwerp een innovatieve methode ontwikkeld om het op processen gebaseerde semi-gedistribueerde hydrologische model SWAT te calibreren. Normaal gesproken wordt bij de calibratie gebruik gemaakt van afvoermetingen, maar voor de ontwikkelde methode is gebruik gemaakt van actuele evapotranspiratie, bepaald met remote sensing. Het gebruik van een ET tijdserie met veel ruimtelijk detail zorgt ervoor dat problemen met equifinaliteit (verschillende combinaties van model parameters leiden tot dezelfde modeluitkomst) beperkt worden. Om de ruimtelijke ET beelden af te leiden is gebruik gemaakt van het wereldwijd toegepaste en gevalideerde SEBAL algoritme. Verschillende sets van bodem, landgebruik en meteorologische parameters werden geoptimaliseerd met behulp van het niet-lineaire parameter optimalisatie software pakket PEST. Het op deze manier gekalibreerde model is vervolgens toegepast om het watergebruik en de waterproductiviteit te evalueren in het stroomgebied van de Upper Bhima in zuid India. Gezien de droogtegevoeligheid, de grote diversiteit in klimatologische omstandigheden, en de afwezigheid van natuurlijke afvoer vanwege een ingewikkeld netwerk van onderling verbonden reservoirs, bleek deze benadering zeer succesvol. De toekomstige uitbreiding van deze methodiek zou zich moeten richten op de verdere integratie van andere remote sensing datasets zoals neerslag en grondwaterberging.

Het laatste hoofdonderwerp heeft een volledig nieuwe component aan de studie toegevoegd en er is een verband gelegd tussen biofysische en economische modellen en het genereren van tijdige, kwantitatieve informatie van voldoende detail voor beleidsmakers. Het "payments for ecosystem services" concept werd geïmplementeerd in een agrarisch stroomgebied op het Tibetaanse plateau, dat een belangrijke watervoorzienende functie heeft voor benedenstroomse gebieden. Het werd aangetoond dat boeren bereid zijn over te stappen van geïrrigeerde naar niet-geïrrigeerde landbouw als zijn een voldoende hoge financiële compensatie krijgen. Dit leidt tot een toename van de afvoer uit het stroomgebied waarvoor benedenstroomse gebruikers bereid zij te betalen. Het SWAT model werd gebruikt om te bepalen hoe hoog de gewasopbrengsten en water besparingen zullen zijn, en een economisch model verschafte inzicht in de relatie tussen de hoogte van de financiële compensatie en het aandeel boeren dat bereid is over te stappen naar het waterbesparende alternatief.

De studie heeft een breed spectrum van onderwerpen behandeld en een aantal relevante aspecten van de hydrologie, klimaatverandering en landbouw in berggebieden zijn uitgebreid behandeld. De integrale benadering heeft fascinerende resultaten opgeleverd, heeft een duidelijke meerwaarde en heeft nieuwe wetenschappelijk deuren geopend voor toekomstig onderzoek.

Curriculum Vitae

Walter Immerzeel was born on 21 June 1975 in Moerkapelle, The Netherlands. From 1993 to 1998 he studied environmental science at Utrecht University. His MSc thesis focused on the effects of pasture management on degraded rangelands in the north of the Philippines. He has nine years working experience in geo-informatics, water resource management and climate change with a special focus on the interface between GIS and simulation models. He has extensive experience in the application of remote sensing in mountain areas for systematically assessing and monitoring droughts and food security. He has worked on projects in the Netherlands as well as in a number of developing countries (China, Mexico, Bangladesh, India, Nepal, Philippines, Kenya). In the Netherlands he has worked for the research institute Alterra on several projects for Dutch water boards focusing on climate change, water retention and flooding. From December 2002 until June 2004 he was attached to the International Centre for Integrated Mountain Development (ICIMOD) in Nepal as associate expert GIS and natural resource management. He is currently working at FutureWater, a research and advisory company that works throughout the world to combine scientific research with practical solutions for water management. He is responsible for a number of projects on the cutting edge of climate change and hydrology. Current research clients include Dutch ministries, water boards and the World Bank.

Peer reviewed publications

Van Loon, A.F., Immerzeel, W.W., Droogers, P., 2007, Evaluating the use of time series and stochastic methods in the assessment of the hydrological effects of climate change. (submitted to Agricultural Water Management)

Immerzeel, W.W., Van Heerwaarden, C.C., Droogers, P., 2007, Modelling climate change in a Dutch polder system using the FutureViewR modelling suite. (submitted to Computers and Geosciences)

Droogers, P., Van Loon, A., Immerzeel, W.W., 2007, Climate change impact assessment as function of model inaccuracy. (submitted to Hydrology and Earth System Sciences)

Immerzeel, W.W., Gaur, A., Zwart, S.J., 2007, Integrating remote sensing and a process-based hydrological model to evaluate water use and productivity in a south Indian catchment. (in press).

Immerzeel, W.W., Droogers, P. 2007, Calibration of a distributed hydrological model based on satellite evapotranspiration. Journal of Hydrology (in press).

Immerzeel, W.W., Stoorvogel, J. and Antle J., 2007, Can payments for ecosystem services save the water tower of Tibet? Agricultural Systems (in press).

Immerzeel, W.W., 2007, Historical trends and future predictions of climate variability in the Brahmaputra basin. The International Journal of Climatology (in press).

Bouma, J., Stoorvogel, J.J., Quiroz, R., Staal, S., Herrero, M., Immerzeel, W., Roetter, R.P., Bosch van den, R., Sterk, G., Rabbinge, R., Chater, S., 2007, Ecoregional Research for Development. Advances in Agronomy 93: 257-311.

Immerzeel, W.W., Quiroz, R.A. and Jong de, S.M., 2005, Understanding complex spatiotemporal weather patterns and land use interaction in the Tibetan Autonomous Region using harmonic analysis of SPOT VGT-S10 NDVI time series, International Journal of Remote Sensing 26: 2281-2296.